

**“SYNTHESIS OF METAL
NANOPARTICLES: NEW LIGANDS FOR
BETTER STABILITY AND WATER
DISPERSIBILITY”**

THESIS SUBMITTED TO THE UNIVERSITY OF PUNE

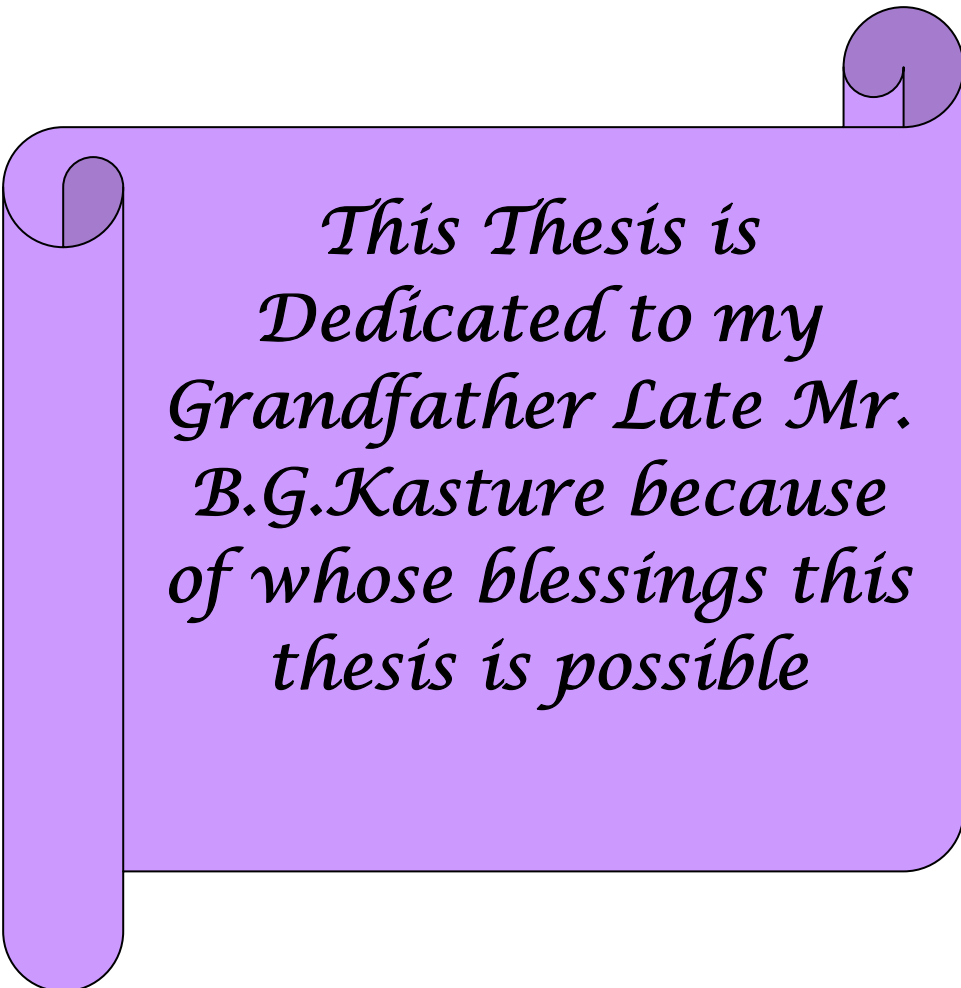
FOR THE DEGREE OF
DOCTOR OF PHILOSOPHY
IN
PHYSICS

BY
MANASI. B. KASTURE

UNDER THE GUIDANCE OF
DR. B. L. V. PRASAD

**PHYSICAL AND MATERIALS CHEMISTRY DIVISION
NATIONAL CHEMICAL LABORATORY
PUNE – 411008, INDIA**

OCTOBER 2010



*This Thesis is
Dedicated to my
Grandfather Late Mr.
B.G.Kasture because
of whose blessings this
thesis is possible*

CERTIFICATE

This is to certify that the work incorporated in the thesis entitled “**SYNTHESIS OF METAL NANOPARTICLES: NEW LIGANDS FOR BETTER STABILITY AND WATER DISPERSIBILITY**” by **MANASI. B. KASTURE**, submitted for the degree *Doctor of Philosophy in Physics* was carried out under my supervision at the Physical and Materials Chemistry Division of National Chemical Laboratory, Pune. Such material as has been obtained by other sources has been duly acknowledged in this thesis. To the best of my knowledge, the present work or any part thereof has not been submitted to any other University for the award of any other degree or diploma.

Date:

Place: Pune

Dr. B. L. V. Prasad

(Research Guide)

DECLARATION

I hereby declare that the work described in the thesis entitled “**SYNTHESIS OF METAL NANOPARTICLES: NEW LIGANDS FOR BETTER STABILITY AND WATER DISPERSIBILITY**” submitted for the degree of *Doctor of Philosophy in Physics* to the University of Pune, has been carried out by me at the Physical and Materials Chemistry Division of National Chemical Laboratory, Pune under the supervision of Dr. B. L. V. Prasad. Such material as has been obtained by other sources has been duly acknowledged in this thesis. The work is original and has not been submitted in part or full by me for any other degree or diploma to other University.

Date:

Place: Pune

Manasi B Kasture

(Research Student)

Acknowledgements

The work presented in this thesis has been made possible by the association of many people and I would like to take this opportunity to acknowledge their contributions.

First and foremost, I would like to extend my sincere gratitude to my guide Dr. B.L.V.Prasad for his invaluable guidance, help, advice, encouragement and continuous support, throughout my PhD. He has provided me with excellent exposure to the field by encouraging and facilitating participation in national as well as international conferences, for which I would like to extend my gratitude towards him.

My special thanks Dr Murali Sastry who introduced me to this field in my initial days of research at NCL. His enthusiasm, integral view on research and his mission has made a deep impression on me. I owe him lots of gratitude for having me shown this way of research. I am really glad to be associated with Dr. Sastry.

I'm grateful to Dr. S. Sivaram, Directors of NCL, Pune for giving me the opportunity to work in this institute and making all the facilities available for my research work,

I also wish to thank Dr Sourav Pal, Head, Physical and Material Chemistry Division, NCL Pune for constant support, encouragement and all the help during my stay at NCL.

It gives me great pleasure to thank Dr Amol A Kulkarni from Chemical Engineering Division, Dr C.V.Ramana from Organic Chemistry Division and Dr Asmita A Prabhune from Biochemical Sciences Division, NCL for the help rendered by them during the collaborative work carried out with them. I also thank them for valuable suggestions and making all the facilities available during the work which I carried out with them. I would like to specially thank Mr. Pitamber P Patel, Dr Ramana's students for providing me the purified sophorolipids and the carboxylic acid. I would also like to thank Prof T Enoji, Tokyo Institute of Technology, Japan and Dr. P. A. Joy, Scientist, NCL, Pune for carrying out all the magnetic measurements of my samples without which I could not have presented my work in the present form.

Dr Georg Thomas and his student Dr P Pramod from National Institute for Interdisciplinary Science and Technology, Trivandrum is acknowledged for the lifetime

measurements. I am also grateful to Dr Arun Banpurkar for the help rendered by him during the prism experiment.

Dr. Vijaymohana, Dr Satish B Ogale Dr Pankaj Potdar for their valuable support and inputs. Mrs. Suguna D. Adyanthaya is greatly acknowledge for her inputs.

I also thank Dr Avinash Kumbhar from the Chemistry Department, University of Pune for being the member of the work evaluation committee.

I would like to extend my sincere thanks to Mrs. Renu Pasricha for TEM measurements. Other members of Center of Material Characterization Mr Gholap for TEM measurements, Dr and Patil for XPS are greatly acknowledged.

My very special thanks goes to my seniors Dr. Senthil, Dr Sumant, Dr Anita, Dr Debabrata, Dr Saikat, Dr. Kannan and Dr Shankar for a sound briefing on the subject and getting me familiarized with all sophisticated characterization techniques and lab culture. My heartfelt thanks to Dr Hrushii, Dr Atul, Dr Sourabh, Dr Ambarish, Dr Akhilesh, Dr Tanushree, Dr Amit, Dr Vipul and Minakshi for all the support I received during my initial PhD days.

I take great pleasure in thanking my labmates Dr Deepti, Dr Prathap, Dr Sanjay, Dr. Vijay, Dr Sonali, Maggie, Priyanka, Sudarshan, Sheetal, Anil, Vilas, Anal, Ravikumar, Ajay, Agnimitra, Balanagalu, Pushpanjali, Prakash and Nikunj. I had a good time with all of them in the lab and outside of it. I also enjoyed the outing with them which was helpful during my PhD days. I thank Dr Deepti, Anal, Ravikumar and Balanagalu for helping me with the thesis corrections. I cherished the days I have spent with Agnimitra in lab and enjoyed the discussions with him on various topics from Food and Football and above all his true passion 'Science'..... Miss You Agni miss you a lot.

Besides, I would also like to acknowledge my project students Gauri, Pallavi, Shabana, Neha and Arpita who have been part of this group for their support. I take this opportunity to thank all my friends Harshada, Yogini, Priya, Aparna, Pradeesh, Dr.Bhalchandra, Vivek, Tushar, Naina, Subhas, Shreeja, Nageshwar, Dr. Mahima, Dr Shena, Dr Shekhar, Mangesh, Kannan, Nivedita, Sindhu, Dr. Ketki, Kuldeep, Sujay, Kunal, Ritwik, all the friends from NCL_TLEP06 group.....Thank You all.

I would like to thanks Mr. Deepak, Mr. Punekar and Mr. Pardesi from the Physical Chemical Division office for helping me extensively with the routine official and administrative

work, I would also like to thank NCL Library staff, administrative staff, and technical staff at CMC for their assistance in the administrative issues during this time.

This thesis would not have been possible without the strong faith, support and encouragement of my family. I wish to express my deep sense of gratitude to my parents Mrs Sunanda B Kasture and Mr Bandu Kasture for being there all the time. I would like to thank my sister Ketki for all the love and affection. I would also like to thank Dr Parshuram, Aae and Baba for their support, love and affection during my thesis.

-Ms Manasi B Kasture

Pune, India

Table of Contents

Chapter I: Introduction

<i>1.1 Introduction</i>	<i>2</i>
<i>1.2 Role of Ligands/surfactant in synthesis of nanoparticles</i>	<i>7</i>
<i>1.2.1 Stabilization of Nanoparticles</i>	<i>7</i>
<i>1.2.2 Influence of ligand on shape and size of nanoparticles</i>	<i>12</i>
<i>1.2.3 Influence of ligand on the crystalline phase of NPs</i>	<i>14</i>
<i>1.2.4 Role of ligand in assembly formation</i>	<i>15</i>
<i>1.3 Objective of thesis</i>	<i>21</i>
<i>1.4 Outline of the thesis</i>	<i>21</i>
<i>1.5 References</i>	<i>23</i>

Chapter II: Effect of ligands on crystal structure and properties of cobalt nanoparticles

<i>2.1 Introduction</i>	<i>39</i>
<i>2.2 Synthesis of sophorolipids and carboxylic acid</i>	<i>42</i>
<i>2.3 Synthesis of cobalt nanoparticles</i>	<i>43</i>
<i>2.4 Results</i>	<i>45</i>
<i>2.5 Discussion</i>	<i>55</i>
<i>2.6 Conclusion</i>	<i>63</i>
<i>2.7 References</i>	<i>64</i>

Chapter III: Sophorolipids as reducing/capping ligands: Understanding the synthetic parameters in batch process an to proceed for continuous process synthesis

<i>3.1 Introduction</i>	<i>69</i>
<i>3.2 Synthesis of sophorolipids</i>	<i>71</i>

Table of content

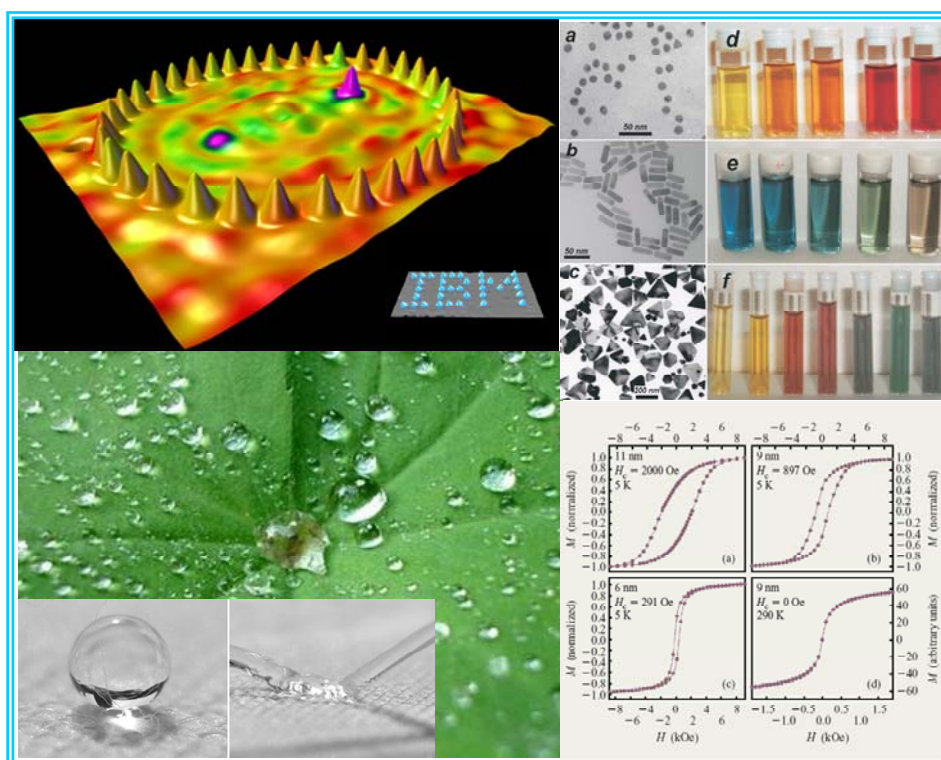
<i>3.3 Synthesis of Ag nanoparticles</i>	<i>71</i>
<i>3.4 Results</i>	<i>74</i>
<i>3.5 Synthesis of Ag nanoparticles in a continuous flow manner</i>	<i>81</i>
<i>3.6 Discussion</i>	<i>84</i>
<i>3.7 Conclusion</i>	<i>89</i>
<i>3.8 References</i>	<i>90</i>
 <i><u>Chapter IV: Halide ion effect on shape of Au nanoparticles: Fluorescence and white light emission</u></i>	
<i>4.1 Introduction</i>	<i>96</i>
<i>4.2 Part A: Synthesis of Au nanoparticles</i>	<i>98</i>
<i>4.3 Results</i>	<i>100</i>
<i>4.4 Discussion: Part A</i>	<i>106</i>
<i>4.5 Part B: White light emission</i>	<i>111</i>
<i>4.6 Fluorescence measurements</i>	<i>113</i>
<i>4.7 Life time measurements</i>	<i>114</i>
<i>4.8 Discussion: Part B</i>	<i>115</i>
<i>4.9 Conclusion</i>	<i>116</i>
<i>4.10 References</i>	<i>117</i>
 <i><u>Chapter V: Conclusions</u></i>	
<i>5.1 Summary of the thesis</i>	<i>123</i>
<i>5.2 Scope for future work</i>	<i>124</i>

Table of content

<i>Appendix I : Instrument Details</i>	<i>125</i>
<i>Appendix II : List of abbreviations</i>	<i>127</i>
<i>Appendix III: Research publications</i>	<i>129</i>

Chapter 1

Introduction



This chapter gives an insight to this thesis and briefly summarizes the different aspects of nanomaterials in terms of its properties, applications and modes of synthesis. The chapter emphasizes the importance of a ligand in the synthesis of nanoparticles. It also highlights the effect of ligand on the size, shape, crystalline phase and formation of assembly of nanomaterials.

1.1 Introduction:

“Nano” today is considered as most happening field and is attracting many researchers to turn towards nanoscience and nanotechnology. The term nanotechnology was coined by Tokyo Science University Professor Taniguchi in 1974 and was popularized in mid 80’s by Dr. K. Eric Drexler, through his books *Engines of Creation: The Coming Era of Nanotechnology* and *Nanosystems: Molecular Machinery, Manufacturing, and Computation*.¹

Term ‘Nano’ can be traced to a Greek root which means dwarf. On the length scale, nano is one billionth of a meter. The use of nanomaterials is documented from the times of Romans. Some of the examples that show use of nanoparticles are the Lycurgus Cup, which consists of gold and silver alloy nanoparticles² and the ‘Damascus Sword’ containing the nanoscale carbon particles etc (Figure 1.1).³ Michael Faraday had demonstrated the synthesis of gold nanoparticles in 1857 in his paper titled ‘Experimental relations of gold (and other metals) to light’ published in *Philosophical Transactions*.⁴ But in last few decades this field has scaled new heights for many reasons including invention of revolutionary imaging methods and techniques that made the characterization of the materials at nanoscale very easy.



Figure 1.1: Examples of use of nanomaterials in ancient times. (A) The Lycurgus Cup, (B) the Damascus Sword and (C) the gold colloids prepared by Michael Faraday (The pictures are taken from ref 2, 3 and 4).

Materials in the micrometer scale exhibit physical properties mostly similar to that of bulk form; however materials in the nanometer scale exhibit properties distinctively different from their bulk counter part. At nanolevel, number of surface

atoms or ions becomes a significant fraction of the total number of atoms or ions and the surface energy plays significant role in the properties of such materials.⁵ The change in the properties is due to the increase in this surface to volume ratio. At nanoscale the electronic structure of materials also gets modified resulting in development of the discrete energy levels in contrast to continuous energy level in bulk materials (Figure 1.2).^{6,7} This leads to dramatic modification of many fundamental properties of nanomaterials such as electrical and thermal conductivity, band gap, density of states, electron affinity, mechanical, magnetic and optical properties etc. These properties are a strong function of size and shape of the particles for a given composition of the nanomaterial.

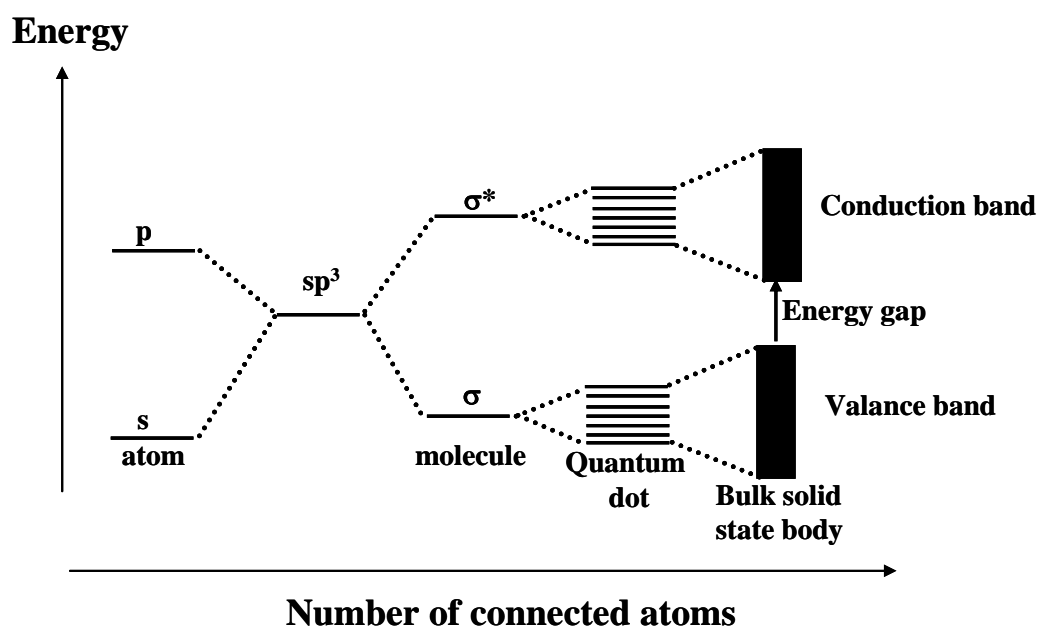


Figure 1.2: Electronic energy levels depending on the number of bound atoms. By binding more number of atoms, the discrete energy levels of the atomic orbital merge into energy bands as shown in the figure. The above figure has been adapted from ref no 6 and 7. Above picture is for semiconductors.

Other properties of materials that are greatly affected by reduction in size to nanolevel are lowering of melting point of the material, reduced lattice constant and the stabilization of crystallographic phases different from the bulk. It is also observed that metal become semiconductors and semiconductors turn insulators at

nanolevel. Figure 1.3 illustrates examples of variation of properties of materials at nanoscale. The fields where nanoparticles are used have a wide spectrum. A partial (not extensive) list of fields they are being used include catalysis,⁸⁻¹⁶ sensors,¹⁷⁻²⁰ electronic devices,²¹⁻²⁶ as photocatalyst,²⁷⁻³⁰ for separation,³¹⁻³⁶ optics,³⁷⁻⁴⁴ data storage,⁴⁵⁻⁴⁷ surface enhanced Raman spectroscopy substrate,⁴⁸⁻⁵⁴ etc. Nanoparticles are also widely used in medical applications like drug and gene delivery,⁵⁵⁻⁶² biosensors,⁶³ in MRI scanners,⁶⁴⁻⁶⁸ hyperthermia⁶⁸⁻⁷⁵ etc.

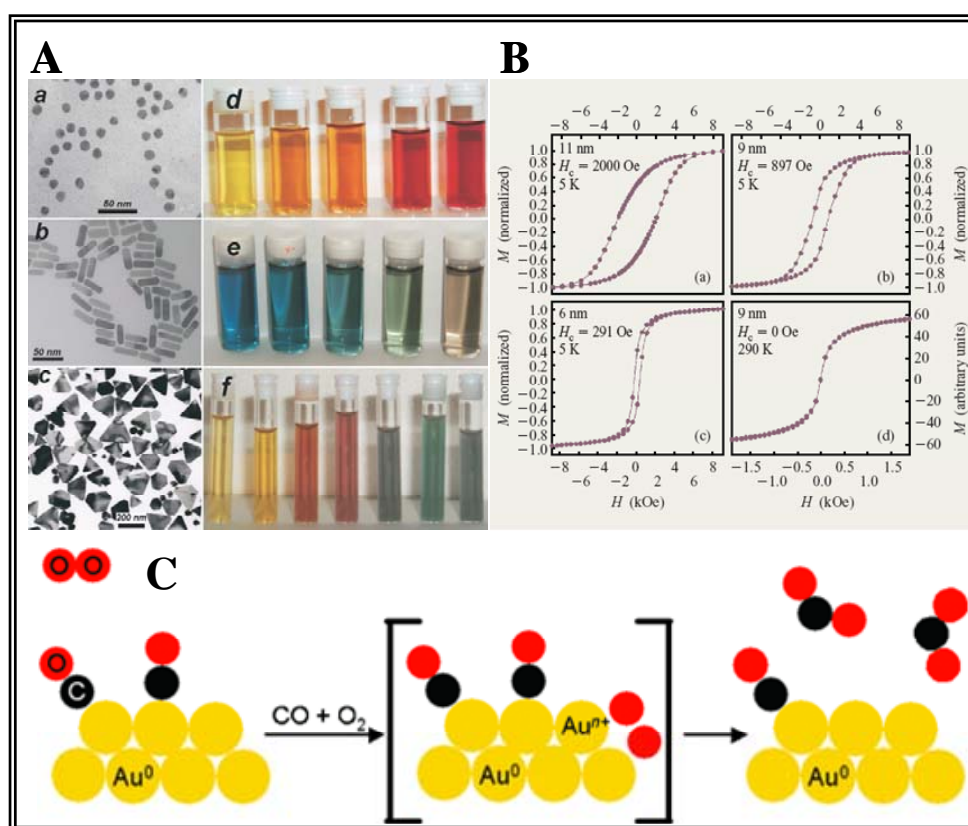


Figure 1.3: Variation of properties of material at nanolevel. (A) Gold at nano-scale possessing different shapes and size. Accordingly, colour of the solution changes with shape and size. (B) Magnetic data as a function of size. (C) Gold nanoparticles acting as a catalyst. Bulk gold does not possess catalytic property.⁷⁶ The images have been taken from reference.^{77,78}

Due to such wide variety of applications, nanoparticles have gained importance and various protocols for synthesis of nanoparticles have been reported. Two classifications that are generally used to distinguish the synthesis of

nanomaterials are i) top down approach which involves slicing or successive cutting of bulk material to obtain nanosize^{5,79,80} and ii) bottom up that involves building up the material atom by atom, molecule by molecule or cluster by cluster.⁸⁰ Figure 1.4 shows the schematics representing these two methods.

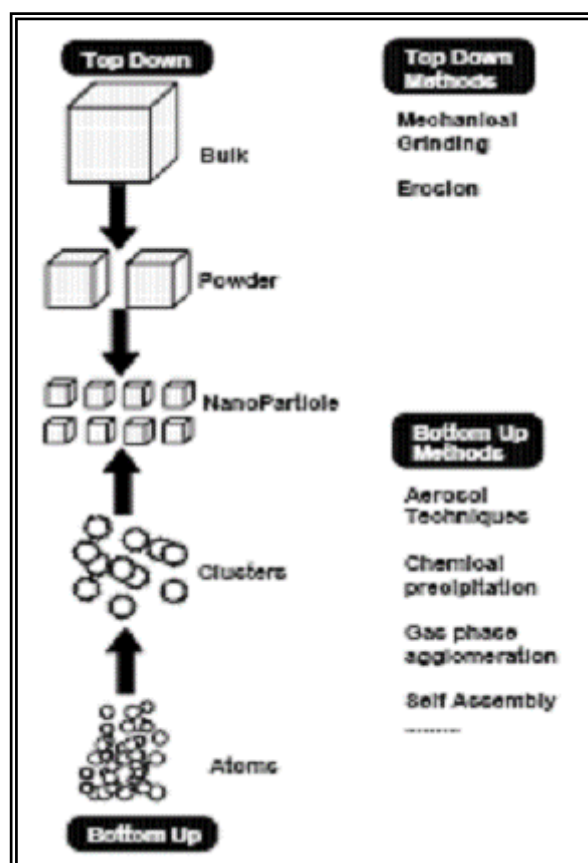


Figure 1.4: Two different approaches for the synthesis of nanoparticles top down and bottom up (taken from ref no.5).

Synthesis of nanoparticles are further broadly classified into three major types

1. Physical Method
2. Chemical Method
3. Biological Method

More detailed classification of the above three methods are summarized in the table 1.1.

Table 1.1: Method for synthesis of nanoparticles

Physical Method	Chemical method	Biological methods	
		Biosynthesis	Bio- mimetic
Evaporation method (Physical vapour deposition , PVD) and (Chemical vapour deposition, CVD) ^{81,82}	Sol-gel method ⁸³⁻⁸⁶	Bacteria, ⁸⁷⁻⁸⁹ Fungi ^{89,90}	DNA/RNA ^{91,92}
Solvated Metal Atom Dispersion (SMAD) ^{93,94}	Chemical precipitation ^{86,95}	Plants and plant extracts ⁹⁶⁻⁹⁸	Viruses ⁹⁹⁻¹⁰¹
Laser ablation ¹⁰²⁻¹⁰⁴	Hydrothermal synthesis ^{86,105}	Amino acids ¹⁰⁶	Proteins ¹⁰⁷
Sonochemical methods ^{108,109}	Micelles or micro-emulsion based synthesis ^{86,110,111}	Peptides ^{112,113}	
Photolytic and Radiolytic methods ^{114,115}	galvanic replacement reaction ^{86,116,117}		

As mentioned before, the properties of nano-materials depend highly on size and shape of nano-materials. Of the above mentioned procedures, chemical methods have proved to be the most reliable ones to produce different sizes and shapes of nanomaterials. As is well known, main ingredient of the chemical synthesis of nanoparticle are the ligands that are used as capping and/ or shape

directing agents. Ligands not only help in achieving stable nanoparticles but also help in achieving nanoparticles of desired shape and size. Custom made ligands perform multiple tasks like capping and reducing the metal ions to metal nanoparticles. Use of ligands which can perform multiple tasks reduces the number of steps involved in the synthesis, thus making the task easy and manageable. Moreover, usage of molecules with multiple functional groups enables the preparation of functional nanoparticles that can be used for targeted drug delivery,¹¹⁸ selective sensitivity¹¹⁹ and multi valent expositions that can be used for specific applications. In the following section we briefly summarize the different roles played by the ligands in the synthesis of nanomaterials.

1.2 Role of Ligands/surfactant in synthesis of nanoparticles:

1.2.1 Stabilization of Nanoparticles:

Stability is one important factor that determines the application potential of the nanoparticles. Stability of nanoparticles especially as dispersion can be achieved by two methods

- a) Electrostatic repulsion.
- b) Steric repulsion (using ligand/surfactants).

1.2.1.1) *Electrostatic interaction.*

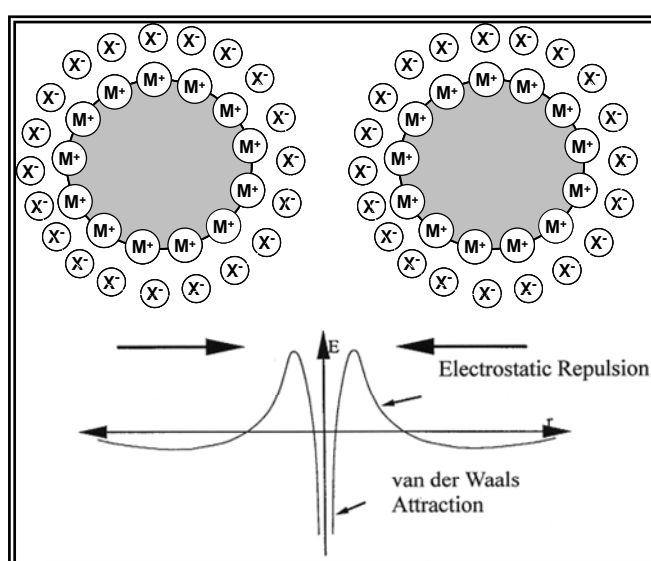
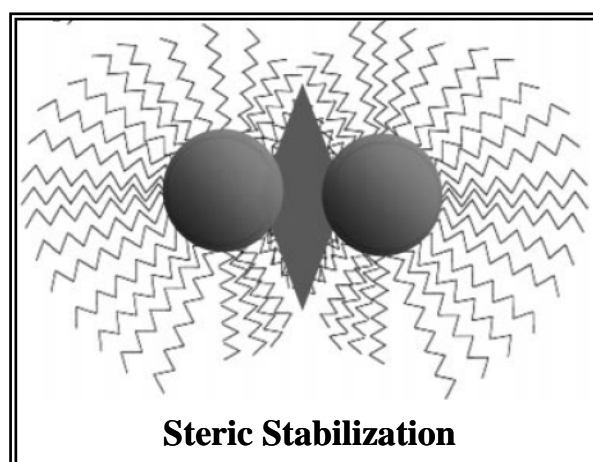


Figure 1.5: Scheme illustrated stabilization of nanoparticles via electrostatic interaction.⁸⁰

In metals, especially noble metals, stabilization of nanoparticles can occur through two modes: electrostatic repulsion and steric repulsion. In the first scenario, subsequent to their reductive preparation, the particles are surrounded by an electric double layer arising due to adsorption of reactant ions on the surface of nanoparticles. This results in two forces acting on nanoparticles, 1) van der Waals force of attraction between metal cores and, 2) electrostatic force of repulsion (potential energy) due to charged ions on the surface. Stability of nanoparticles is dependant on the combination of these two forces. Figure 1.5 shows graph of potential energy versus distance from the surface of spherical particle. At a distance far from the surface, both van der Waals attraction potential and electrostatic repulsion potential is zero. Near the surface, a minimum is observed in potential energy due to van der Waals attraction. At a distance not very far away from the surface where electric repulsion dominates the van der Waal attraction potential and the combination of these two opposing forces leads to a maxima in the energy curve. This maximum is known as repulsive barrier. If the barrier is greater than certain value, two particles cannot overcome the barrier and thus agglomeration is prevented.^{5,120} Electrostatic stabilization is kinetic stabilization process and it is useful only in the case of dilute solutions. Addition of electrolytes screens the double layer charge leading to aggregation. As can be noticed, such stabilization occurring due to electronic repulsion is highly dependent on several factors and the ideal condition for most stable dispersion can be achieved in a very narrow window.

1.2.1.2) Stabilization of nanoparticles using ligands/surfactants:



*Figure 1.6: Steric stabilization of metal nanoparticles.*¹²⁰

Steric stabilization of nanoparticles can be achieved by co-ordination of organic molecules on the surface of nanoparticles, which act as capping ligands. In this way nanoparticle cores are separated from each other and agglomeration is prevented. In case of metal nanoparticles system, ligands that are commonly used as stabilizing agent include thiols, amines, silane, phosphines, carboxylic acid (especially for transition metals) etc.

Table 1.2: Ligand used in synthesis of different nanoparticles

Thiols	used to capped Gold (Au), ¹²¹⁻¹²³ Silver (Ag), ¹²⁴⁻¹²⁶ Platinum (Pt), ¹²⁷ Palladium (Pd) ¹²⁸ and semiconductor nanoparticles. ^{129,130}
Amines	Au, ¹³¹⁻¹³³ Ag, ¹³⁴ Pt, ¹³⁵ Pd ¹³⁶
Carboxylic acid	Ag, ¹³⁷⁻¹³⁹ magnetic nanoparticles (Co, Ni, Fe), ^{140,141}
Phosphines	Au, ^{142,143} magnetic nanoparticles ^{78,144,145}
Silanes	Metals, ^{146,147} Metal oxide ¹⁴⁸

One of the major reasons why these ligands are preferred for capping is due to their binding ability with the surface of nanoparticles.¹⁴⁹ Thiol containing ligands are most widely used as stabilizing agent for metal nanoparticles as the metal-sulfur interaction is known to be strongest as compared to other surfactants. The chemisorption energy between gold and sulfur is estimated to be ~126 kJ.¹²² Extensive studies have been carried out to study the interaction between gold and thiol using various techniques. The thiol-metal bond is most commonly described as a surface bound thiolate. Evidence for thiol being present as it is (without leaving hydrogen) can also be found in literature.¹⁵⁰ Andreoni et al. have carried out detailed experiments to probe the presence and absence of the sulphur bound hydrogen. It was found that apart from presence of thiolates at the bridge sites, intact thiols are also present at “atop” sites and thiolate along with atomic hydrogen adsorbed to the metal surface.^{150,151} Murray and co-workers have based their

argument on ligand place exchange reaction where the hydrogen of the incoming thiol is removed during the replacement step by binding to the leaving thiolate ligand. Brust and co-workers through detailed NMR studies concluded that both the situations (thiolate and thiol binding to gold nanoparticle surface) are possible.¹⁵²

Amines are also known to impart stability to nanoparticles. In depth analysis of interaction of amines with nanoparticle surface has been carried out. Amine-nanoparticle interactions were studied for Au and Ag by recording FTIR, XPS and NMR measurements.^{132,134} Two possibilities of amines binding to gold surface have been proposed: either through co-ordination bond formation or weak co-valent interaction. The analysis carried out by Sastry and co-workers points towards two different modes of binding of alkylamines with nanoparticle surface.^{132,134,135,153,154} The weakly bound component is attributed to the formation of an electrostatic complex between protonated amine molecule and surface bound $\text{AuCl}_4^-/\text{AuCl}_4^-$ ions, while the strong bound entities are assigned to a complex $[\text{AuCl}(\text{NH}_2)]$. Work by Heath and co-workers also suggests that amines form partially covalent bond with gold nanoparticles and that the stability of amine capped gold nanoparticles is a finite size effect which is largely kinetic rather than thermodynamic in origin.¹⁵⁵ Sastry and co-workers showed that gold nanoparticle surface-bound alkanethiols may be replaced by alkylamines by a place-exchange mechanism while the converse process, i.e., exchange of surface bound alkylamines with alkanethiols, does not occur. On the contrary many researchers claim that amines on nanoparticles can be easily replaced by thiols. While the debate goes on, it is a fact that amines are also found to cap nanoparticles and can help stabilizing nanoparticles.

Carboxylic acids are one of the important class of ligand that is used in synthesis of nanoparticles. The carboxylic acid that is being mostly used is oleic acid, which plays a major role in synthesis of magnetic nanoparticles.^{140,141,145,156-158} Interactions of oleic acid with surface of nanoparticles have been discussed in detail.¹³⁷⁻¹⁴⁰ Carboxylic acids generally binds to the metal surface in two different types either a bidentate bond through two equivalent oxygen atoms or a monodentate bond with inequivalent oxygen atoms. In case of the monodentate bond, the C=O bond is still present and the acid hydrogen is substituted by metal atoms.^{140,159,160} However, through detailed FTIR and XPS analysis, Dravid and co-

workers have concluded the bidentate chelating is the type of bonding present in Co nanoparticles case.

It has also been shown that oleic acid can be used to prepare aqueous dispersions of nanoparticles. This aspect is surprising because if the carboxylic acid group binds to the nanoparticle surface then the nanoparticles would not be dispersible in aqueous medium. To address this issue Prasad and co-workers and Efrima and co-workers have studied interaction of oleic acid with silver nanoparticle surface in the aqueous medium.¹³⁷⁻¹³⁹ The studies carried out using FTIR and ¹H NMR reveals that in aqueous medium, oleic acid binds to nanoparticles surface through the double bond. This results in carboxylic acid moiety being exposed to the water medium.

Interaction of phosphine with nanoparticle surfaces has been studied by Hyeon and co-workers. Triphenylphosphine (TPP), trioctylphosphine (TOP) were investigated in detail using NMR. The NMR peak of TOP stabilized palladium nanoparticles appeared at 2.89 ppm while free TOP exhibited a peak at -30.43 ppm. The NMR results indicated that TOP binds weakly to the surface of nanoparticles.

Silanes also are one of the important ligands that are being used for capping surface of nanoparticles. Binding of different silanes like n-hexylsilane (H₁₃C₆SiH₃), n-octylsilane (H₁₇C₈SiH₃), octadecylsilane (H₃₇C₁₈SiH₃) to the surface of nanoparticles are analyzed using reflection-absorption infrared spectroscopy (RAIRS).^{146,147} From RAIRS and XPS results it is proved that the three Si-H bonds of the alkylsilane are broken and a monolayer of the ligand on nanoparticle surface is formed through weak covalent bonds.¹⁶¹⁻¹⁶³

1.2.2: Influence of ligand on shape and size of nanoparticles

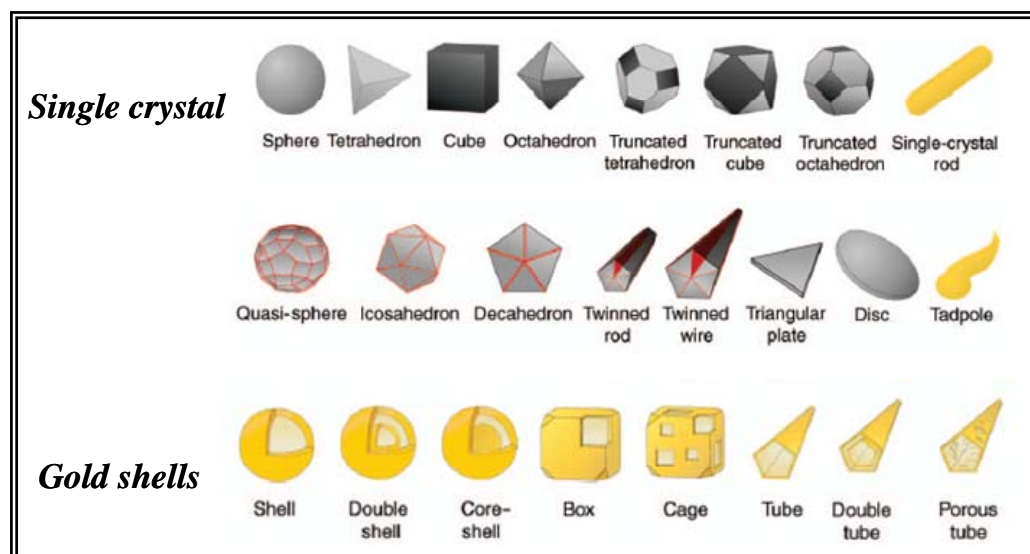


Figure 1.7: Schematic illustration of nanostructure shapes. The shapes in the top row are single crystals, in the second row are particles with twin defects or stacking faults, and in the third row are gold shells. ¹⁶⁴

Factors like temperature of reaction, concentration of reaction, rate of reaction, pH of the reaction solution etc are known to affect the size and shape of the nanoparticles. ¹⁶⁵ Another major factor that plays an important role in governing the shape and size of nanoparticles is the ligands/surfactants that are present during the formation of nanoparticles. ¹⁶⁶ Using the celebrated Brust protocol Heath and co-workers could vary the size of gold nanoparticles ranging from 1.5 to 20 nm. The variation in size of gold nanoparticles was achieved by controlling the initial $\text{AuCl}_4^-/\text{thiol}$ ratio. ^{122,167} Reactivity was controlled by varying the chain length and concentration of the ligands. ¹⁶⁸ Concentration of surfactants like sodium dodecyl sulphate (SDS) and cetyltrimethylammonium bromide (CTAB) were varied and their effects on the size and shape of resulting nanoparticles were investigated in detail. ¹⁶⁹ Change in concentration of these surfactants resulted in formation of different micelle structures which are responsible for control of shape and size of nanoparticles. Using of different concentrations of oleic acid ligand during the cobalt carbonyl decomposition results in the formation of either large nanocrystals

or small clusters. More dramatically, it was shown that by adding or removing free oleic acid ligand from the final reaction product, nanocrystal colloid was turned into a cluster complex solution and vice versa.¹⁷⁰ In order to gain more knowledge on the role of ligands played during the synthesis of nanoparticles, ligand-metal interaction was studied in detail during the growth of nanoparticles. Concentrations of ligand are found to control the size and shape of nanoparticles. At different concentrations, interaction of ligands with metal precursor differs. This results in variety of reaction product formation which ultimately decides the final products.¹⁷¹ Similar ligand effects on particle size were studied in detail by Challa Kumar and co-workers. They demonstrated that usage of different ligands leads to different reaction path ways. This in turn controls the nanoparticle dimensions.^{172,173} The variation in size and shape occurs due to interaction of ligands with the precursor even prior to the nucleation.

Ligands are also known to direct the shape of nanoparticles leading to formation of anisotropic nanoparticles. Murphy and co-worker have extensively synthesized gold nanorods of different aspect ratio using a method called 'seed mediated method'. Based on the systematic studies, they concluded that CTAB is the most suitable surfactant for the formation of gold nanorods and nanowires.¹⁷⁴⁻¹⁷⁷ Detail study on role of CTAB on formation of nanorods/wires reveal that CTA⁺ head group binds to the side surface of nanorods with some preference. The preferential binding is based on steric argument - the Au atom spacing on the side faces is more comparable to the size of the CTA⁺ headgroup than the close-packed {111} face of gold, which is at the end of the nanorods. Such binding stabilizes the side faces, which have relatively large surface energy and stress (tension) compared to other faces. This allows material addition along the [110] common axis on {111} faces, which do not contain the CTA⁺ headgroups.¹⁷⁷

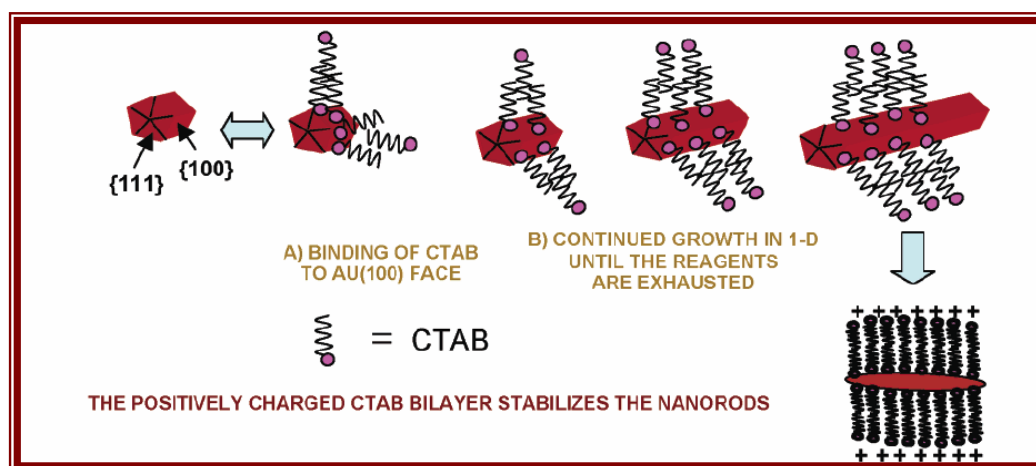


Figure 1.8: Preferential binding of CTAB to specific crystal faces resulting in formation of nanorods. Figure is taken from reference no176.

Detailed investigation of formation of different shapes on nanoparticles has been carried out by Sau and co-workers.¹⁷⁸ Methods like preformed-seed-mediated growth method,¹⁷⁹⁻¹⁸¹ high-temperature reduction method,^{182,183} spatially confined medium/template approach,^{184,185} electrochemical synthesis,¹⁸⁶⁻¹⁸⁸ photochemical method^{189,190} and biosynthesis⁹⁷ which result in different anisotropic nanoparticles in presence of various ligands have been demonstrated. They have concluded that among the many factors that govern the shape of nanoparticles additives like surfactants and ligands play a major role.¹⁹¹⁻¹⁹⁵

1.2.3: Influence of ligand on the crystalline phase of nanoparticles

Properties of nanoparticles are also known to be function of their crystalline phase. This is more prominent in case of magnetic nanoparticles and their magnetic properties.^{196,197} Interestingly the type of crystallographic phase a nanoparticle adopts also has been seen to depend on the type of ligand used. Challa Kumar and co-workers showed formation two different crystal structures when combination of surfactants is used. The two crystal structures obtained in case of cobalt nanoparticles are the hcp phase and the fcc phase.¹⁷³ A new phase ϵ -phase of cobalt nanoparticles was obtained by Bawendi and co-worker when trioctylphosphane oxide (TOPO) was used as capping surfactant. Use of oleylamine at different temperature resulted in formation of different crystalline phases of Ni nanoparticles

(hcp and fcc). Hans *et al.* have synthesized Ni nanoparticles using dodecylamine (DDA) and octadecene (OD) as surfactants. When they used only DDA, cubic phase formation was seen, while the mixture of DDA and DA lead to formation of hexagonal phase. Magnetic measurements were carried out for these two different phases which showed vast difference in nature of magnetic characteristics such as field cooled and zero field cooled curves, Curie temperature etc.¹⁹⁸

Crystal structure of CdTe nanoparticles formed using phosphonic or fatty acid is observed to vary strongly. The nanocrystals grown in presence of the fatty acids had a wurtzite structure, and the reaction in presence of phosphonic acids tended to yield nanocrystals with a zinc blend structure.¹⁹⁹ The exact reason for formation of different crystallographic phases when different ligands are used is not known but one of the reasons cited is binding of ligand and change in aggregation state that can cause phase transformation without particle coarsening.²⁰⁰

1.2.4: Role of ligand in assembly formation

One of the key steps towards the application of nanoparticles in various fields is their assembly into desired architecture.²⁰¹ There are various techniques like i) self assembly of nanoparticles²⁰²⁻²⁰⁴ ii) template directed self assembly²⁰⁵⁻²⁰⁷ iii) assembly by lithography or patterning,²⁰⁸⁻²¹¹ that can lead to the assemblies of nanoparticles. Application of these small clusters in devices requires them to be arranged in one, two or three dimensions (1D, 2D and 3D). Here again, the ligands play an important role.^{86,212-217} In the following we will discuss the assembly of nanoparticles formed by usage of different ligands. Assemblies obtained by usage of ligand depend on various factors like size, stability, solubility of the nanomaterials. Other factors like electrostatic attractions, covalent bonding between the ligands and dipole-dipole interaction incase of magnetic nanoparticles also govern the formation of the assemblies.^{218,219} One of the simplest methods to achieve ligand capped nanoparticle assemblies is to drop coat the nanoparticle solution on a substrate and allow the solvent to evaporate.

The factors that govern the formation of assemblies have been summarized by Prasad and co-workers.²²⁰ The factors that govern the assembly formation include size, ligands used, chain length of the ligand, substrate used for formation of assemblies etc.

We will restrict our discussion to the ligand capping here. As discussed in earlier section, nanoparticle stabilization can be achieved in two ways electrostatic/ligand capping. But the nanoparticles stabilized by electrostatic forces can be destabilized by minor changes. Therefore nanoparticles stabilized by ligands (steric force) are more preferred to obtain reliable assemblies. In this case, stability is imparted by combination of forces viz van der Waals attractive forces between the metal core and the steric repulsive force of the ligand. Expressions for these two forces have been reported by Korgel et al.²²¹

$$E_{steric} = \frac{100R\delta_{SAM}^2}{(C-2R)\Pi\sigma_{thiol}^3} KT \exp\left(\frac{-\Pi(C-2R)}{\delta_{SAM}}\right) \dots \dots \dots (1)$$

Where δ_{SAM} is the thickness of brush and σ_{thiol} is the diameter of the area occupied by the thiol on the particle surface.

$$E_{vdW} = -\frac{A}{12} \left\{ \frac{4R^2}{C^2 - 4R^2} + \frac{4R^2}{C^2} + 2 \ln\left[\frac{C^2 - 4R^2}{C^2}\right] \right\} \dots \dots \dots (2)$$

Where A is the Hamaker's constant and C is the center to center distance between the particles. The above two forces are opposite in nature. When these two are combined a minimum in the total energy can be seen where nanoparticle assemblies can be formed. It can be seen that apart for the above forces, attractive interaction between ligand molecules (interdigitation or bundling) also plays a dominant role.

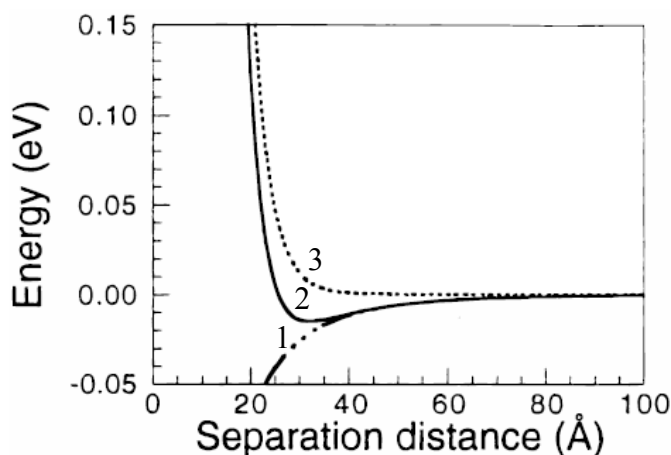


Figure 1.9: Interparticle potential (2) between two nanocrystals: This curve results from a summation of two different forces namely E_{steric} (3) plotted using (eq.1); E_{vdW} (1) plotted using (eq.2) as described in the text. Figure taken from ref no. 220

One of the requisite for formation of assemblies is super saturated solution resulting in formation of assemblies either in solution or on a substrate. Though detail information about the forces responsible for assembly formation is available most of the assemblies obtained are on substrate. There are also examples where assemblies are obtained in solution.²²²⁻²²⁴

Type of ligands and variation in the chain length also govern the formation of nanoparticle assemblies. One of the early reports where assembly of nanoparticles was observed is by Shiffrin and co-workers, where they used thiol based ligands for capping and obtaining the assembly of Au nanoparticles.^{225,226} Superlattices of Au, Ag and Pt were obtained by phase transferring the hydrosols to toluene solution containing thiol ligand.^{127,227} Assemblies of gold nanoparticles were obtained using different ligands like dodecanthiol, dodecylamine, octadecyl silane, trioctyl phosphine, dodecyl bromide, dodecyl iodide, dodecanol and decane. The superlattices formed with these different ligands are different in nature.²²⁸ Dodecylthiol capped nanoparticles formed better assemblies as compared to other ligands. 2-D and 3-D superlattices were synthesized in nonionic inverse micelle and capped with alkanethiol ligands by varying the alkanethiol chain length from C₆ to C₁₈.²²⁹ It is possible to control the interparticle spacing of superlattices over a limited range by capping with organic thiols. Very small alkanethiols cause precipitation, and high alkanethiols restructure the nanoclusters, but intermediate alkanethiols, from C₆SH to C₁₄SH, result in the formation of uniform superlattices with controlled interparticle spacings. Polydispersity of the assembly increases with increase in chain length. Similar chain length dependent studies of superlattice formation were carried out by Prasad et al using thiols. Separate particles were formed when longer chain length (C₁₆) thiols were used while for smaller chain length (C₈ and C₁₀) 3D superlattices are formed.²³⁰

Use of ligands that possess same functional groups at both the ends which can bind to two nanoparticles have also been used in formation of assemblies of nanoparticles. Brust and co-workers have used α,ω -dithiols to assemble Au nanoparticles. Controlling such processes was seen to be difficult, never the less; it was achieved by varying the concentration of the ligand and optimizing it.²¹⁶ Networks of nanoparticles which are photosensitive were prepared by using

azobenzene derivatives. The interparticle spacing could be controlled by the reversible trans–cis isomerization of the azobenzene moiety induced by UV and visible light, respectively.²³¹ One of the examples where assemblies are formed in aqueous medium is reported by Kimura and co-workers. Mercaptosuccinic acid was used to achieve this. In the superlattices that have been obtained Au nanoparticles, arranged in hexagonal closed packed structures were interconnected by interparticle chemical binding due to mercaptosuccinic acid.²³² Assemblies of nanoparticles are formed taking the advantage of specific interactions between the complimentary recognition units. Rotello and co-workers have used this method, where the ligands on surface of nanoparticles bind with complimentary recognition units leading to formation of assemblies.^{204,233}

Assemblies of magnetic nanoparticles are important for their application in recording media.^{144,234} Assembly of these magnetic nanoparticles largely depends on the composition and combination of dispersing solvent and the temperature during the deposition.^{78,235} Ordered array of Fe nanoparticles were obtained by coating these nanoparticles with Oleylamine.²³⁶ Assembly of cobalt nanoparticles were obtained using oleic acid and trioctylphosphine as ligand.¹⁵⁶ Sidhaye et al. have obtained assembly of Ni and Co nanoparticles where the combination of sodium dodecyl sulphate (SDS) and oleic acid have been used to achieve the assembly of nanoparticles.¹⁴¹

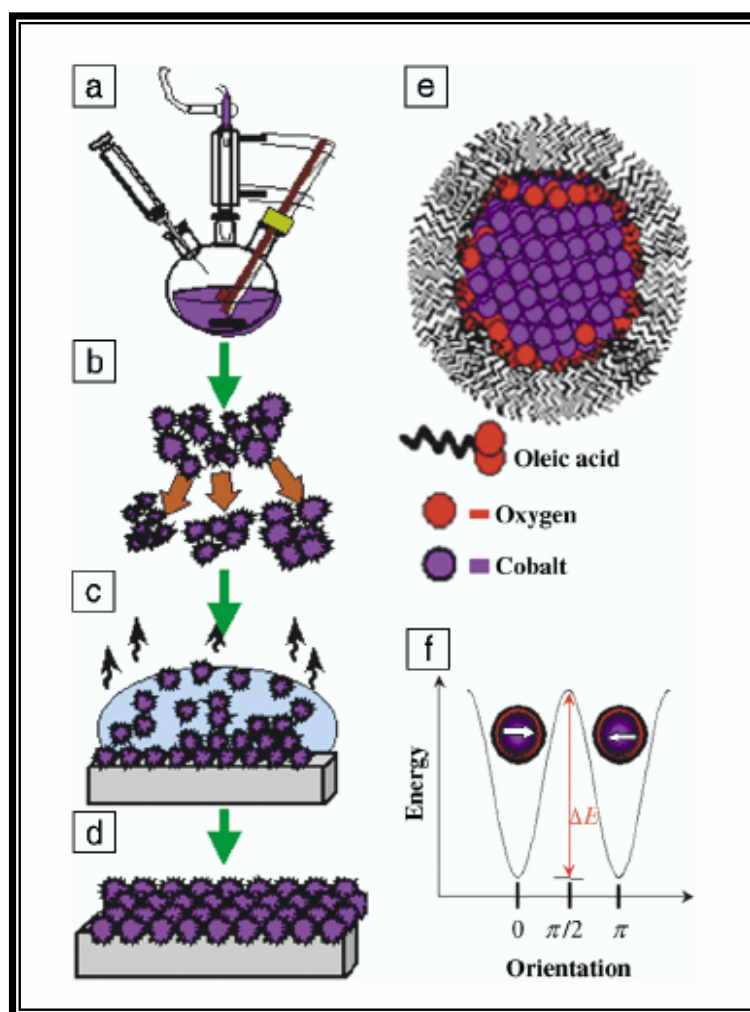


Figure 1.10: Steps involved in formation of assembly of nanoparticles. (a) Nanoparticle synthesis, (b) size selective precipitation (c) self-assembly of nanoparticle dispersion (d) formation of nanoparticle assembly (e) schematic of magnetic nanoparticles coated with ligand along with oxide formation at the surface and (f) graph of the energy dependence of nanoparticle magnetization. This figure has been taken from ref no 198.

Efforts have been taken to assemble anisotropic nanoparticles like rods. Thomas and his group have been successful in achieving chains of gold nanorods using different ligands. Using α,ω -alkanedithiols nanorods were organized in end to end fashion where the alkanedithiols acts as linkers.²³⁷ Similar studies were carried out using other ligands/capping agents like carboxylic acid derivatives, namely, 3-

mercaptopropionic acid (MPA) and 11-mercaptoundecanoic acid (MUA), for assembling Au nanorods.²³⁸

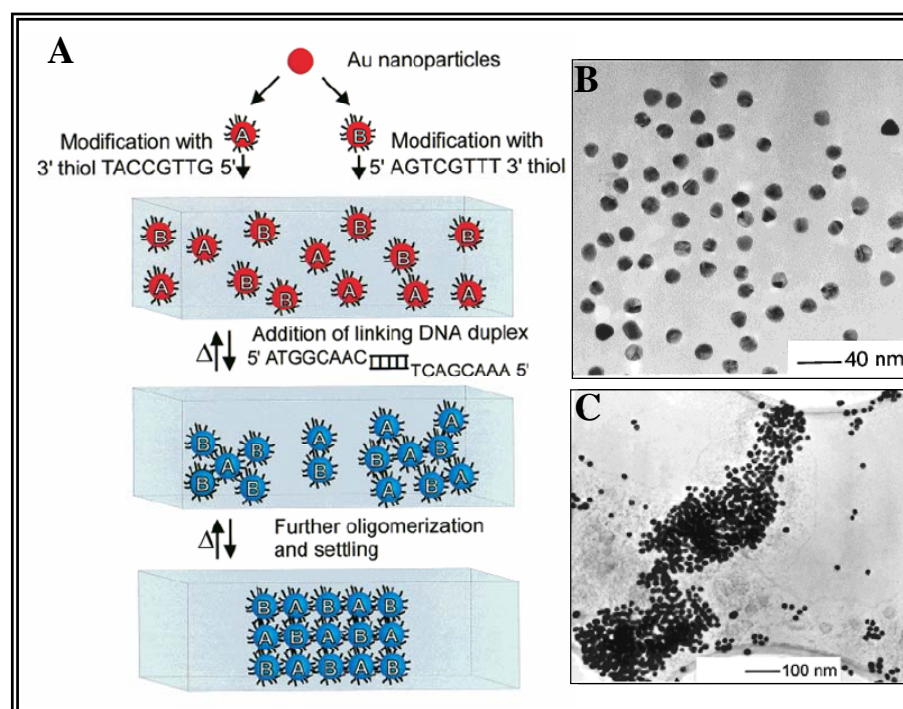


Figure 1.11: (A) Scheme shows DNA-based colloidal nanoparticles assembly method carried out step wise.⁹² (B) Illustrates TEM images of gold nanoparticles as prepared, (C) TEM images of DNA-linked gold nanoparticles show assembly formation.⁹²

Biological entities like DNA have also been employed to achieve assembly of nanoparticles. Mirkin's group⁹¹ have shown DNA based assemblies obtained rationally and reversibly into macroscopic aggregates. This method involves attaching to the surface of two nanoparticles, a non-complimentary DNA-oligonucleotides attached with thiol group, which binds to gold. Addition of oligonucleotides duplex with sticky ends complimentary to two grafted sequences, leads to the formation of nanoparticle assembly.

Thus from above discussion, we observe that ligands/surfactants play a vital role in synthesis, shape control and assemblies of nanoparticles. They are also a key component in the preparation of organo nanoparticles, functional hybrids which find numerous applications like drug delivery and catalysis.

1.3 Objective of this thesis:

We have realized importance of metal and magnetic nanoparticles with their application point of view in different fields. Survey of various methods of synthesis has been described in earlier sections. Apart from this, we have also taken into account the role played by ligand in synthesis of nanoparticles as stabilizing agent, shape directing moiety and also as reducing entity.

In this thesis we concentrate on the effect of surfactant on shape and size of nanoparticles. We have also studied its effect on the crystal structure obtained. Subsequently effect on the properties has also been taken into consideration. We have also demonstrated the dual characteristics of ligand that as reducing agent and as capping moiety.

1.4 Outline of the thesis:

Brief background of the work carried out in the thesis has been described in above section.

Chapter 2 illuminates effects of two ligands, sophorolipid and a new carboxylic acid on the synthesis of cobalt nanoparticles. Synthesis protocol applied is simple reduction of metal salt with sodium borohydride. Different ligands lead to formation of different crystal structures of cobalt nanoparticles. Detailed magnetic measurements like FC-ZFC measurements, field dependent magnetization measurements and ferromagnetic resonance are found to vary depending on the crystal structure. Interaction of these ligands with nanoparticle surface is also studied.

Chapter 3 deals with exploring the dual nature of biosurfactant sophorolipid as reducing and capping moiety. Three different types of sophorolipids namely SA derived sophorolipid, OA derived sophorolipid and LA derived sophorolipid are considered. Synthesis of silver nanoparticles is carried out by two methods namely batch process and continuous flow method. Temperature dependent study is carried out for synthesis of silver nanoparticles using these three ligands as reducing/capping agent. The nanoparticles formed are characterized with UV-visible, FTIR, dynamic light scattering (DLS) and transmission electron

microscopy. Time dependent study is also carried out to optimize the reaction time for synthesis of Ag nanoparticles. Using the optimized reaction conditions the synthesis is carried out in continuous flow method using microreactors. Stainless steel tube was used as microreactor for this synthesis.

In **Chapter 4** we have made use of commonly used ligands cetyltrimethyl ammonium bromide (CTAB) and cetyltrimethyl ammonium chloride (CTAC). Au nanoparticles are synthesized using these ligands. Tryptophan is used as reducing agent for Au nanoparticles. Formation of triangular nanoparticles in case of CTAB and spherical nanoparticles in case of CTAC are seen. Both the species of nanoparticles were characterized by UV-visible, TEM, and XRD. Another interesting feature observed is the emission from triangular nanoparticles while it was absent in case of spherical nanoparticles. To support the observed result, detailed fluorescence and lifetime measurements are carried out.

Chapter 5 summarizes the work carried out in this thesis by highlighting the prominent feature of the work. Here, we also give the possible future work that can be carried out using this work as the basis.

1.5 Reference:

- (1) Eric, D. K.; *Engines of Creation: The Coming Era of Nanotechnology* Anchor Books: 1986.
- (2) Freestone, I.; Meeks, N.; Sax, M.; Higgitt, C. *Gold Bulletin* **2007**, *40*, 270.
- (3) Verhoeven, J. D.; Pendray, A. H.; Dauksch, W. E. *JOM Journal of the Minerals, Metals and Materials Society* **1998**, *50*, 58.
- (4) Thompson, D. *Gold Bulletin* **2007**, *40*, 267.
- (5) Cao, G. *Nanostructures & nanomaterials: synthesis, properties & applications*; Imperial College Pr, 2004.
- (6) Alivisatos, A. P. *Endeavour* **1997**, *21*, 56.
- (7) Schmid, G. *Nanoparticles: from theory to application*; Wiley-VCH Weinheim, 2004.
- (8) Haruta, M. *Catalysis Today* **1997**, *36*, 153.
- (9) Narayanan, R.; El-Sayed, M. A. *Nano Letters* **2004**, *4*, 1343.
- (10) Narayanan, R.; El-Sayed, M. A. *Journal of Physical Chemistry B* **2004**, *108*, 5726.
- (11) Narayanan, R.; El-Sayed, M. A. *Journal of the American Chemical Society* **2004**, *126*, 7194.
- (12) Moiseev, II; Vargaftik, M. N. *Russian Journal of General Chemistry* **2002**, *72*, 512.
- (13) Mayer, A. B. R. *Polymers for Advanced Technologies* **2001**, *12*, 96.
- (14) Siepen, K.; Bonnemann, H.; Brijoux, W.; Rothe, J.; Hormes, J. *Applied Organometallic Chemistry* **2000**, *14*, 549.
- (15) Toshima, N. In *Fine Particles Science and Technology - from Micro to Nanoparticles*; Pelizzetti, E., Ed. **1996**; Vol. 12, p 371.
- (16) Pasricha, R.; Bala, T.; Biradar, A. V.; Umbarkar, S.; Sastry, M. *Small* **2009**, *5*, 1467.
- (17) Han, M.; Gao, X.; Su, J. Z.; Nie, S. *Nature Biotechnology* **2001**, *19*, 631.
- (18) Moreno-Manas, M.; Pleixats, R. *Accounts of Chemical Research* **2003**, *36*, 638.

- (19) Shi, J.; Zhu, Y.; Zhang, X.; Baeyens, W. R. G.; García-Campaña, A. M. *TrAC Trends in Analytical Chemistry* **2004**, *23*, 351.
- (20) Yoon, H.; Chang, M.; Jang, J. *Advanced functional materials* **2007**, *17*, 431.
- (21) Service, R. F. *Science* **2001**, *293*, 782.
- (22) Tseng, G. Y.; Ellenbogen, J. C. *Science* **2001**, *294*, 1293.
- (23) Schon, J. H.; Meng, H.; Bao, Z. *Nature* **2001**, *413*, 713.
- (24) Schon, J. H.; Meng, H.; Bao, Z. N. *Science* **2001**, *294*, 2138.
- (25) Aviram, A.; Ratner, M. A. *Chemical Physics Letters* **1974**, *29*, 277.
- (26) Bachtold, A.; Hadley, P.; Nakanishi, T.; Dekker, C. *Science* **2001**, *294*, 1317.
- (27) Gratzel, M. *Nature* **2001**, *414*, 338.
- (28) Fujishima, A.; Honda, K. *Nature* **1972**, *238*, 37.
- (29) Fujishima, A.; Rao, T. N.; Tryk, D. A. *Journal of Photochemistry and Photobiology C: Photochemistry Reviews* **2000**, *1*, 1.
- (30) Tryk, D. A.; Fujishima, A.; Honda, K. *Electrochimica Acta* **2000**, *45*, 2363.
- (31) Dunnill, P.; Lilly, M. D. *Biotechnology and Bioengineering* **1974**, *16*, 987.
- (32) Zhengxiang, Z.; Zhiyong, W.; Yiping, L.; Huwei, L. *Journal of Separation Science* **2006**, *29*, 1872.
- (33) Xu, C. J.; Xu, K. M.; Gu, H. W.; Zheng, R. K.; Liu, H.; Zhang, X. X.; Guo, Z. H.; Xu, B. *Journal of the American Chemical Society* **2004**, *126*, 9938.
- (34) Safarik, I.; Safarikova, M. *Journal of Chromatography B* **1999**, *722*, 33.
- (35) Gu, H. W.; Xu, K. M.; Xu, C. J.; Xu, B. *Chemical Communications* **2006**, 941.
- (36) Zhao, X. J.; Tapeç-Dytioco, R.; Wang, K. M.; Tan, W. H. *Analytical Chemistry* **2003**, *75*, 3476.
- (37) Haynes, C. L.; Van Duyne, R. P. *J. Phys. Chem. B* **2001**, *105*, 5599.
- (38) Barnes, W. L.; Dereux, A.; Ebbesen, T. W. *Nature* **2003**, *424*, 824.

- (39) Haynes, C. L.; Van Duyne, R. P. *Journal of Physical Chemistry B* **2001**, *105*, 5599.
- (40) Kamat, P. V. *The Journal of Physical Chemistry B* **2002**, *106*, 7729.
- (41) Mansour, K.; Soileau, M. J.; Vanstryland, E. W. *Journal of the Optical Society of America B-Optical Physics* **1992**, *9*, 1100.
- (42) Lidorikis, E.; Li, Q. M.; Soukoulis, C. M. *Physical Review E* **1997**, *55*, 3613.
- (43) Schubert, E. F.; Hunt, N. E. J.; Micovic, M.; Malik, R. J.; Sivco, D. L.; Cho, A. Y.; Zydzik, G. J. *Science* **1994**, *265*, 943.
- (44) Wanke, M. C.; Lehmann, O.; Muller, K.; Wen, Q. Z.; Stuke, M. *Science* **1997**, *275*, 1284.
- (45) Chou, S. Y.; Krauss, P. R.; Zhang, W.; Guo, L. J.; Zhuang, L. *Journal of Vacuum Science & Technology B* **1997**, *15*, 2897.
- (46) Emmelius, M.; Pawlowski, G.; Vollmann, H. W. *Angewandte Chemie-International Edition in English* **1989**, *28*, 1445.
- (47) Ethirajan, A.; Wiedwald, U.; Boyen, H. G.; Kern, B.; Han, L.; Klimmer, A.; Weigl, F.; Kästle, G.; Ziemann, P.; Fauth, K. *Advanced Materials* **2007**, *19*, 406.
- (48) Zou, S. Z.; Williams, C. T.; Chen, E. K. Y.; Weaver, M. J. *Journal of the American Chemical Society* **1998**, *120*, 3811.
- (49) Emory, S. R.; Nie, S. *Journal of Physical Chemistry B* **1998**, *102*, 493.
- (50) Krug, J. T.; Wang, G. D.; Emory, S. R.; Nie, S. M. *Journal of the American Chemical Society* **1999**, *121*, 9208.
- (51) Pipino, A. C. R.; VanDuyne, R. P.; Schatz, G. C. *Physical Review B* **1996**, *53*, 4162.
- (52) Yang, W. H.; Hulteen, J.; Schatz, G. C.; VanDuyne, R. P. *Journal of Chemical Physics* **1996**, *104*, 4313.
- (53) Freeman, R. G.; Grabar, K. C.; Allison, K. J.; Bright, R. M.; Davis, J. A.; Guthrie, A. P.; Hommer, M. B.; Jackson, M. A.; Smith, P. C.; Walter, D. G.; Natan, M. J. *Science* **1995**, *267*, 1629.
-
-

- (54) Liu, Y. Y.; Hu, J. Q.; Kong, Q. C.; Feng, X. M. *Materials Letters*, **64**, 422.
- (55) Neuberger, T.; Schöpf, B.; Hofmann, H.; Hofmann, M.; Von Rechenberg, B. *Journal of magnetism and Magnetic Materials* **2005**, *293*, 483.
- (56) Panyam, J.; Labhassetwar, V. *Advanced drug delivery reviews* **2003**, *55*, 329.
- (57) Goldberg, M.; Langer, R.; Jia, X. *Journal of Biomaterials Science, Polymer Edition* **2007**, *18*, 241.
- (58) Slowing, II; Trewyn, B. G.; Giri, S.; Lin, V. S. Y. *Advanced Functional Materials* **2007**, *17*, 1225.
- (59) Cho, K.; Wang, X.; Nie, S.; Chen, Z. G.; Shin, D. M. *Clinical Cancer Research* **2008**, *14*, 1310.
- (60) Pantarotto, D.; Partidos, C. D.; Hoebeke, J.; Brown, F.; Kramer, E.; Briand, J. P.; Muller, S.; Prato, M.; Bianco, A. *Chemistry & Biology* **2003**, *10*, 961.
- (61) Salata, O. V. *Journal of Nanobiotechnology* **2004**, *2*, 3.
- (62) Dhar, S.; Reddy, E. M.; Shiras, A.; Pokharkar, V.; Prasad, B. L. V. *Chemistry-A European Journal* **2008**, *14*, 10244.
- (63) Edelstein, R. L.; Tamanaha, C. R.; Sheehan, P. E.; Miller, M. M.; Baselt, D. R.; Whitman, L. J.; Colton, R. J. *Biosensors & Bioelectronics* **2000**, *14*, 805.
- (64) Shapiro, E. M.; Skrtic, S.; Sharer, K.; Hill, J. M.; Dunbar, C. E.; Koretsky, A. P. *Proceedings of the National Academy of Sciences of the United States of America* **2004**, *101*, 10901.
- (65) Huh, Y. M.; Jun, Y. W.; Song, H. T.; Kim, S.; Choi, J. S.; Lee, J. H.; Yoon, S.; Kim, K. S.; Shin, J. S.; Suh, J. S.; Cheon, J. *Journal of the American Chemical Society* **2005**, *127*, 12387.
- (66) Cunningham, C. H.; Arai, T.; Yang, P. C.; McConnell, M. V.; Pauly, J. M.; Conolly, S. M. *Magnetic Resonance in Medicine* **2005**, *53*, 999.
-
-

-
-
- (67) Weissleder, R.; Elizondo, G.; Wittenberg, J.; Rabito, C. A.; Bengel, H. H.; Josephson, L. *Radiology* **1990**, *175*, 489.
- (68) Mornet, S.; Vasseur, S.; Grasset, F.; Duguet, E. *Journal of Materials Chemistry* **2004**, *14*, 2161.
- (69) Shinkai, M.; Yanase, M.; Suzuki, M.; Honda, H.; Wakabayashi, T.; Yoshida, J.; Kobayashi, T. *Journal of Magnetism and Magnetic Materials* **1999**, *194*, 176.
- (70) Jordan, A.; Scholz, R.; Wust, P.; Fahling, H.; Felix, R. *Journal of Magnetism and Magnetic Materials* **1999**, *201*, 413.
- (71) Jordan, A.; Scholz, R.; Wust, P.; Fahling, H.; Krause, J.; Wlodarczyk, W.; Sander, B.; Vogl, T.; Felix, R. *International Journal of Hyperthermia* **1997**, *13*, 587.
- (72) Jordan, A.; Scholz, R.; Wust, P.; Schirra, H.; Schiestel, T.; Schmidt, H.; Felix, R. *Journal of magnetism and Magnetic Materials* **1999**, *194*, 185.
- (73) Jordan, A.; Wust, P.; Scholz, R.; Tesche, B.; Fahling, H.; Mitrovics, T.; Vogl, T.; CervosNavarro, J.; Felix, R. *International Journal of Hyperthermia* **1996**, *12*, 705.
- (74) Hirsch, L. R.; Stafford, R. J.; Bankson, J. A.; Sershen, S. R.; Rivera, B.; Price, R. E.; Hazle, J. D.; Halas, N. J.; West, J. L. *Proceedings of the National Academy of Sciences of the United States of America* **2003**, *100*, 13549.
- (75) Loo, C.; Lowery, A.; Halas, N.; West, J.; Drezek, R. *Nano Letters* **2005**, *5*, 709.
- (76) Bond, G. C. *Catalysis Today* **2002**, *72*, 5.
- (77) <http://www.esrf.eu/news/spotlight/spotlight35catalysts/>.
- (78) Murray, C. B.; Sun, S.; Gaschler, W.; Doyle, H.; Betley, T. A.; Kagan, C. R. *IBM Journal of Research and Development* **2001**, *45*, 47.
- (79) Whitesides, G. M.; Love, J. C. *Scientific American* **2001**, *285*, 38.
- (80) Klabunde, K. J. *Nanoscale materials in chemistry*; Wiley-Interscience New York, 2001.
-
-

- (81) Wolf, E. L. *Nanophysics and nanotechnology: an introduction to modern concepts in nanoscience*; Vch Verlagsgesellschaft Mbh, 2006.
- (82) Okumura, M.; Tsubota, S.; Iwamoto, M.; Haruta, M. *Chemistry Letters* **1998**, 315.
- (83) Murray, C. B.; Norris, D. J.; Bawendi, M. G. *Journal of the American Chemical Society* **1993**, *115*, 8706.
- (84) Peng, Z. A.; Peng, X. G. *Journal of the American Chemical Society* **2001**, *123*, 183.
- (85) Qu, L. H.; Peng, Z. A.; Peng, X. G. *Nano Letters* **2001**, *1*, 333.
- (86) Burda, C.; Chen, X. B.; Narayanan, R.; El-Sayed, M. A. *Chemical Reviews* **2005**, *105*, 1025.
- (87) Bharde, A.; Wani, A.; Shouche, Y.; Joy, P. A.; Prasad, B. L. V.; Sastry, M. *Journal of the American Chemical Society* **2005**, *127*, 9326.
- (88) Bharde, A. A.; Parikh, R. Y.; Baidakova, M.; Jouen, S.; Hannover, B.; Enoki, T.; Prasad, B. L. V.; Shouche, Y. S.; Ogale, S.; Sastry, M. *Langmuir* **2008**, *24*, 5787.
- (89) Mandal, D.; Bolander, M. E.; Mukhopadhyay, D.; Sarkar, G.; Mukherjee, P. *Applied Microbiology and Biotechnology* **2006**, *69*, 485.
- (90) Kowshik, M.; Ashtaputre, S.; Kharrazi, S.; Vogel, W.; Urban, J.; Kulkarni, S. K.; Paknikar, K. M. *Nanotechnology* **2003**, *14*, 95.
- (91) Mirkin, C. A.; Letsinger, R. L.; Mucic, R. C.; Storhoff, J. J. *Nature* **1996**, *382*, 607.
- (92) Mirkin, C. A. *Inorganic Chemistry* **2000**, *39*, 2258.
- (93) Lin, S. T.; Franklin, M. T.; Klabunde, K. J. *Langmuir* **1986**, *2*, 259.
- (94) Klabunde, K. J. *Accounts of Chemical Research* **1975**, *8*, 393.
- (95) Huang, Y. X.; Guo, C. J. *Powder Technology* **1992**, *72*, 101.
- (96) Gardea-Torresdey, J. L.; Parsons, J. G.; Gomez, E.; Peralta-Videa, J.; Troiani, H. E.; Santiago, P.; Yacaman, M. J. *Nano Letters* **2002**, *2*, 397.
-
-

- (97) Shankar, S. S.; Rai, A.; Ankamwar, B.; Singh, A.; Ahmad, A.; Sastry, M. *Nature Materials* **2004**, *3*, 482.
- (98) Armendariz, V.; Herrera, I.; Peralta-Videa, J. R.; Jose-Yacaman, M.; Troiani, H.; Santiago, P.; Gardea-Torresdey, J. L. *Journal of Nanoparticle Research* **2004**, *6*, 377.
- (99) Nam, K. T.; Kim, D. W.; Yoo, P. J.; Chiang, C. Y.; Meethong, N.; Hammond, P. T.; Chiang, Y. M.; Belcher, A. M. *Science* **2006**, *312*, 885.
- (100) Royston, E.; Ghosh, A.; Kofinas, P.; Harris, M. T.; Culver, J. N. *Langmuir* **2008**, *24*, 906.
- (101) Slocik, J. M.; Naik, R. R.; Stone, M. O.; Wright, D. W. *Journal of Materials Chemistry* **2005**, *15*, 749.
- (102) Becker, M. F.; Brock, J. R.; Cai, H.; Henneke, D. E.; Keto, J. W.; Lee, J. Y.; Nichols, W. T.; Glicksman, H. D. *Nanostructured Materials* **1998**, *10*, 853.
- (103) Mafune, F.; Kohno, J. Y.; Takeda, Y.; Kondow, T. *Journal of Physical Chemistry B* **2003**, *107*, 4218.
- (104) Mafune, F.; Kohno, J.; Takeda, Y.; Kondow, T.; Sawabe, H. *Journal of Physical Chemistry B* **2000**, *104*, 9111.
- (105) Yang, J.; Mei, S.; Ferreira, J. M. F. *Materials Science and Engineering: C* **2001**, *15*, 183.
- (106) Selvakannan, P.; Mandal, S.; Phadtare, S.; Gole, A.; Pasricha, R.; Adyanthaya, S. D.; Sastry, M. *Journal of Colloid and Interface Science* **2004**, *269*, 97.
- (107) Niemeyer, C. M. *Angewandte Chemie-International Edition* **2001**, *40*, 4128.
- (108) Caruso, F. *Colloids and colloid assemblies*; Wiley-VCH Weinheim, 2004.
- (109) Salkar, R. A.; Jeevanandam, P.; Aruna, S. T.; Kolytyn, Y.; Gedanken, A. *Journal of Materials Chemistry* **1999**, *9*, 1333.
- (110) Tanori, J.; Pileni, M. P. *Langmuir* **1997**, *13*, 639.
-
-

- (111) Turkevich, J.; Stevenson, P. C.; Hillier, J. *Discussions of the Faraday Society* **1951**, 55.
- (112) Mann, S. *Angewandte Chemie-International Edition* **2000**, 39, 3393.
- (113) Kroger, N.; Deutzmann, R.; Sumper, M. *Science* **1999**, 286, 1129.
- (114) Yonezawa, Y.; Sato, T.; Ohno, M.; Hada, H. *Journal of the Chemical Society-Faraday Transactions I* **1987**, 83, 1559.
- (115) Gachard, E.; Remita, H.; Khatouri, J.; Keita, B.; Nadjo, L.; Belloni, J. *New Journal of Chemistry* **1998**, 22, 1257.
- (116) Sun, Y. G.; Xia, Y. A. *Nano Letters* **2003**, 3, 1569.
- (117) Sun, Y. G.; Xia, Y. N. *Journal of the American Chemical Society* **2004**, 126, 3892.
- (118) De Jong, W. H.; Borm, P. J. A. *International Journal of Nanomedicine* **2008**, 3, 133.
- (119) Li, B.; Du, Y.; Dong, S. *Analytica Chimica Acta* **2009**, 644, 78.
- (120) Bonnemann, H.; Richards, R. M. *European Journal of Inorganic Chemistry* **2001**, 2455.
- (121) Brust, M.; Fink, J.; Bethell, D.; Schiffrin, D. J.; Kiely, C. *Journal of the Chemical Society-Chemical Communications* **1995**, 1655.
- (122) Leff, D. V.; Ohara, P. C.; Heath, J. R.; Gelbart, W. M. *Journal of Physical Chemistry* **1995**, 99, 7036.
- (123) Weisbecker, C. S.; Merritt, M. V.; Whitesides, G. M. *Langmuir* **1996**, 12, 3763.
- (124) Smetana, A. B.; Klabunde, K. J.; Sorensen, C. M. *Journal of Colloid and Interface Science* **2005**, 284, 521.
- (125) Linnert, T.; Mulvaney, P.; Henglein, A. *Journal of Physical Chemistry* **1993**, 97, 679.
- (126) Doty, R. C.; Tshikhudo, T. R.; Brust, M.; Fernig, D. G. *Chemistry of Materials* **2005**, 17, 4630.
- (127) Sarathy, K. V.; Raina, G.; Yadav, R. T.; Kulkarni, G. U.; Rao, C. N. R. *Journal of Physical Chemistry B* **1997**, 101, 9876.
- (128) Cook, S. C.; Padmos, J. D.; Zhang, P. *Journal of Chemical Physics* **2008**, 128, 154705.
-
-

-
-
- (129) Rogach, A. L.; Kornowski, A.; Gao, M.; Eychmuller, A.; Weller, H. *J. Phys. Chem. B* **1999**, *103*, 3065.
- (130) Abd El-Sadek, M. S.; Ram Kumar, J.; Moorthy Babu, S. *International Journal of Nanoparticles* **2009**, *2*, 20.
- (131) Green, M.; O'Brien, P. *Chemical Communications* **2000**, 183.
- (132) Kumar, A.; Mandal, S.; Selvakannan, P. R.; Pasricha, R.; Mandale, A. B.; Sastry, M. *Langmuir* **2003**, *19*, 6277.
- (133) Datar, S.; Chaudhari, M.; Sastry, M.; Dharmadhikari, C. V. *Applied Surface Science* **2007**, *253*, 5109.
- (134) Kumar, A.; Joshi, H.; Pasricha, R.; Mandale, A. B.; Sastry, M. *Journal of Colloid and Interface Science* **2003**, *264*, 396.
- (135) Kumar, A.; Joshi, H. M.; Mandale, A. B.; Srivastava, R.; Adyanthaya, S. D.; Pasricha, R.; Sastry, M. *Journal of Chemical Sciences* **2004**, *116*, 293.
- (136) Ramirez, E.; Jansat, S.; Philippot, K.; Lecante, P.; Gomez, M.; Masdeu-Bulto, A. M.; Chaudret, B. *Journal of Organometallic Chemistry* **2004**, *689*, 4601.
- (137) Wang, W.; Efrima, S.; Regev, O. *Langmuir* **1998**, *14*, 602.
- (138) Wang, W.; Chen, X.; Efrima, S. *Journal of Physical Chemistry B* **1999**, *103*, 7238.
- (139) Bala, T.; Swami, A.; Prasad, B. L. V.; Sastry, M. *Journal of Colloid and Interface Science* **2005**, *283*, 422.
- (140) Wu, N.; Fu, L.; Su, M.; Aslam, M.; Wong, K. C.; Dravid, V. P. *Nano Letters* **2004**, *4*, 383.
- (141) Sidhaye, D. S.; Bala, T.; Srinath, S.; Srikanth, H.; Poddar, P.; Sastry, M.; Prasad, B. L. V. *Journal of Physical Chemistry C* **2009**, *113*, 3426.
- (142) Schmid, G.; Pfeil, R.; Boese, R.; Bandermann, F.; Meyer, S.; Calis, G. H. M.; Vandervelden, W. A. *Chemische Berichte-Recueil* **1981**, *114*, 3634.
- (143) Schmid, G.; Klein, N.; Korste, L.; Kreibig, U.; Schonauer, D. *Polyhedron* **1988**, *7*, 605.
-
-

- (144) Murray, C. B.; Sun, S. H.; Doyle, H.; Betley, T. *Mrs Bulletin* **2001**, 26, 985.
- (145) Hyeon, T. *Chemical Communications* **2003**, 9, 927.
- (146) Owens, T. M.; Nicholson, K. T.; Holl, M. M. B.; Suzer, S. *Journal of the American Chemical Society* **2002**, 124, 6800.
- (147) Owens, T. M.; Nicholson, K. T.; Fosnacht, D. R.; Orr, B. G.; Holl, M. M. B. *Langmuir* **2006**, 22, 9619.
- (148) Fadeev, A. Y.; McCarthy, T. J. *Journal of the American Chemical Society* **1999**, 121, 12184.
- (149) Neouze, M. A.; Schubert, U. *Monatshefte Fur Chemie* **2008**, 139, 183.
- (150) Andreoni, W.; Curioni, A.; Gronbeck, H. *International Journal of Quantum Chemistry* **2000**, 80, 598.
- (151) Gronbeck, H.; Curioni, A.; Andreoni, W. *Journal of the American Chemical Society* **2000**, 122, 3839.
- (152) Hasan, M.; Bethell, D.; Brust, M. *Journal of the American Chemical Society* **2002**, 124, 1132.
- (153) Sastry, M.; Kumar, A.; Mukherjee, P. *Colloids and Surfaces a-Physicochemical and Engineering Aspects* **2001**, 181, 255.
- (154) Kumar, A.; Mandale, A. B.; Sastry, M. *Langmuir* **2000**, 16, 9299.
- (155) Leff, D. V.; Brandt, L.; Heath, J. R. *Langmuir* **1996**, 12, 4723.
- (156) Sun, S.; Murray, C. B. *Journal of Applied Physics* **1999**, 85, 4325.
- (157) Puentes, V. F.; Krishnan, K. M.; Alivisatos, A. P. *Science* **2001**, 291, 2115.
- (158) Puentes, V. F.; Krishnan, K.; Alivisatos, A. P. *Topics in Catalysis* **2002**, 19, 145.
- (159) Dubois, L. H.; Zegarski, B. R.; Nuzzo, R. G. *Langmuir* **1986**, 2, 412.
- (160) Wuhn, A.; Weckesser, J.; Woll, C. *Langmuir* **2001**, 17, 7605.
- (161) Wiegand, B. C.; Lohokare, S. P.; Nuzzo, R. G. *Journal of Physical Chemistry* **1993**, 97, 11553.
- (162) Nuzzo, R. G.; Dubois, L. H.; Allara, D. L. *Journal of the American Chemical Society* **1990**, 112, 558.
-
-

- (163) Hostetler, M. J.; Nuzzo, R. G.; Girolami, G. S. *Journal of the American Chemical Society* **1994**, *116*, 11608.
- (164) Xia, Y. N.; Halas, N. J. *Mrs Bulletin* **2005**, *30*, 338.
- (165) Viswanath, B.; Kundu, P.; Mukherjee, B.; Ravishankar, N. *Nanotechnology* **2008**, *19*, 195603.
- (166) Reetz, M. T.; Helbig, W. *Journal of the American Chemical Society* **1994**, *116*, 7401.
- (167) Hostetler, M. J.; Wingate, J. E.; Zhong, C. J.; Harris, J. E.; Vachet, R. W.; Clark, M. R.; Londono, J. D.; Green, S. J.; Stokes, J. J.; Wignall, G. D.; Glish, G. L.; Porter, M. D.; Evans, N. D.; Murray, R. W. *Langmuir* **1998**, *14*, 17.
- (168) Jana, N. R.; Chen, Y. F.; Peng, X. G. *Chemistry of Materials* **2004**, *16*, 3931.
- (169) Pileni, M. P. *Nature Materials* **2003**, *2*, 145.
- (170) Samia, A. C. S.; Hyzer, K.; Schlueter, J. A.; Qin, C. J.; Jiang, J. S.; Bader, S. D.; Lin, X. M. *J. Am. Chem. Soc* **2005**, *127*, 4126.
- (171) Samia, A. C. S.; Schlueter, J. A.; Jiang, J. S.; Bader, S. D.; Qin, C. J.; Lin, X. M. *Chem. Mater* **2006**, *18*, 5203.
- (172) De Silva, R. M.; Palshin, V.; Fronczek, F. R.; Hormes, J.; Kumar, C. S. S. R. *Journal of Physical Chemistry C* **2007**, *111*, 10320.
- (173) De Silva, R. M.; Palshin, V.; de Silva, K. M. N.; Henry, L. L.; Kumar, C. J. *Mater. Chem* **2008**, *18*, 738.
- (174) Jana, N. R.; Gearheart, L.; Murphy, C. J. *Journal of Physical Chemistry B* **2001**, *105*, 4065.
- (175) Jana, N. R.; Gearheart, L.; Murphy, C. J. *Chemical Communications* **2001**, 617.
- (176) Murphy, C. J.; Jana, N. R. *Advanced Materials* **2002**, *14*, 80.
- (177) Murphy, C. J.; San, T. K.; Gole, A. M.; Orendorff, C. J.; Gao, J. X.; Gou, L.; Hunyadi, S. E.; Li, T. *Journal of Physical Chemistry B* **2005**, *109*, 13857.
- (178) Sau, T. K.; Rogach, A. L. *Advanced Materials*, *22*, 1781.

- (179) Sau, T. K.; Murphy, C. J. *Journal of the American Chemical Society* **2004**, *126*, 8648.
- (180) Niu, W. X.; Li, Z. Y.; Shi, L. H.; Liu, X. Q.; Li, H. J.; Han, S.; Chen, J.; Xu, G. B. *Crystal Growth & Design* **2008**, *8*, 4440.
- (181) Seo, D.; Yoo, C. I.; Park, J. C.; Park, S. M.; Ryu, S.; Song, H. *Angewandte Chemie-International Edition* **2008**, *47*, 763.
- (182) Liu, X.; Huang, R.; Zhu, J. *Chemistry of Materials* **2007**, *20*, 192.
- (183) Yener, D. O.; Sindel, J.; Randall, C. A.; Adair, J. H. *Langmuir* **2002**, *18*, 8692.
- (184) Huang, L. M.; Wang, H. T.; Wang, Z. B.; Mitra, A.; Bozhilov, K. N.; Yan, Y. S. *Advanced Materials* **2002**, *14*, 61.
- (185) Wang, L. Y.; Chen, X.; Zhan, J.; Chai, Y. C.; Yang, C. J.; Xu, L. M.; Zhuang, W. C.; Jing, B. *Journal of Physical Chemistry B* **2005**, *109*, 3189.
- (186) Wirtz, M.; Martin, C. R. *Advanced Materials* **2003**, *15*, 455.
- (187) Preston, C. K.; Moskovits, M. *Journal of Physical Chemistry* **1988**, *92*, 2957.
- (188) Payne, E. K.; Shuford, K. L.; Park, S.; Schatz, G. C.; Mirkin, C. A. *Journal of Physical Chemistry B* **2006**, *110*, 2150.
- (189) Yang, S. C.; Zhang, R. L.; Wang, Q. F.; Ding, B. J.; Wang, Y. P. *Colloids and Surfaces A-Physicochemical and Engineering Aspects* **2007**, *311*, 174.
- (190) Yang, S. C.; Wang, Y. P.; Wang, Q. F.; Zhang, R. L.; Ding, B. J. *Colloids and Surfaces A-Physicochemical and Engineering Aspects* **2007**, *301*, 174.
- (191) Murphy, C. J.; Sau, T. K.; Gole, A. M.; Orendorff, C. J.; Gao, J.; Gou, L.; Hunyadi, S. E.; Li, T. *J. Phys. Chem. B* **2005**, *109*, 13857.
- (192) Kuo, C. H.; Huang, M. H. *Langmuir* **2005**, *21*, 2012.
- (193) Hu, J. Q.; Zhang, Y.; Liu, B.; Liu, J. X.; Zhou, H. H.; Xu, Y. F.; Jiang, Y. X.; Yang, Z. L.; Tian, Z. Q. *Journal of the American Chemical Society* **2004**, *126*, 9470.
-
-

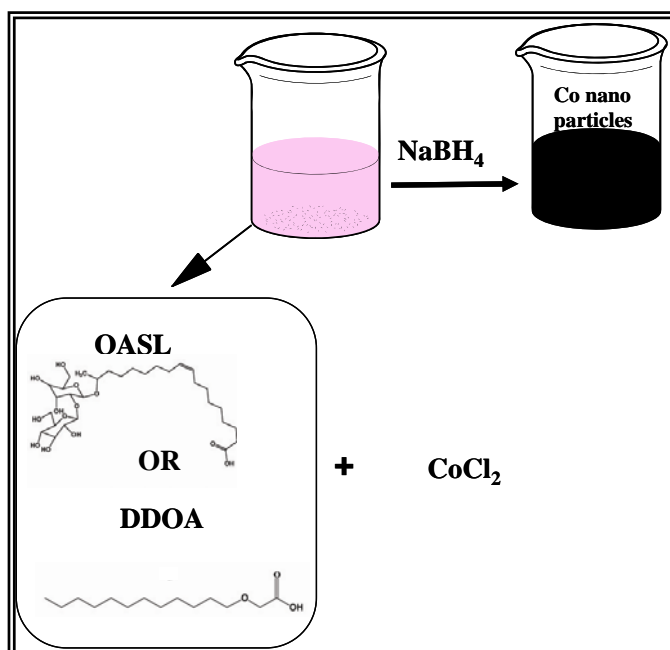
-
-
- (194) Skrabalak, S. E.; Au, L.; Li, X. D.; Xia, Y. *Nature Protocols* **2007**, *2*, 2182.
- (195) Millstone, J. E.; Wei, W.; Jones, M. R.; Yoo, H. J.; Mirkin, C. A. *Nano Letters* **2008**, *8*, 2526.
- (196) Diehl, M. R.; Yu, J. Y.; Heath, J. R.; Held, G. A.; Doyle, H.; Sun, S.; Murray, C. B. *J. Phys. Chem. B* **2001**, *105*, 7913.
- (197) Jeon, Y. T.; Moon, J. Y.; Lee, G. H.; Park, J.; Chang, Y. *Journal of Physical Chemistry B* **2006**, *110*, 1187.
- (198) Han, M.; Liu, Q.; He, J. H.; Song, Y.; Xu, Z.; Zhu, J. M. *Advanced Materials* **2007**, *19*, 1096.
- (199) Yu, W. W.; Wang, Y. A.; Peng, X. *Chem. Mater* **2003**, *15*, 4300.
- (200) Gilbert, B.; Zhang, H.; Huang, F.; Finnegan, M. P.; Waychunas, G. A.; Banfield, J. F. *Geochemical Transactions* **2003**, *4*, 20.
- (201) Fendler, J. H. *Chem. Mater* **2001**, *13*, 3196.
- (202) Nuzzo, R. G.; Allara, D. L. *Journal of the American Chemical Society* **1983**, *105*, 4481.
- (203) Bain, C. D.; Troughton, E. B.; Tao, Y. T.; Evall, J.; Whitesides, G. M.; Nuzzo, R. G. *Journal of the American Chemical Society* **1989**, *111*, 321.
- (204) Boal, A. K.; Ilhan, F.; DeRouchey, J. E.; Thurn-Albrecht, T.; Russell, T. P.; Rotello, V. M. *Nature* **2000**, *404*, 746.
- (205) Li, Z.; Chung, S. W.; Nam, J. M.; Ginger, D. S.; Mirkin, C. A. *Angewandte Chemie-International Edition* **2003**, *42*, 2306.
- (206) Lazzari, M.; Rodriguez-Abreu, C.; Rivas, J.; Lopez-Quintela, M. A. *Journal of Nanoscience and Nanotechnology* **2006**, *6*, 892.
- (207) Sotiropoulou, S.; Sierra-Sastre, Y.; Mark, S. S.; Batt, C. A. *Chemistry of Materials* **2008**, *20*, 821.
- (208) Xia, Y. N.; Rogers, J. A.; Paul, K. E.; Whitesides, G. M. *Chemical Reviews* **1999**, *99*, 1823.
- (209) Xia, Y. N.; Whitesides, G. M. *Annual Review of Materials Science* **1998**, *28*, 153.
- (210) Mirkin, C. A. *Acs Nano* **2007**, *1*, 79.
-
-

- (211) Lim, J. H.; Ginger, D. S.; Lee, K. B.; Heo, J.; Nam, J. M.; Mirkin, C. *A. Angewandte Chemie-International Edition* **2003**, *42*, 2309.
- (212) Schmid, G.; Chi, L. F. *Advanced Materials* **1998**, *10*, 515.
- (213) Burghard, M.; Philipp, G.; Roth, S.; von Klitzing, K.; Pugin, R.; Schmid, G. *Advanced Materials* **1998**, *10*, 842.
- (214) Hu, M.; Yamaguchi, Y.; Okubo, T. *Journal of Nanoparticle Research* **2005**, *7*, 187.
- (215) Rao, C. N. R.; Kulkarni, G. U.; Thomas, P. J.; Edwards, P. P. *Chemical Society Reviews* **2000**, *29*, 27.
- (216) Brust, M.; Bethell, D.; Schiffrin, D. J.; Kiely, C. J. *Advanced Materials* **1995**, *7*, 795.
- (217) Hu, T.; Gao, Y.; Wang, Z. L.; Tang, Z. Y. *Frontiers of Physics in China* **2009**, *4*, 487.
- (218) Min, Y. J.; Akbulut, M.; Kristiansen, K.; Golan, Y.; Israelachvili, J. *Nature Materials* **2008**, *7*, 527.
- (219) Bishop, K. J. M.; Wilmer, C. E.; Soh, S.; Grzybowski, B. A. *Small* **2009**, *5*, 1600.
- (220) Prasad, B. L. V.; Sorensen, C. M.; Klabunde, K. J. *Chemical Society Reviews* **2008**, *37*, 1871.
- (221) Korgel, B. A.; Fullam, S.; Connolly, S.; Fitzmaurice, D. *Journal of Physical Chemistry B* **1998**, *102*, 8379.
- (222) Whetten, R. L.; Khoury, J. T.; Alvarez, M. M.; Murthy, S.; Vezmar, I.; Wang, Z. L.; Stephens, P. W.; Cleveland, C. L.; Luedtke, W. D.; Landman, U. *Advanced Materials* **1996**, *8*, 428.
- (223) Weitz, D. A.; Oliveria, M. *Physical Review Letters* **1984**, *52*, 1433.
- (224) Stoeva, S. I.; Prasad, B. L. V.; Uma, S.; Stoimenov, P. K.; Zaikovski, V.; Sorensen, C. M.; Klabunde, K. J. *Journal of Physical Chemistry B* **2003**, *107*, 7441.
- (225) Brust, M.; Bethell, D.; Schiffrin, D. J.; Kiely, C. J. *Advanced Materials* **1995**, *7*, 795.

- (226) Brust, M.; Walker, M.; Bethell, D.; Schiffrin, D. J.; Whyman, R. *Journal of the Chemical Society-Chemical Communications* **1994**, 801.
- (227) Sarathy, K. V.; Kulkarni, G. U.; Rao, C. N. R. *Chemical Communications* **1997**, 1997, 537.
- (228) Prasad, B. L. V.; Stoeva, S. I.; Sorensen, C. M.; Klabunde, K. J. *Chemistry of Materials* **2003**, *15*, 935.
- (229) Martin, J. E.; Wilcoxon, J. P.; Odinek, J.; Provencio, P. *Journal of Physical Chemistry B* **2000**, *104*, 9475.
- (230) Prasad, B. L. V.; Stoeva, S. I.; Sorensen, C. M.; Klabunde, K. J. *Langmuir* **2002**, *18*, 7515.
- (231) Sidhaye, D. S.; Kashyap, S.; Sastry, M.; Hotha, S.; Prasad, B. L. V. *Langmuir* **2005**, *21*, 7979.
- (232) Wang, S. H.; Sato, S.; Kimura, K. *Chemistry of Materials* **2003**, *15*, 2445.
- (233) Shenhar, R.; Rotello, V. M. *Accounts of Chemical Research* **2003**, *36*, 549.
- (234) Martin, J. I.; Nogues, J.; Liu, K.; Vicent, J. L.; Schuller, I. K. *Journal of magnetism and Magnetic Materials* **2003**, *256*, 449.
- (235) Murray, C. B.; Kagan, C. R.; Bawendi, M. G. *Annual Review of Materials Science* **2000**, *30*, 545.
- (236) Peng, S.; Wang, C.; Xie, J.; Sun, S. *J. Am. Chem. Soc* **2006**, *128*, 10676.
- (237) Joseph, S. T. S.; Ipe, B. I.; Pramod, P.; Thomas, K. G. *Journal of Physical Chemistry B* **2006**, *110*, 150.
- (238) Thomas, K. G.; Barazzouk, S.; Ipe, B. I.; Joseph, S. T. S.; Kamat, P. V. *Journal of Physical Chemistry B* **2004**, *108*, 13066.

Chapter 2

Effect of ligands on crystal structure and properties of cobalt nanoparticles.



This chapter discusses the role played by the ligands in the synthesis of cobalt nanoparticles. It is observed that usage of different ligands lead to formation of different crystal phases of cobalt nanoparticles. Variation in magnetic properties from these different crystalline phases was studied in detail. The mode of interaction of ligand with the nanoparticle surface was also investigated.

Part of this work has been published in:

- 1) Manasi Kasture, Sanjay Singh, Pitamber Patel, P.A.Joy, A.A.Prabhune, C.V.Ramana and B.L.V.Prasad, *Langmuir*, **2007**, 23, 11409-11412.
- 2) A Sendilkumar, Manasi Kasture, Pitamber Patel, C.V.Ramana, B.L.V.Prasad and S Srinath, *Journal of Physics: Conference Series*, **2010**, 200, 075088.

2.1 Introduction:

Magnetic nanoparticles have become an important class of the nanomaterial family due to their applications in numerous areas like data storage, catalysis, motors, magnetic refrigeration and electrical power transformers.¹⁻¹³ They are also being used in magnetic separation¹⁴ and as magnetic seals.^{15,16} Apart from these applications magnetic nanoparticles are finding applications in biomedical fields as MRI enhancers, drug delivery agent, separating matrices of bio entities etc.^{1,17-22} Important magnetic nanoparticles that are being used are cobalt (Co), nickel (Ni) and iron (Fe). These find application in the field of catalysis too.¹ During the synthesis of these magnetic nanoparticles, the challenge is to maintain the metallic state as Co, Ni and Fe are highly prone to oxidation especially in aqueous environment. The inter-particle attraction arising from the large van der Waals forces between polarizable metal particles and from magnetic dipole interactions in these materials are also very large.²³ This makes it difficult to keep them in a dispersed state. Thus, to obtain stable magnetic nanoparticle dispersion, it is important to protect the nanoparticle surface. This can be easily achieved by using capping ligands /surfactants. Most of the practiced methods for the synthesis of these protected and stable Fe, Co and Ni nanoparticle dispersion are accomplished in organic solvent.²⁴⁻²⁹ This is due to the structure of the capping agent used which generally bears one functional group that can bind to the nanoparticle surface thus preventing it from getting oxidized. The other end of these molecules is generally a hydrophobic group. This makes it easy for nanoparticles capped by these molecules to be dispersed in non-polar organic media. As some of the important applications of these nanoparticles require them to be dispersed in aqueous media; the need for developing methods for their synthesis in aqueous media can be immediately understood.

Another major drawback in these reported synthetic procedures is the lack of proper understanding of the mode of interaction between the nanoparticle surface and the ligand. In fact we firmly believe that this understanding is very crucial for developing reliable synthetic procedure of these magnetic metal nanoparticle systems in any solvent media.

Based on the knowledge that oleic acid is one of the extensively used molecules as a capping agent during the synthesis of magnetic metal nanoparticles, in this chapter we wish to address two issues.

1. Whether the structural modification of oleic acid could provide us access to the synthesis of magnetic metal nanoparticles in aqueous media.
2. Whether new ligands that possess similar structural moiety as present in oleic acid can act as good capping agents for such nanoparticles.

As the three transition metals (Fe, Ni and Co) behave more or less in similar fashion we chose one of them, namely cobalt as the test case. As we have observed in chapter 1, oleic acid (OA) is one of the major surfactant during the synthesis of cobalt nanoparticles. It has been shown that in organic media the oleic acid molecule binds to the nanoparticle surface through the $-\text{COOH}$ group (Figure 2.1A). The few reports that tested the utility of oleic acid as a capping molecule in aqueous medium used the ethanol/methanol-water mixture for the synthesis instead of pure water.^{30,31} This was necessary because oleic acid is insoluble in water. Through detailed FTIR and NMR spectral characterization, it has been demonstrated that in aqueous media the oleic acid molecule binds to the nanoparticle surface through the double bond.³² A quick look at the structure of the oleic acid suggests that if a hydrophilic moiety can be attached towards the $-\text{CH}_3$ end it may be possible to make it water soluble. Such modification can be achieved by organic synthesis which involves multiple steps and are tedious. On the other hand it is well known that when fatty acids are added to yeast cells in presence of excess of glucose a class of bio-surfactants called sophorolipids are formed. In these sophorolipids (SLs) a sophorose – a dimeric glucose – is attached to either ω or $\omega-1$ carbons of the fatty acids through a β -glycosidic linkage (Figure 2.1 B).^{33,34}

As mentioned above, OA can bind to the nanoparticle surface through the double bond or the carboxylic end. In OA, the double bond is located at the center of the molecule and the carboxylic acid end is separated by six carbon atoms from this double bond. As has been already mentioned, both olefin and the carboxylic

acid can play the role of stabilizing moiety during the nanoparticle synthesis.³² However in case of OA both of them (from a single molecule) cannot bind to the nanoparticle surface because of their spatial separation. We envisaged that a molecule in which two functional moieties that can bind to the nanoparticle surface have been placed next to each other, may act as a good stabilizing agent. Our search concluded that 2-(dodecyloxy) acetic acid (DDOA) could be one such candidate. Here, the -O-CH₂-COOH group can stabilize the metal surface by forming a 5 membered ring (Figure 2.1C).

Thus, in this chapter, we investigate the role played by two hitherto unused surfactants in the formation of cobalt nanoparticles. The two surfactants that have been considered are:

1. A biomolecule called sophorolipid of oleic acid obtained by challenging yeast cells like *Candida Bombicola* with oleic acid in presence of glucose.
2. 2-(dodecyloxy) acetic acid (DDOA) which is synthesized by chemical route.

We have also studied the interaction of these surfactants with nanoparticles. Our results indicate that both the surfactants show good capping capability and the cobalt nanoparticle synthesis thus formed are stable and show good magnetic properties. This chapter also illustrates the role played by surfactants in controlling the crystallographic phase of cobalt nanoparticles.

2.2 Synthesis of sophorolipids and carboxylic acid:

Sophorolipid used in this work was synthesized in our lab by using the reported procedure in literature.³⁵⁻³⁷

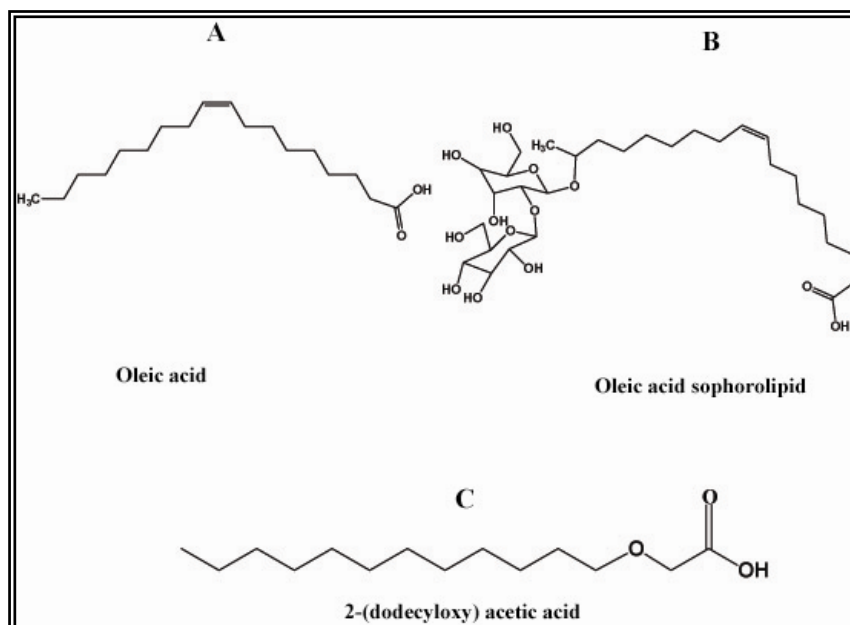


Figure 2.1: Structure of oleic acid (A), oleic acid derived sophorolipid (B), dodecyloxy acetic acid (C).

In brief, yeast cells like *Candida bombicola* are challenged with fatty acids such as oleic acid, linoleic acid etc. in presence of glucose. The well established biotransformation follows by the attachment of the hydroxy group to the penultimate carbon and then two glucose molecules are attached to this hydroxyl group by β -glycosidic linkage. Crude sophorolipid obtained are mixture of acetylated acidic and acetylated lactonic form. This crude sophorolipid was subjected to base hydrolysis to obtain pure acidic form of sophorolipid. In this chapter, we have used oleic acid derived sophorolipid (OASL).³⁸ The DDOA molecule used in our study was synthesized by Dr C.V.Ramana's group at NCL and was used as received. In brief, to obtain these molecules monoalkylation of glycol by alkyl bromide in presence of base followed by oxidation of primary alcohol was carried out. The structure has been verified by NMR and other characterizations.

2.3 Synthesis of cobalt nanoparticles:

This section describes synthesis protocols used for synthesis of cobalt nanoparticles using sophorolipid, oleic acid and DDOA as capping ligands. Schematic method for synthesis of cobalt nanoparticles is shown in Figure 2.2.

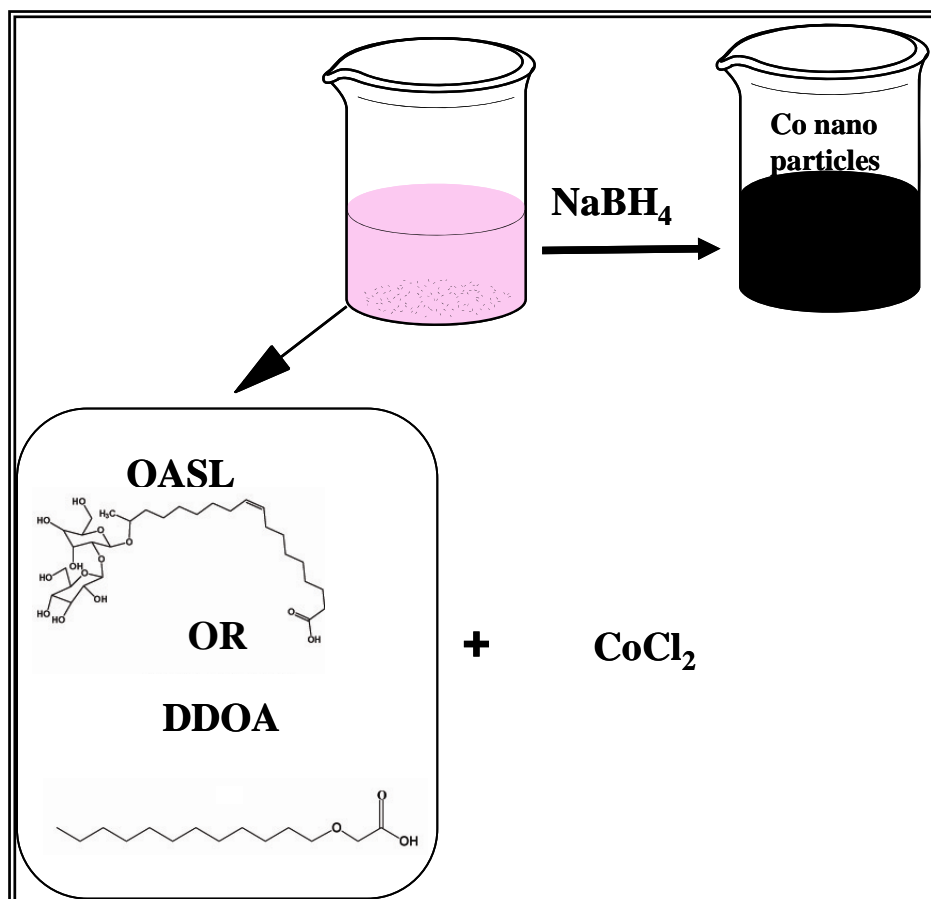


Figure 2.2: Method for synthesis of cobalt nanoparticles using OASL and DDOA as capping ligands.

2.3.1: Using sophorolipid as capping agent

Synthesis of cobalt nanoparticles was carried out by using sodium borohydride (NaBH_4) as reducing agent. In a typical experiment, 100 mL of sophorolipid solution was taken and cobalt chloride (CoCl_2) was added to this. The final concentration of SL was 10^{-4} M and that of CoCl_2 was 10^{-3} M. This mixture was purged with nitrogen for 30 min to remove the dissolved oxygen. 20 mg of sodium borohydride was dissolved in 1 mL deionized water and added to the

mixture drop wise using a syringe. On addition of NaBH_4 the colour of the solution changed from light pink to black indicating the formation of cobalt nanoparticles. The formed cobalt nanoparticles were also purged with nitrogen to ensure complete removal of dissolved oxygen to avoid contamination. The nanoparticle solution was then centrifuged at 8000 rpm for 20 min to remove uncoordinated surfactant and un-reacted NaBH_4 . The obtained pellet was re-dispersed in deionized water and used for further characterization. The obtained pellet was vacuum dried to form powder for X-ray and magnetic measurements.

2.3.2: Using pure oleic acid (OA)

Procedure for cobalt nanoparticles synthesized using pure OA was similar to the procedure followed for OASL. In this case ethanol-water mixture was used to dissolve OA. The final concentration of oleic acid in water was 10^{-4} M. To this solution, 1 mL of 10^{-2} M CoCl_2 was added so that the final concentration of CoCl_2 is 10^{-3} M. This mixture was purged with nitrogen to remove the dissolved oxygen impurities. This mixture was reduced by adding sodium borohydride. Change in colour from light pink to black indicates the formation of Co nanoparticles. Purging of nitrogen was carried out even after formation of nanoparticles. The obtained nanoparticles are subjected to centrifugation at 8000 rpm for 20 min. The pellet obtained was re-dispersed in water and further used for characterization. Powder sample was obtained by drying the pellet. Powder samples were used for XRD and magnetic characterization.

2.3.3: Using carboxylic acid

The synthesis of cobalt nanoparticles using DDOA as capping ligand was similar to that carried out for cobalt nanoparticles prepared using OA. In this case, again since the DDOA is not soluble in water ethanol/ water mixture was used and then the synthesis was carried out in deionized water. Similar methods as described above were used for purification and characterization of the cobalt nanoparticles formed.

2.4: Results

2.4.1: Fourier Transform infrared spectroscopy (FTIR)

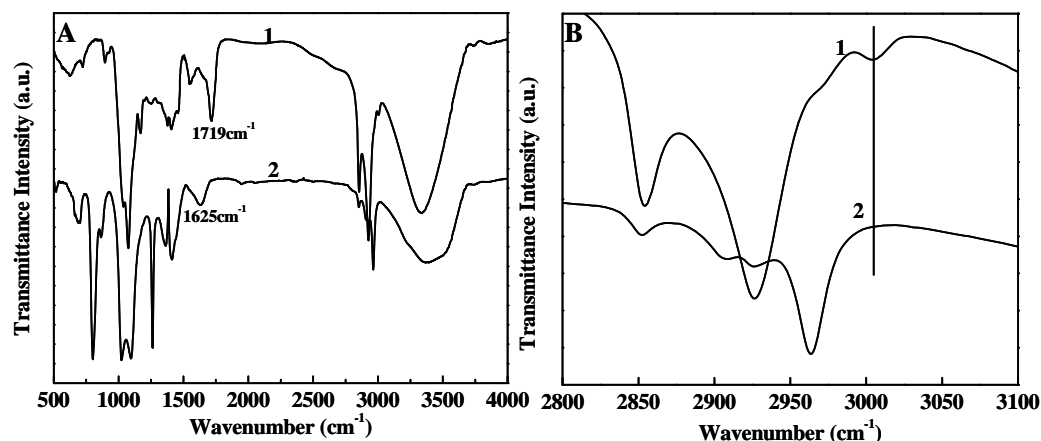


Figure 2.3: (A) FTIR spectrum analysis of pure OASL (curve 1), OASL-CoNPs (curve 2). (B) Shows the magnified region in the range 2850 to 3100 cm^{-1} corresponding to the olefinic band.

FTIR is a powerful tool to study the capping of surfactants to the surface of the nanoparticles. Figure 2.3A shows the FTIR data for pure OASL and OASL-CoNPs. The notable features of the spectrum in OASL (curve 1) are a band centered at 1719 cm^{-1} and a peak occurring at 3004 cm^{-1} (Figure 2.3, curve 1). We also observe bands positioned at 2853 and 2926 cm^{-1} which are designated to symmetric and antisymmetric stretching of CH_2 .^{29,39} The spectrum recorded for OASL-CoNPs are shown in Figure 2.3 A&B, curve 2. The most important differences in this spectrum from that of pure OASL are a shift in the 1719 cm^{-1} band to 1625 cm^{-1} and the disappearance of 3004 cm^{-1} peak.

A comparison of FTIR of pure OA and OA capped nanoparticles represents (OA-CoNPs) similar features as observed for OASL and OASL-CoNPs. Figure 2.4 represents FTIR spectra of pure OA (curve 1) and OA-CoNPs (curve 2) for comparison. The comparative FTIR spectra of OA-CoNPs spectra also display the disappearance of the 3004 cm^{-1} peak and a shift in the $-\text{C}=\text{O}$ stretch (Figure 2.4, curve 1 and 2) from 1709 cm^{-1} to 1632 cm^{-1} .

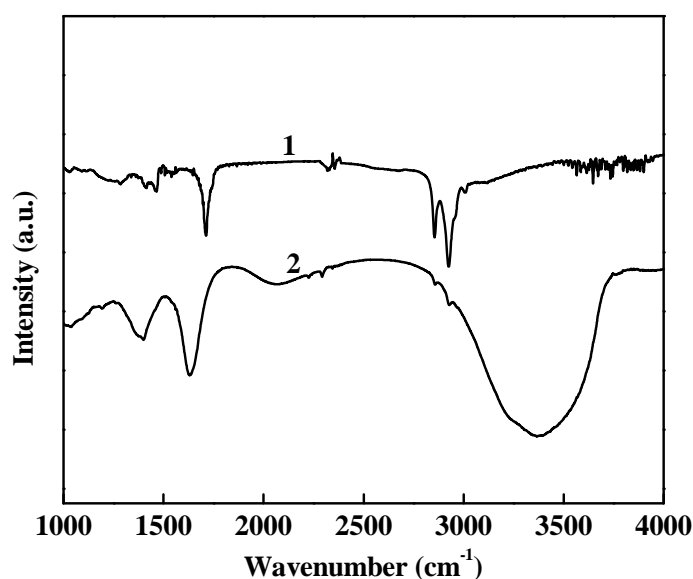


Figure 2.4: FTIR spectrum of pure OA (curve 1) and OA capped cobalt nanoparticles (curve 2).

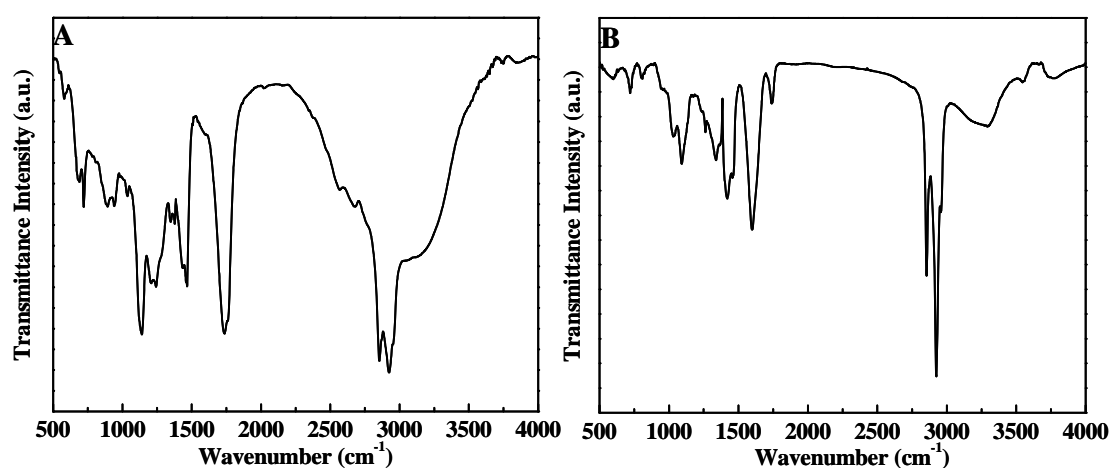


Figure 2.5: (A) FTIR spectra for pure DDOA. (B) FTIR spectra for cobalt nanoparticles capped DDOA.

The FTIR spectrum for purified DDOA molecule is shown in Figure 2.5A. Band at 1737 cm^{-1} is assigned to C=O stretch while the peaks appearing at 2853 and 2926 cm^{-1} are assigned to symmetric and antisymmetric stretching of CH_2 . Here the most prominent difference when this molecule is present on CoNPs surface is the shift observed in 1737 cm^{-1} peak to 1593 cm^{-1} (Figure 2.5 B).

2.4.2: Transmission Electron microscopy

(a) OASL capped Co nanoparticles

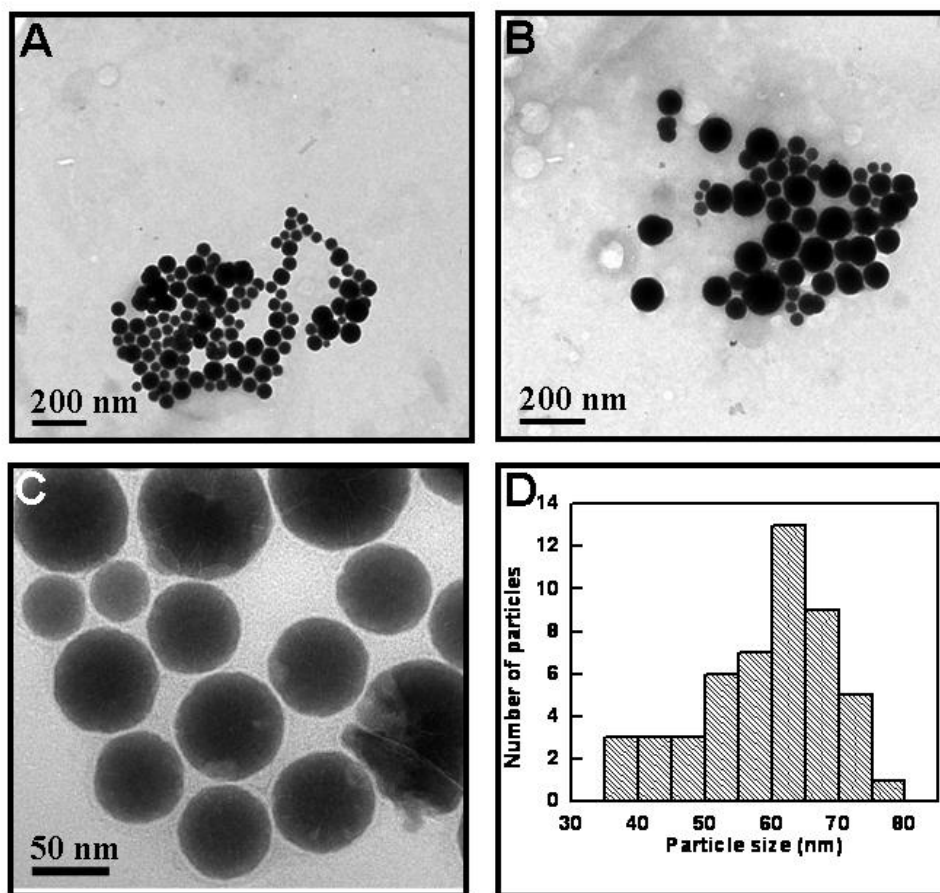


Figure 2.6: (A-C) Representative TEM micrographs of OASL capped cobalt nanoparticles at different magnifications. (D) Particle size distribution of the particles observed in the images A-C.

The representative TEM images of OASL-CoNPs shown in Figure 2.6 (A-C). From the figure we observe that the cobalt nanoparticles are spherical in shape. The particle size distribution determined from the TEM analysis also indicates the polydisperse nature of the nanoparticles. Average particle size obtained is ~ 60 nm (Figure 2.6 D).

The selected area electron diffraction (SAED) pattern obtained from TEM analysis is shown in Figure 2.7. The diffraction pattern displays a spotty pattern overlaid on rings indicative of polycrystalline nature of the particles.

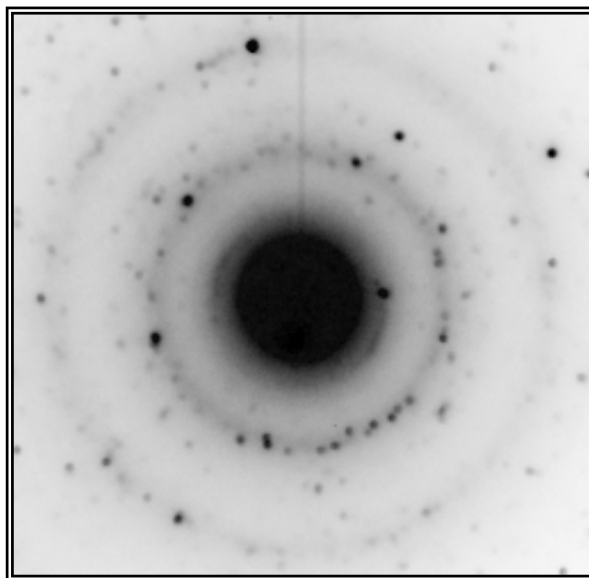


Figure 2.7: Selected Area electron diffraction of OASL-CoNPs.

(b) OA capped Co nanoparticles:

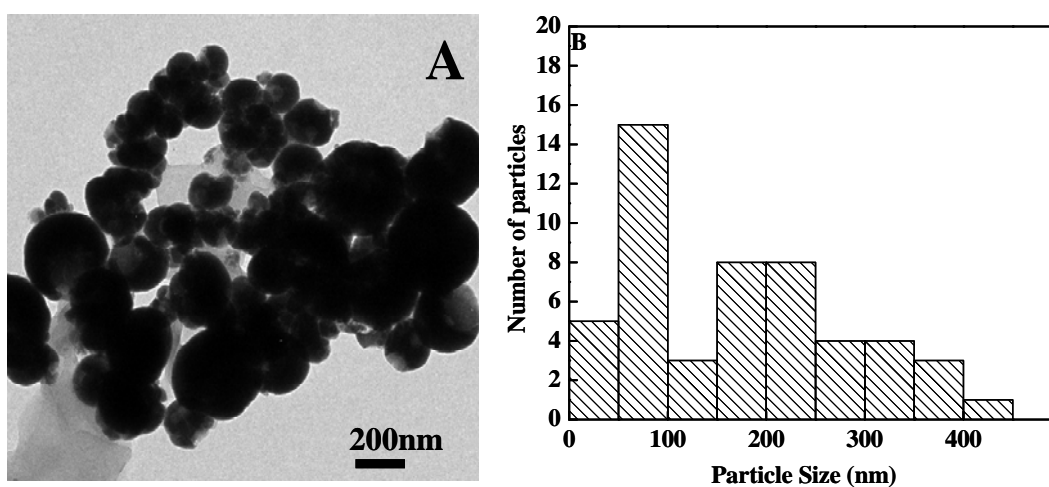


Figure 2.8: (A) TEM micrographs of pure OA capped cobalt nanoparticles. (B) The particle size distribution of OA capped cobalt nanoparticles.

A comparative TEM images for OA-CoNPs are shown in Figure 2.8 along with particle size distribution. The TEM images indicate that the particles are irregular in shape and are clustered. Particle size distribution indicates that size of particle vary from 40 nm to about 400 nm (Figure 2.8 B).

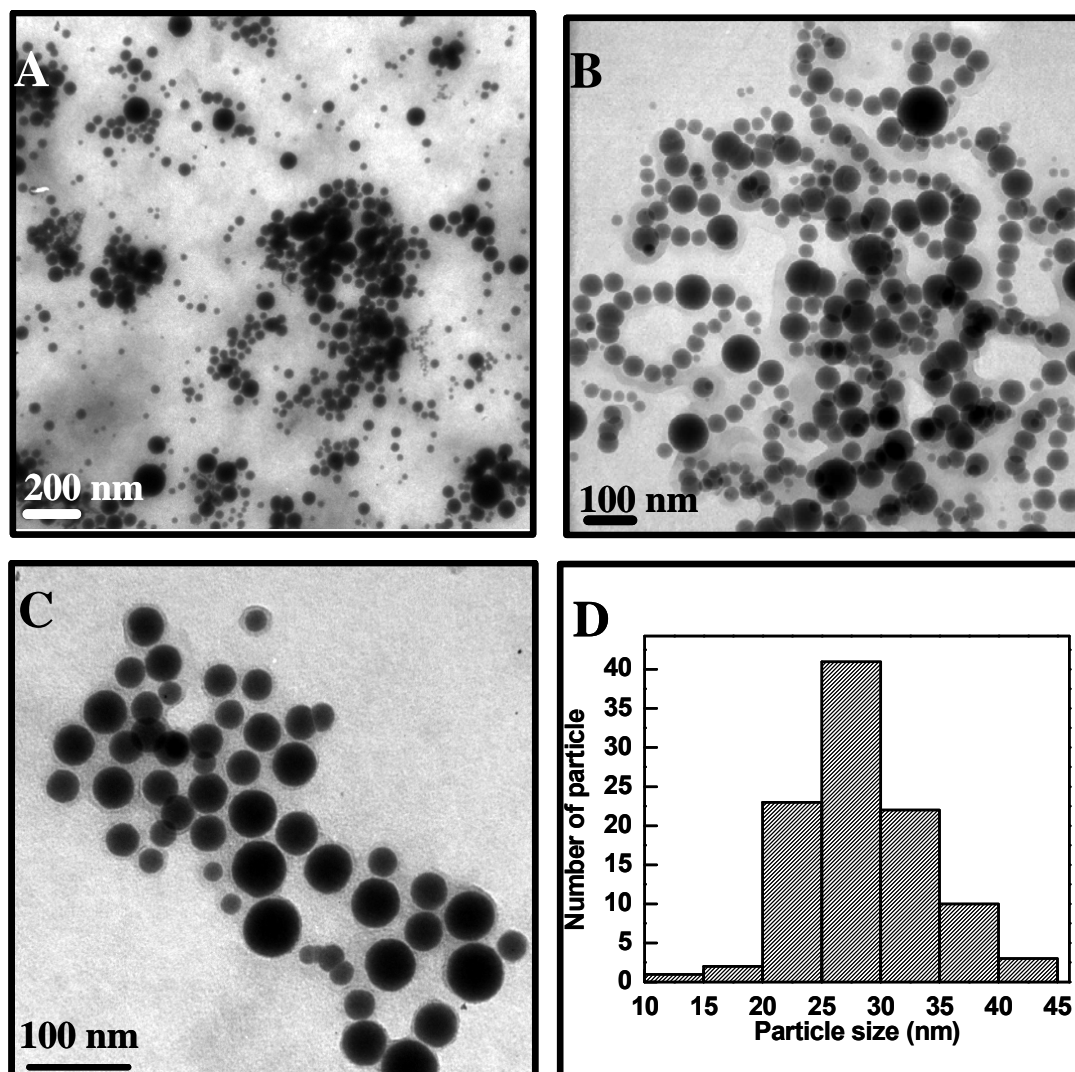
(c) DDOA capped Co nanoparticles:

Figure 2.9: (A-C) TEM micrographs of (DDOA) capped cobalt nanoparticles at different magnifications. (D) Histogram of the particle size distribution.

Figure 2.9 (A-C) illustrates the TEM micrographs at different magnifications of cobalt nanoparticles synthesized using DDOA as capping molecule. From the image we can observe that the particles are spherical in shape and polydisperse in nature. Size distribution analysis (Figure 2.9 D) indicates that the average particle size is ~ 28 nm.

2.4.3: X-ray Diffraction (XRD)

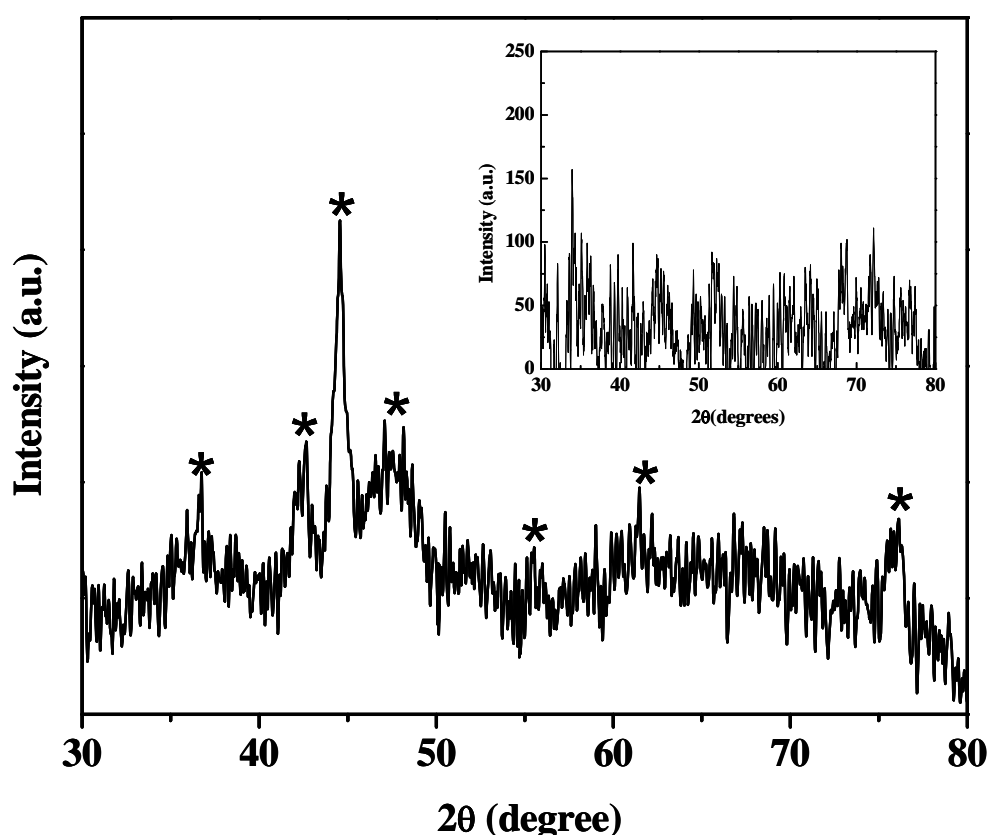


Figure 2.10: XRD spectrum of OASL capped cobalt nanoparticles heated at 300 °C. Inset of the figure shows the powder XRD recorded for as synthesized OASL-CoNPs.

Figure 2.10 demonstrates the X-ray diffraction pattern for OASL-CoNPs. The as prepared sample displays no features (inset, Figure 2.10). Therefore the sample was heat treated at 300 °C for 30 min under N₂ environment. Clear and distinguishable peaks are observed upon heating. The ‘d’ value of peak designated with ‘*’ are 2.45, 2.11, 2.03, 1.69, 1.65, 1.49, 0.79 Å.

Figure 2.11 demonstrates the X-ray diffraction pattern for DDOA capped Co nanoparticles. In this case also the diffraction pattern was recorded for the powder sample heated at 300 °C as no diffraction was observed for as prepared sample (curve1). The peak observed corresponds to the ‘d’ value 2.15, 2.03, and 1.48 Å.

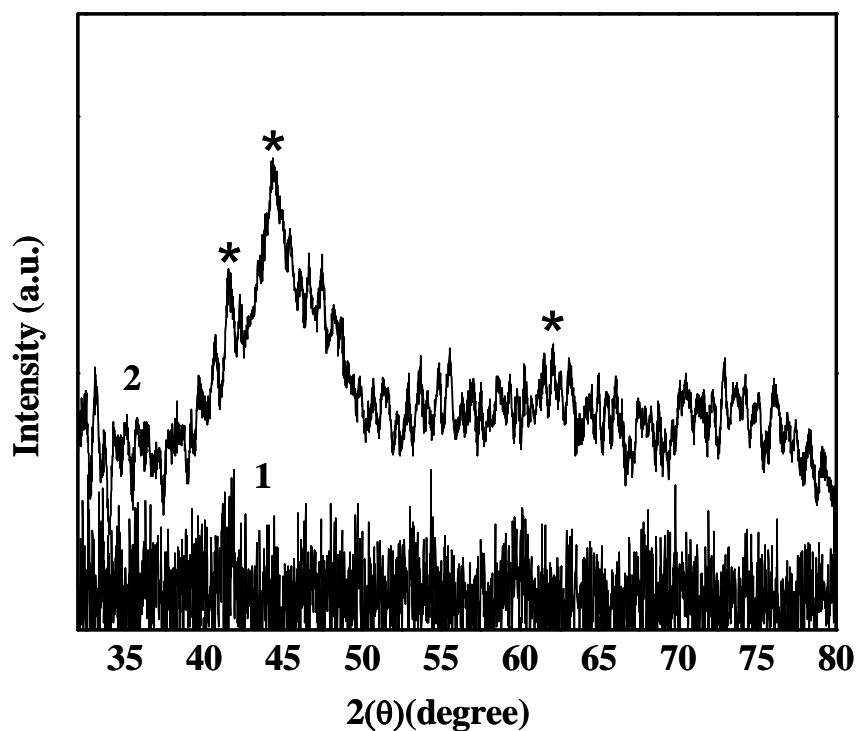


Figure 2.11: XRD pattern for as prepared cobalt nanoparticles capped with DDOA nanoparticles, curve 1. Curve 2 displays the diffractogram of the heat treated sample.

2.4.4 Comparative room temperature magnetic measurement for OA and OASL capped cobalt nanoparticles.

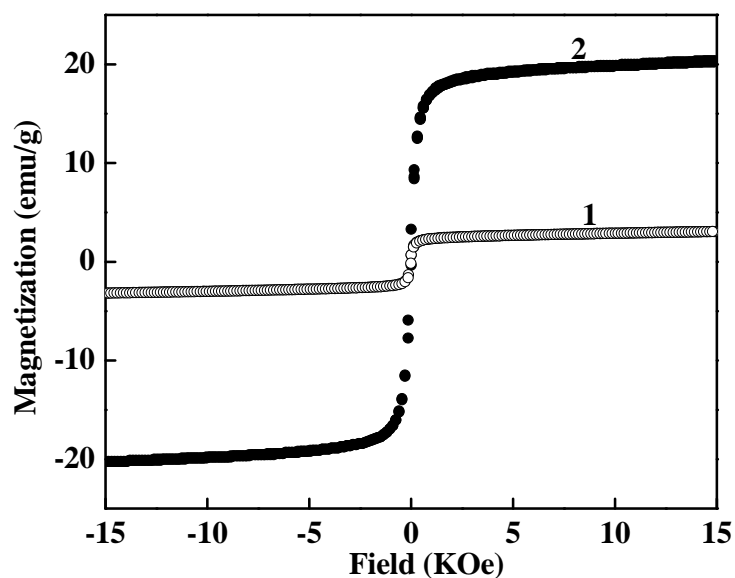


Figure 2.12: Comparative room temperature magnetic measurement data for OA-CoNPs (curve 1) and OASL-CoNPs (curve 2).

A comparative room temperature magnetic measurement was carried out between pure OA-CoNPs and OASL-CoNPs (Figure 2.12, curve 1 and 2 respectively). Both the samples show no hysteresis at room temperature and the saturation magnetization value for OASL-CoNPs (23 emu/g) is much higher than the value for OA-CoNPs (3 emu/g). The probable reason for higher magnetization for OASL-CoNPs could point to the stabilization imparted to cobalt nanoparticles as a result of the better capping nature and stability of OASL in a aqueous environment as compared to OA. There is also a possibility of oxide formation in case of OA-CoNPs which can result in lower magnetization value.

2.4.5: Magnetic measurement:

a) FC-ZFC measurements

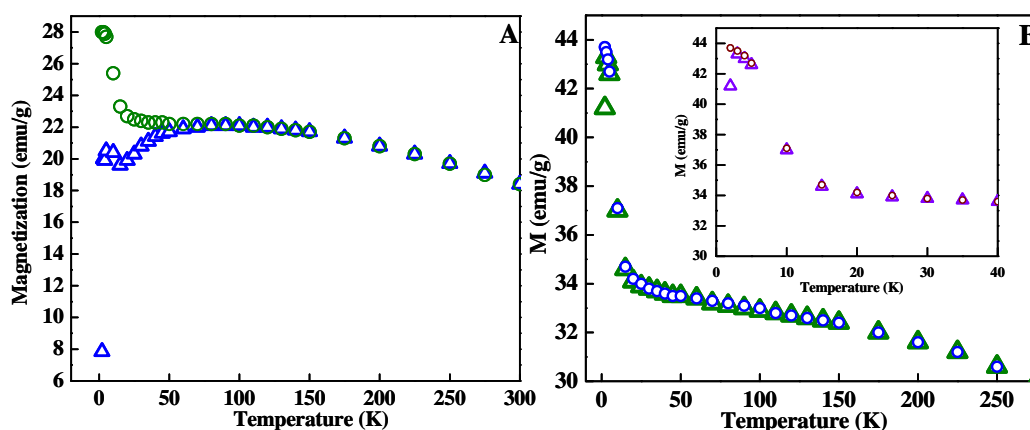


Figure 2.13: Zero Field cooled (ZFC- data points denoted by Δ) and field cooled (FC-data points denoted by 'o') for OASL-CoNPs (A) and DDOA-CoNPs (B). Inset B shows the magnified region from 0 to 40 K demonstrating the blocking temperature.

Temperature dependent magnetization curves for OASL-CoNPs and DDOA-CoNPs are shown in Figure 2.13. Magnetic field applied in this case was 50 Oe. Data points denoted by 'o' corresponds to field cooled (FC) mode while those marked with ' Δ ' corresponds to zero field cooled mode (ZFC). For OASL-CoNPs the FC and ZFC data points overlap with each other down to 50 K and below that we see a divergence between the data points (Figure 2.13 A). Below 50 K ZFC shows a decrease in magnetization with decrease in temperature while the FC

shows an increase in magnetization with decrease in temperature. Again a peak is observed at 10 K in the ZFC trace.

FC-ZFC curves for cobalt nanoparticles capped with DDOA again show very similar features where the divergence between FC and ZFC curves is seen at 20 K with similar trends in magnetization values.

b) Field dependent magnetic measurement.

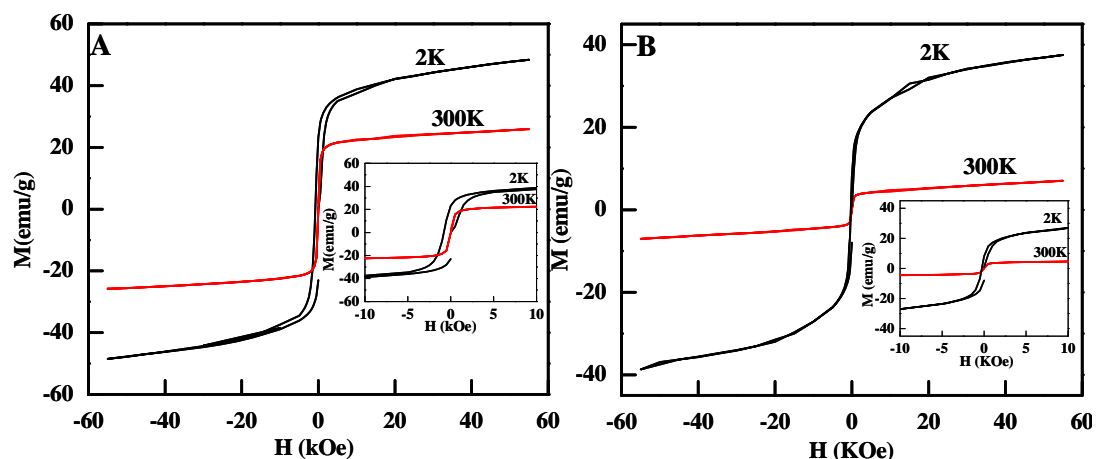


Figure 2.14: Field dependent magnetic measurement recorded at room temperature (red) and at 2 K (black). (A) Represents measurements carried out for OASL-CoNPs and (B) is for DDOA-CoNPs. The inset in the figure shows magnified traces around 0 Oe.

The field dependent magnetic measurements at different temperatures (room temperature and 2 K) are shown in Figure 2.14. Here the notable features are that for room temperature no saturation is observed and hysteresis is absent (inset, red curve). The magnetic measurements carried out at 5 K shows a small loop opening with coercivity value of 800 Oe. The magnetization values observed for room temperature is 23 emu/g while for temperature below 5 K it is 55 emu/g.

Similar field dependent magnetization was also carried out for cobalt nanoparticles capped with DDOA at temperatures (300 K) and at (2 K). Figure 2.14 B shows the magnetization curves at room temperature (curve 1) and at low temperature, 2 K (curve 2). It can be noticed that at room temperature no hysteresis is seen while at 2K small hysteresis loop opening up can be observed from the inset of Figure 2.14 B. Magnetization value obtained for the sample at room temperature

is 12 emu/g, while at 2 K it is 35 emu/g. The coercivity value determined at 2 K is 260 Oe.

c) Ferromagnetic Resonance (FMR):

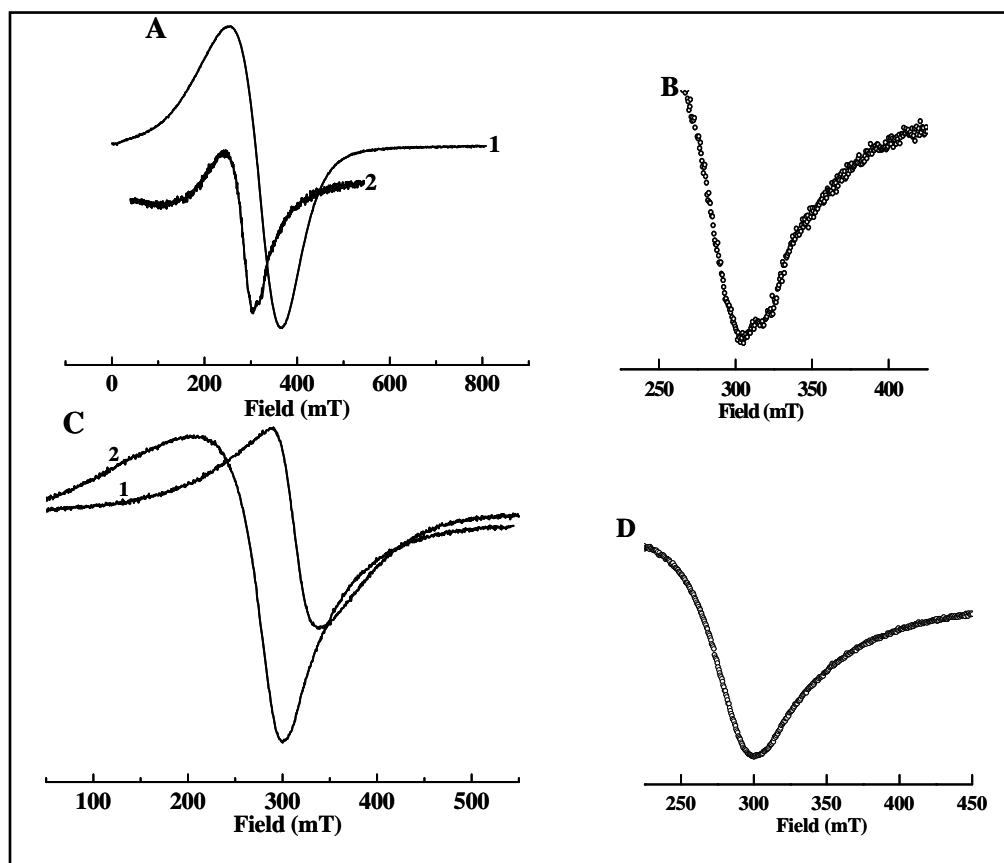


Figure 2.15: Ferromagnetic resonance (FMR) for OASL-CoNPs (A) and DDOA-CoNPs (C) recorded at RT (A and C, curve 1) and at 2 K (A and C, curve 2). B and D shows the magnified image of FMR recorded at low temperatures.

For the FMR measurements the OASL-CoNPs and DDOA-CoNPs powder was dispersed in paraffin to minimize the interaction between the particles.

FMR measurements were carried out at different temperature. As representative the traces recorded for two temperatures (a) room temperature and (b) low temperature (2K) are displayed in Figure 2.15A and C, curve 1 and 2 respectively. FMR for OASL-CoNPs is shown in Figure 2.15 A and B. The curves recorded at room temperature are sharp while we observe that at lower temperature there is broadening and concomitant split in the peak.

Ferromagnetic resonance for DDOA-CoNPs is shown in Figure 2.15 C and D. The graphs show FMR recorded at room temperature (300 K, curve 1) and at low temperature (4 K, curve 2). Here we can see that compared to the room temperature spectrum, the spectrum at lower temperature is sharp and does not show any splitting as was observed in the case of OASL-CoNPs.

2.5 Discussion:

The results obtained so far on the cobalt nanoparticles synthesized with OASL and DDOA as capping agent would be discussed in the following section. The sequence will be maintained in same manner as the results. Synthesis of cobalt nanoparticles was carried out using two surfactants: first being oleic acid derived sophorolipid (OASL) and second one was organically prepared 2-(dodecyloxy) acetic acid (DDOA). Using these ligands cobalt nanoparticle synthesis was carried out as per the procedure reported in section 2.2. Interaction of these ligands with nanoparticle surface was studied by FTIR.

Table 2.1: Major FTIR peaks

Peaks	Pure OASL	OASL-CoNPs	Pure DDOA	DDOA-CoNPs
C=O stretch	1719 cm ⁻¹	1625 cm ⁻¹	1735 cm ⁻¹	1723 cm ⁻¹
Olefinic stretching	3004 cm ⁻¹	vanishes	absent	absent

Table 2.1 gives the values of prominent FTIR peaks occurring in OASL before and after binding to Co surface. It also shows the FTIR peaks for DDOA case.

FTIR spectroscopy is useful technique to study the binding of ligands to the surface of nanoparticles. In the pure OASL spectrum, peak positioned at 1719 cm⁻¹ is assigned to C=O stretch while peak occurring at 3004 cm⁻¹ represents the stretching of olefinic C-H. In the FTIR spectra of OASL-CoNPs, a shift in peak corresponding to C=O peak is observed while the peak corresponding to C=C-H

stretch vanishes. Disappearance of this peak indicates binding of double bond to surface of nanoparticles while the shift in C=O peak is due to carboxylate formation (Figure 2.3 A and B).^{29,32,40,41} Comparative FTIR study carried out for OA-CoNPs also shows similar feature as observed for OASL-CoNPs (Figure 2.4). These results highlight the similarity in the binding of SL and oleic acid on the nanoparticle surface and that it might take place both through the double bond and carboxylate formation (Figure 2.16 A and B). We wish to highlight here that in the pure OA case, if the binding to the CoNPs is through the double bond or carboxylic ends with CoNPs surface an unfavorable situation where $-CH_3$ end is exposed to aqueous environment would result. This could be the reason why OA does not act as good capping agent in aqueous environment. On the other hand, in case of OASL whether the carboxylic acid or the double bond binds to the Co surface (Figure 2.16 B) hydrophilic groups are present on the exterior. This would make a favorable condition for the particles to be dispersed in aqueous media. This is probably the reason why OASL acts as a good capping agent in water. At this juncture, it is difficult to say how many molecules are attached through the double bond and how many are attached through the $-COOH$ group. In case of DDOA, binding to surface of nanoparticles occurs only through $-COOH$ group as it does not contain a double bond (Figure 2.16 C). This is indicated by shift in peak (Figure 2.5 A and B, curve1). At this juncture the DDOA-CoNPs are dispersible only in non-polar organic media. However, by changing appropriate precursors and organic transformation changes to this ligand structure can be accomplished. This can lead to newer synthetic methods for the preparation of CoNPs in the aqueous environment a relatively easier task.

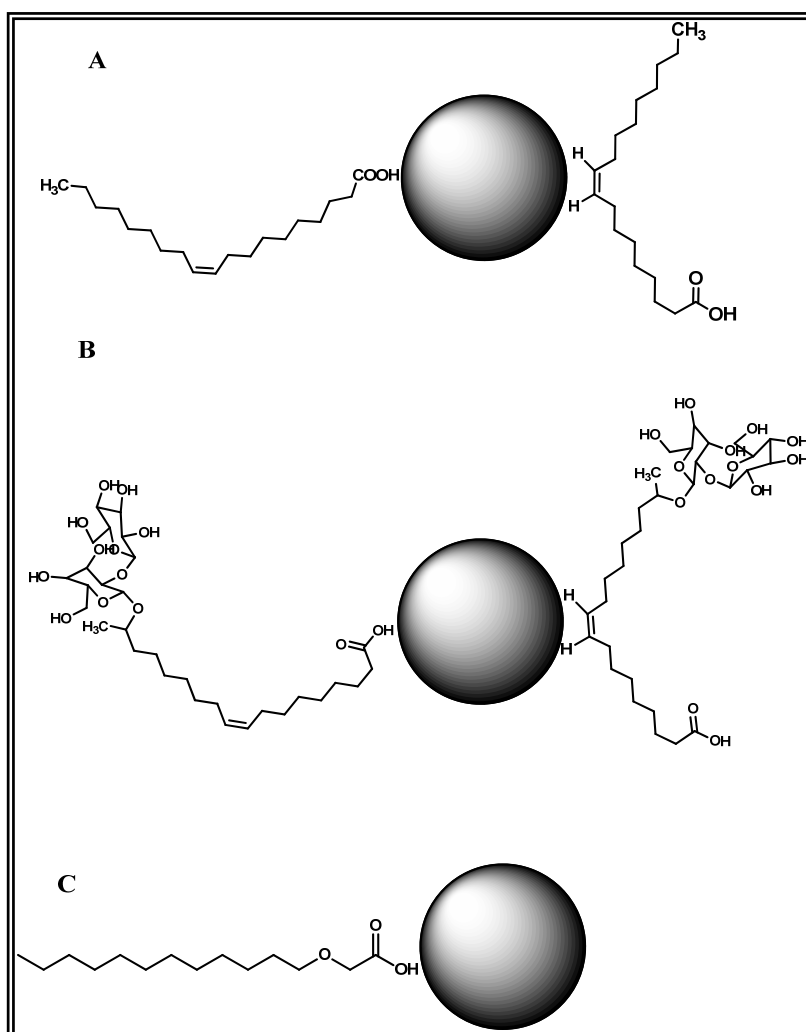


Figure 2.16: Schematic showing mode of binding of OA (A), OASL (B) and DDOA (C) to the surface of cobalt nanoparticles.

TEM analysis is used to determine the nature and size of nanoparticles formed. In both the cases the nanoparticles were polydisperse (Figure 2.6 and 2.9 A-C). Particle size obtained with DDOA as capping agent was smaller than particles obtained with OASL capping (Figure 2.6 and 2.9, D). TEM analysis carried out for pure OA-CoNPs as a comparative study with OASL-CoNPs shows aggregated nanoparticles with larger particle size (Figure 2.8). The poor capping ability of OA in water can be implicated for this observation as OA cannot stabilize CoNPs leading to coalescence of particles.

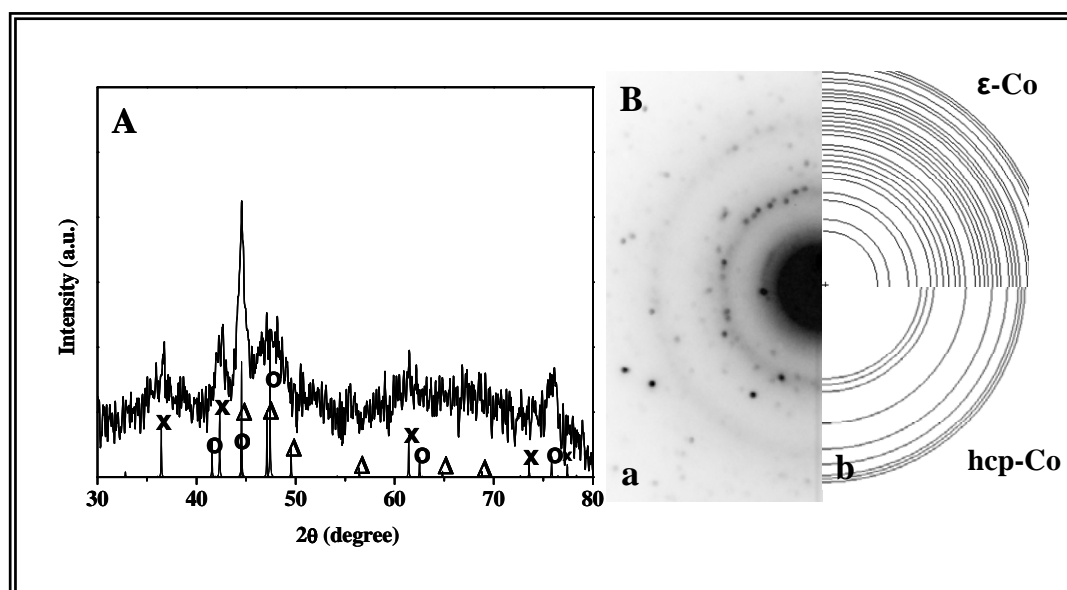


Figure 2.17: Simulated XRD pattern (line spectrum) and simulated electron diffraction (circular lines) for OASL capped cobalt nanoparticles along with the experimental data.

It is known that cobalt nanoparticles prepared in aqueous medium do not show any diffraction at room temperature while slight heating renders crystallinity to Co nanoparticles.^{31,42,43} Our observation also supports this result. Upon heat treating the CoNPs at 300 °C the crystallinity of the sample increases and we see clearly discernible peaks in the X-ray diffractogram. In case of OASL-CoNPs the observed XRD pattern could not be indexed to any single phase of Co. Therefore, we tried to index it to a mixture of different phases (Figure 2.17A) where the peak position of hcp, ϵ -phase and CoO are given by ‘O’, ‘ Δ ’ and ‘X’ respectively. Electron diffraction for OASL-CoNPs could also be indexed to mixed phase corresponding to hcp structure and the ϵ -phase (Figure 2.7 and 2.17 B). OASL-CoNPs sample also shows traces of CoO. Most of the cobalt nanoparticles formed are known to possess one or two layers of CoO.^{42,44} It is possible that our as prepared sample itself contains few layers of CoO. Other possibility would be that the sophorolipid on the surface may decompose during heating resulting in release of oxygen which may convert few layers of Co to CoO.⁴⁵

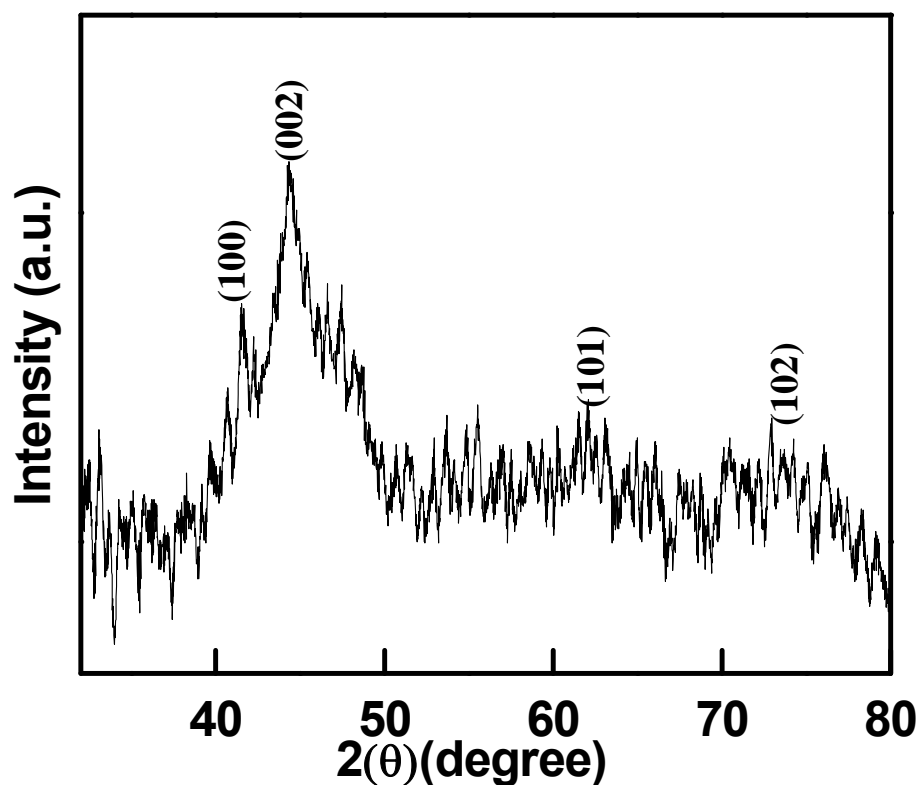


Figure 2.18: X-ray diffraction pattern for DDOA-CoNPs for sample heated at 300 °C indexed to hcp phase of CoNPs.

The DDOA-CoNPs XRD traces could be indexed to pure hcp phase (Figure 2.11, curve 2). Prominent peak occurs at $d=0.77$ Å corresponding to interplaner spacing of (002) phase of hcp. Other peaks corresponding interplaner spacing of (100), (101), (102) and (110) also match with the hcp phase of Co nanoparticles (Figure 2.18). It is well documented that cobalt nanoparticles synthesized by borohydride reduction do not show any diffraction pattern. It may also form borides.⁴⁶ Simple annealing leads to formation of crystalline material as were also observed in our case.^{47,48} Heating of the sample also results in eliminating the defects and improve crystallinity.⁴⁹

Detailed magnetic measurements were carried out for both the samples. Magnetic properties depend on the crystalline phase of nanoparticles.⁵⁰ In the present instant the nature of the FC-ZFC measurements of both OASL-CoNPs and DDOA-CoNPs display characteristics resembling super-paramagnetic particles.^{51,52} Ferromagnetic materials below certain size regime become single domain systems

and display superparamagnetic characteristic. The main features of superparamagnetism are

1. Divergence of FC-ZFC curves below certain temperature called blocking temperature (T_B).
2. No hysteresis loop in the M-H trace above T_B .
3. Hysteresis in the M-H curve below T_B .

In case of OASL capped cobalt nanoparticles the ZFC curves depict two peaks at 55 K and 10 K. These could be the blocking temperature (T_B) for cobalt nanoparticles corresponding to two different phases present (Figure 2.13A). When two phases co-exist two phase transitions are observed in the nature of ZFC curve.⁵³ Thus M-T measurements also confirm the presence of mixed phase in OASL-CoNPs nanoparticles. For DDOA-CoNPs FC-ZFC curve co-inside with each other and the blocking temperature (T_B) observed is very low (5 K) (Figure 2.13 B). One of the reasons for appearance of blocking temperature at lower value can be the size of the nanoparticles which is clear from the following equation of magneto crystalline anisotropy $K = \frac{K_\beta T_B}{V}$ where K is anisotropy constant, K_β is the Boltzman constant, T_B is the blocking temperature and V is the volume of the particle. It is also known that decrease in blocking temperature is observed when the interaction between the particles is decreased.^{27,54} Defects are also responsible for lower blocking temperature of magnetic nanoparticles.⁵⁴ It is also worth remembering here in case of DDOA-CoNPs belongs to the hcp crystalline phase. The hcp phase of Co is known to display lower blocking temperature.⁵⁰ In the present case of DDOA capping any one of the reasons mentioned above or all of them could be contributing to the lower T_B observe.

M-H measurements carried out on OASL-CoNPs and DDOA-CoNPs show typical superparamagnetic behavior (Figure 2.14 A and B). Both the sample do not show any hysteresis at room temperature i.e. above the blocking temperature (Figure 2.14 A, red curve and Figure 2.14 B, red curve) , while for lower temperature 2 K (below blocking temperature), samples show small hysteresis indicating ferromagnetic behavior below T_B . Magnetization value (M_s) increases at

lower temperature. OASL-CoNPs possess higher M_s value than M_s value obtained for DDOA-CoNPs both at room temperature and 2K. Also the coercivity at lower temperature for DDOA-CoNPs is smaller than coercivity value for OASL-CoNPs. This again could be related to the different phases observed in the system.

Ferromagnetic resonance (FMR) is a tool that enables study of superparamagnetic particles that possess different crystalline structure and different sizes.⁴⁵ FMR data were recorded for different temperatures. Room temperature FMR data for OASL-CoNPs and DDOA-CoNPs (Figure 3.15 A and C respectively) shows smaller line width and the resonance for OASL-CoNPs is at higher magnetic field than for DDOA-CoNPs. At lower temperatures we observe line splitting in case of OASL-CoNPs while this is not observed in case of DDOA-CoNPs. The probable reason for occurrence of this splitting is

- 1) Presence of two crystalline structures in OASL capped cobalt nanoparticles (hcp phase and ϵ -phase).
- 2) OASL capped cobalt nanoparticles consist of ϵ -phase which has been known to display splitting in the FMR curve at low temperature.⁴⁵
- 3) Particle sizes in case of OASL capped cobalt nanoparticles are bigger than DDOA-CoNPs.

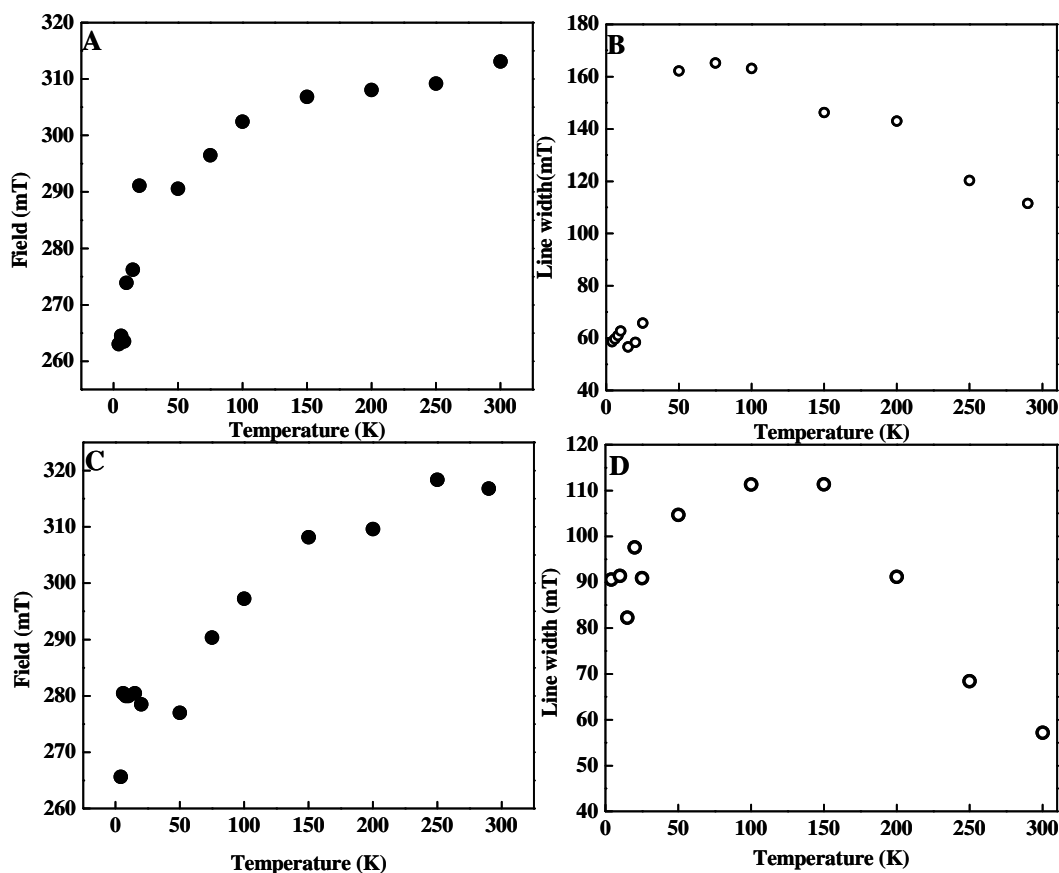


Figure 2.19: Variation in resonance with temperature and line width variation as a function of temperature for OASL-CoNPs (A and B) and DDOA-CoNPs.

In Figure 2.19 we plot the variation in resonance as a function of temperature and variation in line width as a function of temperature. We observe that as the temperature decreases the resonance shifts towards lower magnetic field value. This trend is observed for both the samples (Figure 2.18 A and C). However, small kinks in the trend are observed at 50 K (for OASL-CoNPs) and at 10 K (for DDOA-CoNPs). It is interesting to note that these kinks arise around blocking temperature for the samples. Decrease in resonance field H_0 with temperature can be attributed to increase in internal magnetic field.^{55,56} However we do not know why there should be marginal increase in the resonance at T_B . The line width increase gradually and then starts to become sharper in both the cases below 50 K. But in case of DDOA-CoNPs peaks are broad at lower temperature as compared to higher temperatures. Increase in line width with temperature for most of the temperature (except lower temperatures) can be attributed to the fact that as

temperatures are decreased the particle moments are unable to overcome the local anisotropy barrier and these become trapped in meta stable state.⁴⁵

2.6 Conclusion:

We have successfully shown the ability of sophorolipid to act as capping ligand for cobalt nanoparticle in aqueous medium. The cobalt nanoparticles obtained show good magnetic properties than the cobalt nanoparticles synthesized using pure oleic acid as capping ligand. The use of sophorolipid provides capability of synthesizing cobalt nanoparticles for application where they are required as stable dispersion in aqueous medium.

The second ligand used is 2 (dodecyloxy) acetic acid and it also act as a reasonably good stabilizing agent for CoNPs. From our studies it is observed that ligand used in the syntheses play an important role in governing the crystal structure of cobalt nanoparticles. The magnetic characteristics also crucially depend on the crystalline phase of the nanoparticles formed.

2.7 References:

- (1) Fertman, V. E. *Magnetic fluids guidebook: properties and applications*; Hemisphere New York, 1990.
- (2) Weller, D.; Moser, A.; Folks, L.; Best, M. E.; Lee, W.; Toney, M. F.; Schwickert, M. *IEEE Transactions on Magnetics* **2000**, *36*, 10.
- (3) Berkovsky, B. M.; Medvedev, V. F.; Krakov, M. S. *Magnetic Fluids: Engineering Applications* **1993**.
- (4) Feyen, M.; Heim, E.; Ludwig, F.; Schmidt, A. M. *Chemistry of Materials* **2008**, *20*, 2942.
- (5) Michalek, F.; Lagunas, A.; Jimeno, C.; Pericás, M. A. *Journal of Materials Chemistry* **2008**, *18*, 4692.
- (6) Ziolo, R. F.; Giannelis, E. P.; Weinstein, B. A.; O'Horo, M. P.; Ganguly, B. N.; Mehrotra, V.; Russell, M. W.; Huffman, D. R. *Science* **1992**, *257*, 219.
- (7) Awschalom, D. D.; Divincenzo, D. P. *Physics Today* **1995**, *48*, 43.
- (8) Raj, K.; Moskowitz, R. *Journal of Magnetism and Magnetic Materials* **1990**, *85*, 233.
- (9) Billas, I. M. L.; Chatelain, A.; Deheer, W. A. *Science* **1994**, *265*, 1682.
- (10) O'Handley, R. C. *Modern magnetic materials: principles and applications*; Wiley New York, 2000.
- (11) Ross, C. A. *Annual Review of Materials Research* **2001**, *31*, 203.
- (12) Skomski, R. *Journal of Physics: Condensed Matter* **2003**, *15*, R841.
- (13) Weller, D.; Doerner, M. F. *Annual Review of Materials Science* **2000**, *30*, 611.
- (14) Zhao, X. L.; Shi, Y. L.; Ca, Y. Q.; Mou, S. F. *Environmental Science & Technology* **2008**, *42*, 1201.
- (15) Odenbach, S. *Colloids and Surfaces a-Physicochemical and Engineering Aspects* **2003**, *217*, 171.
- (16) De Volder, M.; Reynaerts, D. *Sensors and Actuators a-Physical* **2009**, *152*, 234.

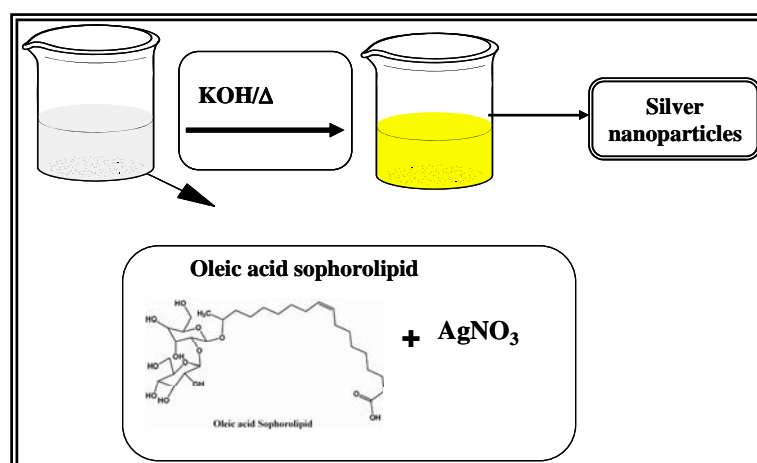
- (17) Jeong, U.; Teng, X.; Wang, Y.; Yang, H.; Xia, Y. *Advanced Materials* **2007**, *19*, 33.
- (18) Whitesides, G. M.; Kazlauskas, R. J.; Josephson, L. *Trends Biotechnol* **1983**, *1*, 144.
- (19) Wu, E. X.; Tang, H.; Jensen, J. H. *NMR in Biomedicine* **2004**, *17*, 478.
- (20) Xu, Y.; Mahmood, M.; Li, Z.; Dervishi, E.; Trigwell, S.; Zharov, V. P.; Ali, N.; Saini, V.; Biris, A. R.; Lupu, D.; Boldor, D.; Biris, A. S. *Nanotechnology* **2008**, *19*, 435102.
- (21) Sun, C.; Lee, J. S. H.; Zhang, M. *Advanced Drug Delivery Reviews* **2008**, *60*, 1252.
- (22) Jun, Y. W.; Seo, J. W.; Cheon, J. *Accounts of Chemical Research* **2008**, *41*, 179.
- (23) Puentes, V. F.; Krishnan, K. M.; Alivisatos, A. P. *Science* **2001**, *291*, 2115.
- (24) Murray, C. B.; Sun, S.; Gaschler, W.; Doyle, H.; Betley, T. A.; Kagan, C. R. *IBM Journal of Research and Development* **2001**, *45*, 47.
- (25) Chen, J. P.; Lee, K. M.; Sorensen, C. M.; Klabunde, K. J.; Hadjipanayis, G. C. *Journal of Applied Physics* **1994**, *75*, 5876.
- (26) Chen, J. P.; Sorensen, C. M.; Klabunde, K. J.; Hadjipanayis, G. C. *Journal of Applied Physics* **1994**, *76*, 6316.
- (27) Sun, S.; Murray, C. B. *Journal of Applied Physics* **1999**, *85*, 4325.
- (28) Hyeon, T. *Chemical Communications* **2003**, *9*, 927.
- (29) Wu, N.; Fu, L.; Su, M.; Aslam, M.; Wong, K. C.; Dravid, V. P. *Nano Letters* **2004**, *4*, 383.
- (30) Bala, T.; Arumugam, S. K.; Pasricha, R.; Prasad, B. L. V.; Sastry, M. *Journal of Materials Chemistry* **2004**, *14*, 1057.
- (31) Sidhaye, D. S.; Bala, T.; Srinath, S.; Srikanth, H.; Poddar, P.; Sastry, M.; Prasad, B. L. V. *Journal of Physical Chemistry C* **2009**, *113*, 3426.

-
-
- (32) Bala, T.; Swami, A.; Prasad, B. L. V.; Sastry, M. *Journal of Colloid and Interface Science* **2005**, 283, 422.
- (33) Zhang, L.; Somasundaran, P.; Singh, S. K.; Felse, A. P.; Gross, R. *Colloids and Surfaces A: Physicochemical and Engineering Aspects* **2004**, 240, 75.
- (34) Zhou, S.; Xu, C.; Wang, J.; Gao, W.; Akhverdiyeva, R.; Shah, V.; Gross, R. *Langmuir* **2004**, 20, 7926.
- (35) Shah, V.; Doncel, G. F.; Seyoum, T.; Eaton, K. M.; Zalenskaya, I.; Hagver, R.; Azim, A.; Gross, R. *Antimicrobial agents and chemotherapy* **2005**, 49, 4093.
- (36) Singh, S. K.; Felse, A. P.; Nunez, A.; Foglia, T. A.; Gross, R. A. *J. Org. Chem* **2003**, 68, 5466.
- (37) Van Bogaert, I. N. A.; Saerens, K.; De Muynck, C.; Develter, D.; Soetaert, W.; Vandamme, E. J. *Applied Microbiology and Biotechnology* **2007**, 76, 23.
- (38) Kasture, M.; Singh, S.; Patel, P.; Joy, P. A.; Prabhune, A. A.; Ramana, C. V.; Prasad, B. L. V. *Langmuir* **2007**, 23, 11409.
- (39) Silverstein, R. M.; Webster, F. X.; *Spectrometric Identification of Organic Compound* John Wiley & Sons, Inc.
- (40) Wang, W.; Chen, X.; Efrima, S. *Journal of Physical Chemistry B* **1999**, 103, 7238.
- (41) Wang, W.; Efrima, S.; Regev, O. *Langmuir* **1998**, 14, 602.
- (42) Dinega, D. P.; Bawendi, M. G. *Angewandte Chemie - International Edition* **1999**, 38, 1788.
- (43) Petit, C.; Taleb, A.; Pileni, M. P. *J. Phys. Chem. B* **1999**, 103, 1805.
- (44) Wiedwald, U.; Spasova, M.; Salabas, E. L.; Ulmeanu, M.; Farle, M.; Frait, Z.; Fraile Rodriguez, A.; Arvanitis, D.; Sobal, N. S.; Hilgendorff, M.; Giersig, M. *Physical Review B - Condensed Matter and Materials Physics* **2003**, 68, 644241.
- (45) Diehl, M. R.; Yu, J. Y.; Heath, J. R.; Held, G. A.; Doyle, H.; Sun, S.; Murray, C. B. *Journal of Physical Chemistry B* **2001**, 105, 7913.
-
-

- (46) Glavee, G. N.; Klabunde, K. J.; Sorensen, C. M.; Hadjipanayis, G. *C. Inorganic Chemistry* **1993**, *32*, 474.
- (47) Petit, C.; Taleb, A.; Pileni, M. P. *Journal of Physical Chemistry B* **1999**, *103*, 1805.
- (48) Petit, C.; Wang, Z. L.; Pileni, M. P. *Journal of Physical Chemistry B* **2005**, *109*, 15309.
- (49) Kotov, N. A. *Nanoparticle assemblies and superstructures*; CRC, **2006**.
- (50) Han, M.; Liu, Q.; He, J. H.; Song, Y.; Xu, Z.; Zhu, J. M. *Advanced Materials* **2007**, *19*, 1096.
- (51) Klabunde, K. J.; Richards, R. *Nanoscale materials in chemistry*; Wiley-Interscience New York, 2001.
- (52) Cullity, B. D.; Graham, C. D. *Introduction to magnetic materials*; Wiley-IEEE Press, **2008**.
- (53) Jeon, Y. T.; Moon, J. Y.; Lee, G. H.; Park, J.; Chang, Y. *Journal of Physical Chemistry B* **2006**, *110*, 1187.
- (54) Hanson, M.; Johansson, C.; Pedersen, M. S.; Morup, S. *Journal of Physics: Condensed Matter* **1995**, *7*, 9269.
- (55) Sobon, M.; Lipinski, I. E.; Typek, J.; Guskos, A.; Narkiewicz, U.; Podsiadly, M. In *Doped Nanopowders: Synthesis, Characterisation Applications*; Lojkowski, W., Blizzard, J. R., Narkiewicz, U., Fidelus, J. D., Eds. **2007**; Vol. 128, p 193-198.
- (56) Sobon, M.; Lipinski, I. E.; Guskos, A.; Typek, J.; Aidinis, K.; Guskos, N.; Narkiewicz, U.; Podsiadly, M. *Reviews on Advanced Materials Science* **2007**, *14*, 11.

Chapter 3

Sophorolipids as reducing/capping ligands: Understanding the synthetic parameters in batch process and to proceed for continuous process synthesis



This chapter discusses role of sophorolipid as reducing/capping ligand in synthesis of silver nanoparticles. Comparative study has been carried out using three different types of sophorolipids mainly stearic acid sophorolipid, oleic acid sophorolipid and linoleic acid sophorolipid which differ in number of double bonds present. Temperature and time dependent synthesis has been carried out and reaction conditions have been optimized in batch process. Using the optimized reaction conditions in batch process, synthesis of silver nanoparticles has been accomplished in continuous flow conditions in micro-reactors.

Part of the work described in this chapter has been published in:

- 1) M.B.Kasture, P Patel, A A Prabhune, C V Ramana, A A Kulkarni and B L V Prasad, *Journal of Chemical Science*, **2008**, 120, 6, 515-520.
- 2) D. V. Ravi Kumar, Manasi Kasture, A. A. Prabhune, C. V. Ramana, B. L. V. Prasad, A. A. Kulkarni, *Green Chemistry*, **2010**, 12, 609-615.

3.1 Introduction:

Metal nanoparticles mainly those of gold (Au) and silver (Ag) have generated huge interest in researchers as they possess size dependent properties that are profoundly different from their bulk counterparts. These nanoparticles possess a very strong absorption in the visible region due to surface plasmon resonance and by a higher extinction coefficients ($\epsilon > 10^8 \text{ M}^{-1} \text{ cm}^{-1}$) than commonly used organic fluorophores.¹ These properties enable their application in field like photonics,² electrochemical analysis,³ electronics,⁴ optoelectronics,⁵ catalysis,⁵⁻⁸ information storage,^{9,10} photography.¹¹

Extensive studies are carried out on silver nanoparticles to explore their optical properties.¹²⁻¹⁴ Silver nanoparticles are also being used in biosensing,¹⁵⁻¹⁸ biolabeling,¹⁹ imaging.¹⁹ Ag nanoparticles are also used as antimicrobial agent²⁰⁻²⁴ and as SERS substrates.²⁵⁻²⁷ Such enormous number of applications and interesting properties has naturally lead to the development of numerous methods for synthesis of Ag nanoparticles.

Common synthesis protocols used for synthesis of silver nanoparticles include solution based methods,²⁸⁻³² micelles,³³ reverse micelles,^{34,35} chemical deposition,³⁶ electrochemical,³⁷ pulse laser irradiation.^{12,38-40} Ligands that possess dual characteristic of reducing/capping are being preferred now a days by researchers as their use minimizes the number of reagents and number of steps involved in the synthetic procedures.⁴¹⁻⁴³ Utility of biomolecules for such dual activity is particularly preferred. The main motive behind this is to obtain environmentally friendly nanoparticles in the 'green synthesis' manner. Panáček et al. have synthesized Ag nanoparticles by reducing $[\text{Ag}(\text{NH}_3)_2]^+$ complex with four different saccharides namely glucose, galactose, maltose and lactose.³¹ Yin et al. have followed the Tollens reagent path for synthesis of Ag nanoparticles.²⁸ Hasell et al. have used water soluble polymers as capping ligands for synthesis of Ag nanoparticles.⁴⁴ Following the 'green chemistry' route Raveendran et al. have fabricated Ag nanoparticles using starch as capping/reducing agent.^{45,46} Huang et al. also have used polysaccharide method for synthesis of Ag and Au nanoparticles.⁴⁷ Such one step procedure for the synthesis of nanoparticles can also play a major

role for finding methods to scale up the synthesis of nanoparticles. Recent developments point out to continuous flow methods as an attractive strategy towards this goal.⁴⁸⁻⁵⁰ Continuous flow based methods are known to overcome the drawback of batch processes like reagent addition, mixing and non-uniform temperature distribution.⁵¹ Micro-fluidic syntheses can also be monitored online. Last few years have seen the emergence of micro-fluidic syntheses for nanoparticles as a better alternative for batch process based synthesis. This method has been used in syntheses of semiconducting,⁵²⁻⁵⁵ metallic,⁵⁶⁻⁵⁹ dielectric, magnetic,⁶⁰ and core-shell⁶¹ nanoparticles.⁴⁹

In our studies, a class of biosurfactant called sophorolipids attracted our attention as they can reduce metal ions to metal nanoparticles and cap the nanoparticles. In this chapter we discuss the role of sophorolipid as reducing and capping molecule on the synthesis of silver nanoparticles. We have used three different types of sophorolipids namely 1) linoleic acid derived sophorolipid (LASL), 2) oleic acid derived sophorolipid (OASL) and 3) stearic acid sophorolipid (SASL). Difference between these three SLs is number of cis double bonds present in the lipid part. LASL has 2; OASL has 1 while SASL has no double bond. A comparative study of synthesis of Ag nanoparticles in batch process has been carried out using these three sophorolipids. Reactions have been carried out at different temperatures and for different interval of time. The optimized reaction conditions obtained from the batch processes of nanoparticles have then been utilized in continuous flow method.

3.2 Synthesis of sophorolipids:

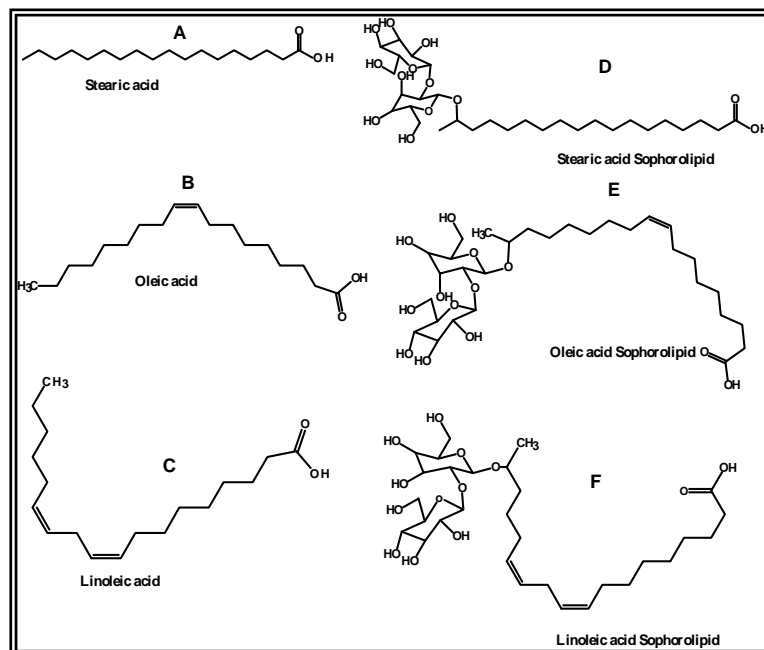


Figure 3.1: Structure of three lipids stearic acid (A), oleic acid (B) and linoleic acid (C) along with structure of sophorolipids, SASL (D), OASL (E), LASL (F).

Synthesis of sophorolipids was carried out in our group according to the reported procedure.⁶²⁻⁶⁴ Obtained sophorolipids were purified and characterized by NMR spectroscopy. The spectra agree well with the reported literature. Based on the spectral characteristics the structures of sophorolipids have been assigned and the same are shown in Figure 3.1.

3.3 Synthesis of Ag nanoparticles:

3.3.1 Using batch process:

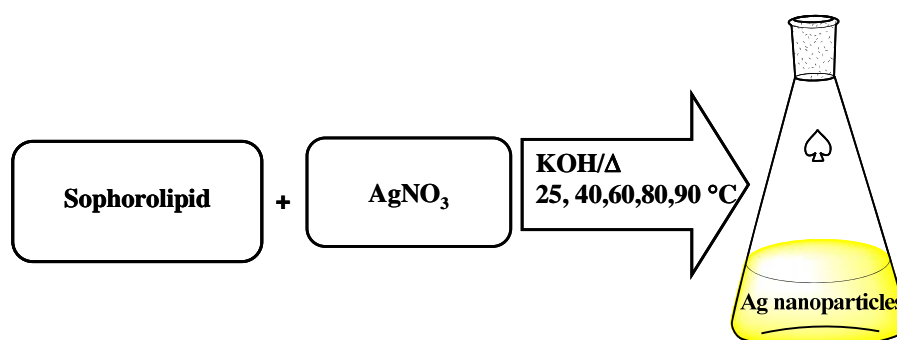


Figure 3.2: Schematics showing the batch process synthesis of Ag nanoparticles.

Synthesis of Ag nanoparticles using three different sophorolipids was carried out under basic pH condition. Schematic for synthesis of Ag nanoparticles using sophorolipid as reducing/capping moiety is shown in Figure 3.2. A mixture of SL and AgNO₃ is prepared in 100 mL of deionized water. The final concentration of both the solutions is 10⁻³ M. While maintaining the temperature of this mixture at various temperatures (25, 40, 60, 80, and 90°C), concentrated KOH is added. The colour of SL+AgNO₃ mixture turns yellow on addition of KOH. Time required for colour change to occur depends on the temperature at which the reaction is carried out. For the time dependent studies, mixture of AgNO₃ and sophorolipid (10⁻³ M each) were taken and heated to 90 °C and KOH was added to it at 90 °C. The mixture was constantly stirred while maintaining constant temperature using a thermostat (Julabo, Germany). To monitor the reaction the aliquots from the reaction mixture were sampled at equal time interval and analyzed with UV-Visible spectrophotometer. Same aliquots were used for dynamic light scattering (DLS) and transmission electron microscopy (TEM).

We will designate LASL capped/reduced Ag nanoparticles as Ag_LASL, OASL reduced/capped Ag nanoparticles as Ag_OASL and with SASL as Ag_SASL in the rest of this chapter.

3.3.2 Synthesis of Ag nanoparticles using stainless steel (SS) micro-reactor:

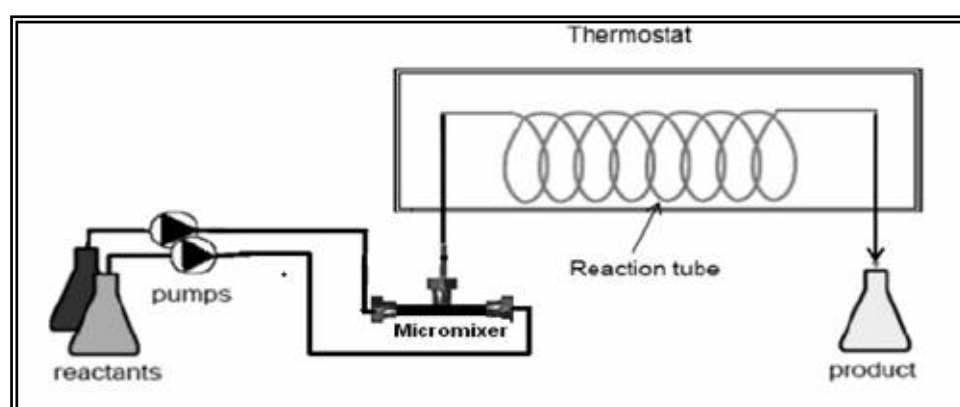


Figure 3.3: Set up for continuous flow synthesis of Ag nanoparticles using micro-reactor.

The optimized reaction conditions obtained in the batch process were used to carry out the reaction in continuous flow experiments in stainless steel (SS) tube. A stainless steel tube (SS316) of length 1m with 1.38 mm i.d. and 1.58 mm o.d. was used. For the synthesis two solutions were prepared 1) mixture of sophorolipid and AgNO₃ (10⁻³ M each) 2) KOH solution. These solutions were filled in two different syringes of volume 20 mL and 2 mL respectively. A dual syringe pump (Boading Longer, China) was used for driving the reactants into the micro-mixer and the reaction tube. The flow rate maintained was 0.27 mL/min for 20 mL syringe and 0.027 mL/min for 2 mL syringe. Outlet from two syringes was connected to a simple T-mixer (0.8 mm i.d.) using in-house designed and fabricated (Glass to Metal) Teflon connectors. The fluids mixed in the T-mixer subsequently entered the reaction tube. The T-mixture and the reaction tube were immersed in a thermostat (Julabo, Germany) and the temperature was maintained at 90 °C. The flow rates were maintained to achieve a residence time of 5 minutes, which is required to complete the reaction and the samples were collected at the outlet. Samples from batch process and from the micro-reactors were characterized by FTIR, TEM, DLS, and XRD.

3.4 Results

3.4.1 Temperature dependent studies.

(a) *UV-Visible spectroscopy:*

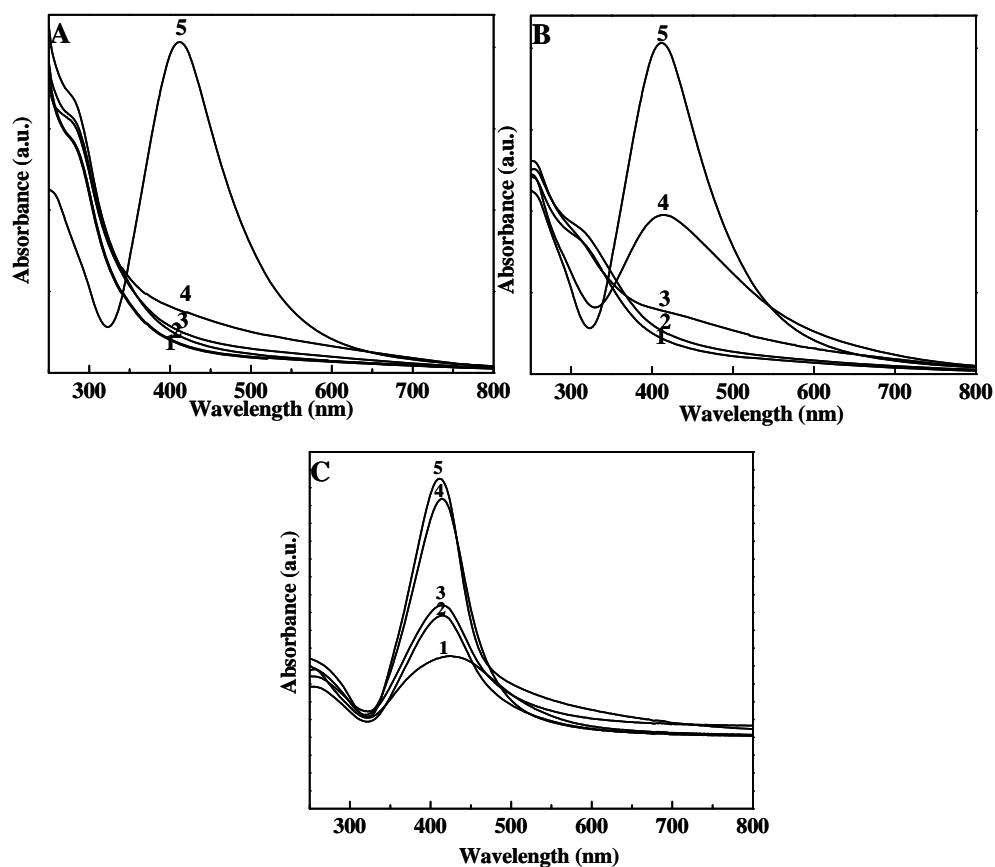


Figure 3.4: UV-visible spectra for Ag nanoparticles synthesized using LASL (A), OASL (B) and SASL (C) as reducing/capping ligand at different temperatures 25, 40, 60, 80 and 90 °C (curves 1 to 5 respectively).

Ag nanoparticles synthesized using three different sophorolipids were characterized by UV-visible spectroscopy. Figure 3.4 demonstrates the temperature dependent UV-visible spectra recorded after 5 min of reaction time for Ag nanoparticles synthesized using LASL (A), OASL (B) and SASL (C) as reducing and capping agent. Curves 1-5 correspond to different temperatures at which the reaction was carried out (25, 40, 60, 80 and 90 °C respectively). We observe that for Ag_LASL (Figure 3.4A) at lower temperatures no clear peak corresponding to

Ag is observed. But at higher temperature (i.e. 90 °C) we observe a sharp peak appearing at 420 nm which is characteristic feature of Ag nanoparticles. In Ag_OASL (Figure 3.4B) case at lower temperatures (25, 40 and 60 °C), no discernible peak is observed but a hump like feature at 420 nm could be seen (curve 1-3). As the temperature increases (80 and 90 °C), we observe the appearance of peak centered around 420 nm (curve 4 and 5). In case of SASL, the SPR peak is observed even at lower temperatures (Figure 4.5C, curves 1-5). In this case, as the temperature increases the intensity of the SPR peaks goes on increasing and is maximum at 90 °C.

(b) Transmission electron microscopy (TEM):

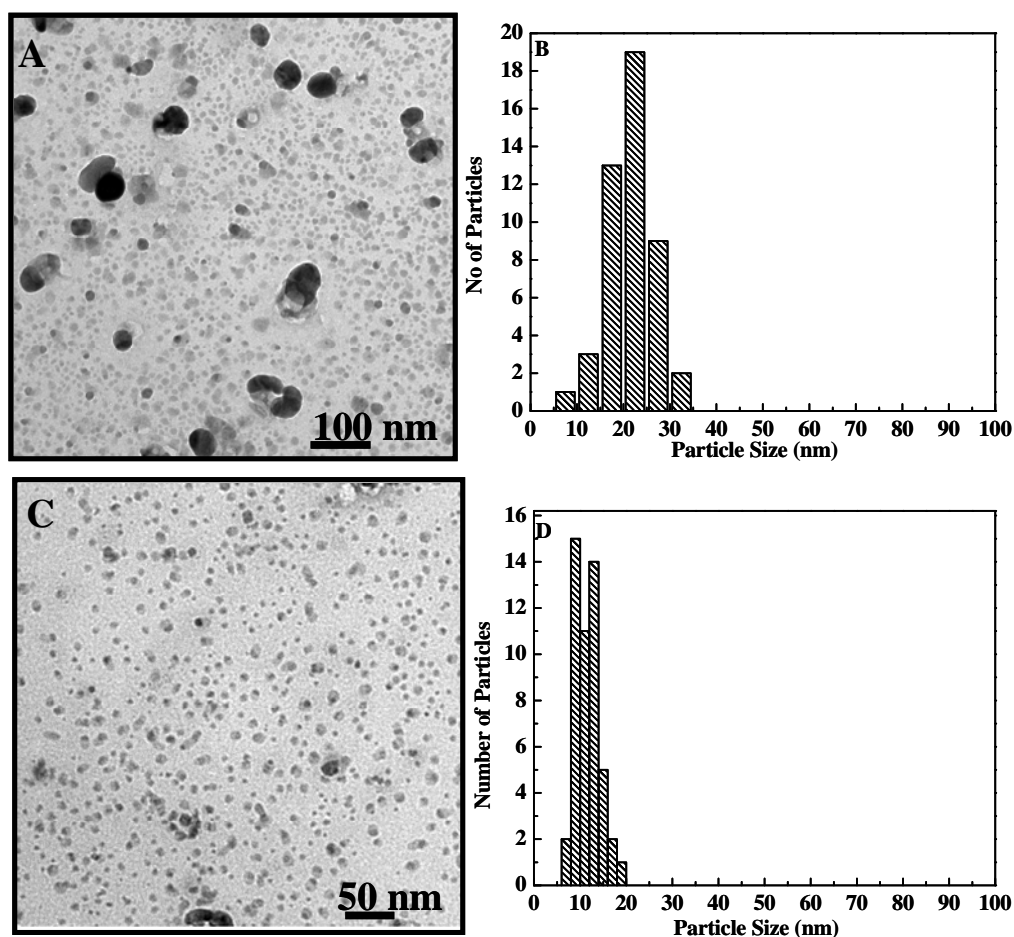


Figure 3.5: TEM images of Ag_LASL at 40 °C (A) and at 90 °C (C). Particle size measurement calculated from TEM analysis are shown in B and D for synthesis carried at 40 and 90 °C respectively.

TEM measurements were performed on Ag_LASL at different temperatures. The images along with respective particle size distribution are shown in Figure 3.5. Figure 3.5A illustrates the TEM image for Ag_LASL nanoparticles synthesized at lower temperature (40 °C). We observe that particles are irregular and poly-disperse in nature. The average particle size obtained was 22 nm (Figure 3.5 B). TEM images for Ag_LASL synthesized at 90 °C reveals that the particles are smaller in size with average particle size 11 nm as can be seen from particle size distribution (Figure 3.5 D).

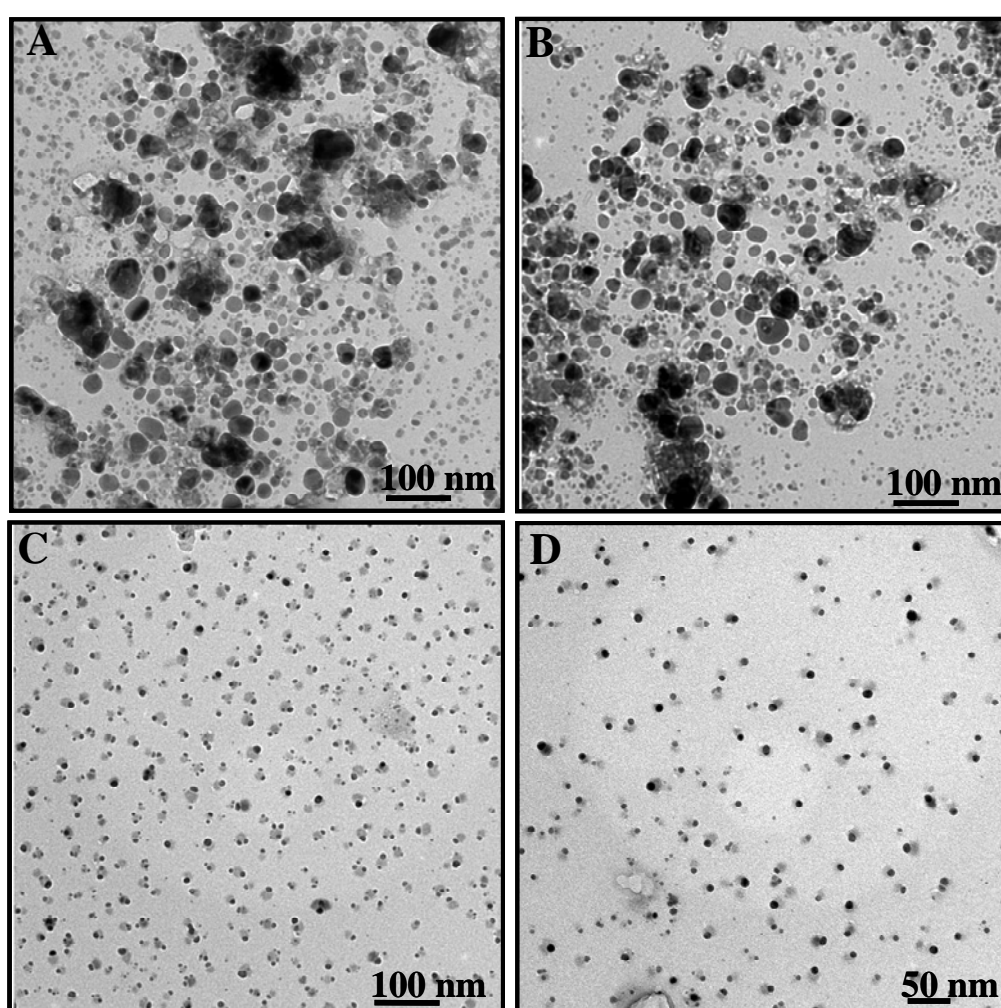
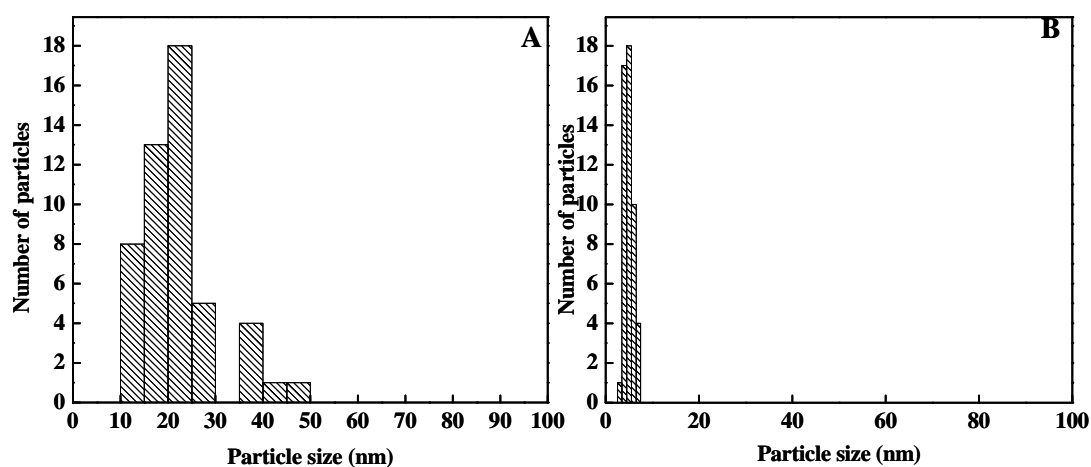


Figure 3.6: TEM images of Ag nanoparticles synthesized using OASL as reducing/capping moiety at different temperatures 40 °C (A-B) and 90 °C (C-D).

In a similar fashion the TEM images of Ag nanoparticles synthesized using OASL as reducing/capping ligand at two different temperatures (40 and 90 °C) are displayed in Figure 3.6. Here also similar trend is observed as was observed for LASL case. For particles synthesized at 40 °C, the particles are irregular and bigger in size (Figure 3.6 A and B) while Ag nanoparticles synthesized at higher temperature resulted in spherical and smaller particles (Figure 3.6 C and D). Particle size obtained from TEM measurements are shown in Figure 3.7A & B. The average particle size obtained for reaction at 40 and 90 °C are 23 and 5.5 nm



respectively.

Figure 3.7: Particle size distribution obtained from TEM analysis for Ag nanoparticles synthesized at 40 (A) and 90 °C (B).

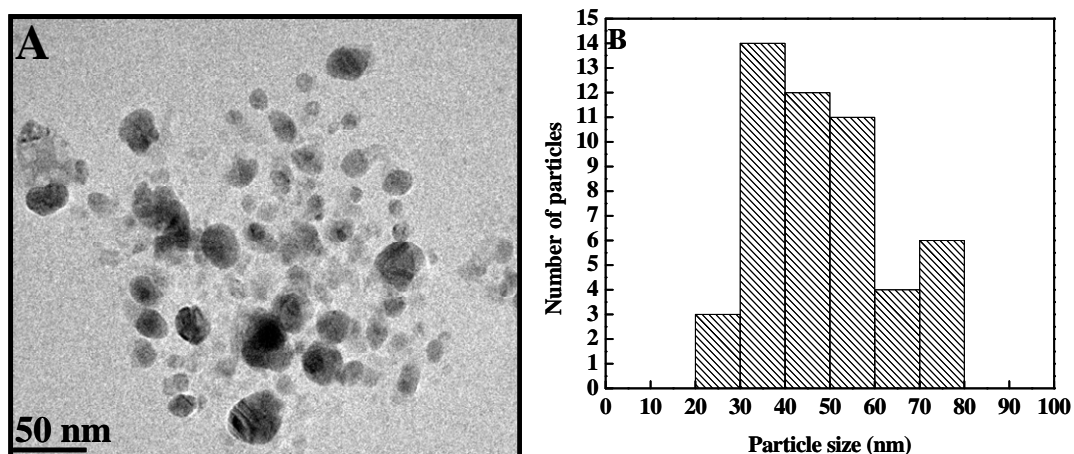


Figure 3.8: (A) TEM micrograph of Ag_SASL synthesized at 40 °C. (B) Particle size distribution obtained from the TEM images.

TEM analysis for Ag nanoparticles synthesized using SASL at lower temperatures (40 °C) is shown in Figure 3.8 A. Micrographs illustrates irregular and polydisperse particles with average particles size of 50 nm (Figure 3.8 B).

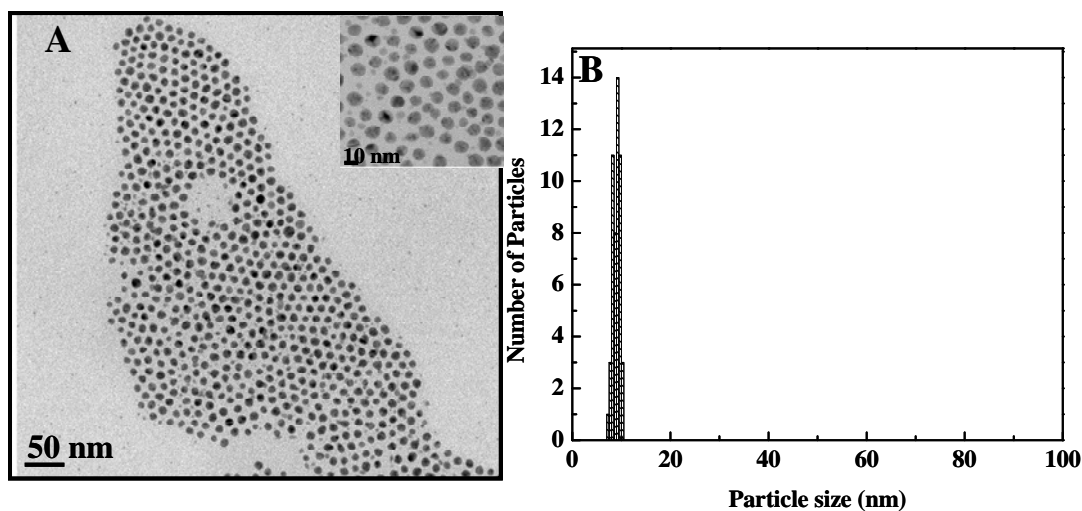


Figure 3.9: (A) TEM micrograph of Ag_SASL synthesized at 90 °C. (B) Particle size distribution obtained from the TEM images.

TEM analysis for Ag nanoparticles synthesized using SASL at higher temperatures (90 °C) is shown in Figure 3.9 A. Inset shows the magnified image. Particle size distribution is seen to be very narrow.

(c) *Dynamic Light Scattering (DLS)*

DLS measurements carried out for Ag nanoparticles synthesized using different sophorolipids is shown in Figure 3.10. Particle size measurements were carried out for 40 and 90 °C are shown for Ag_LASL (A and B), Ag_OASL (C and D) and Ag_SASL (E and F). We observe that at lower temperatures particles are bigger in size and polydisperse in nature while at higher temperatures particles are smaller (< 10 nm) showing mono-disperse nature. Obtained particle sizes and nature match with particle size distribution obtained from TEM measurements.

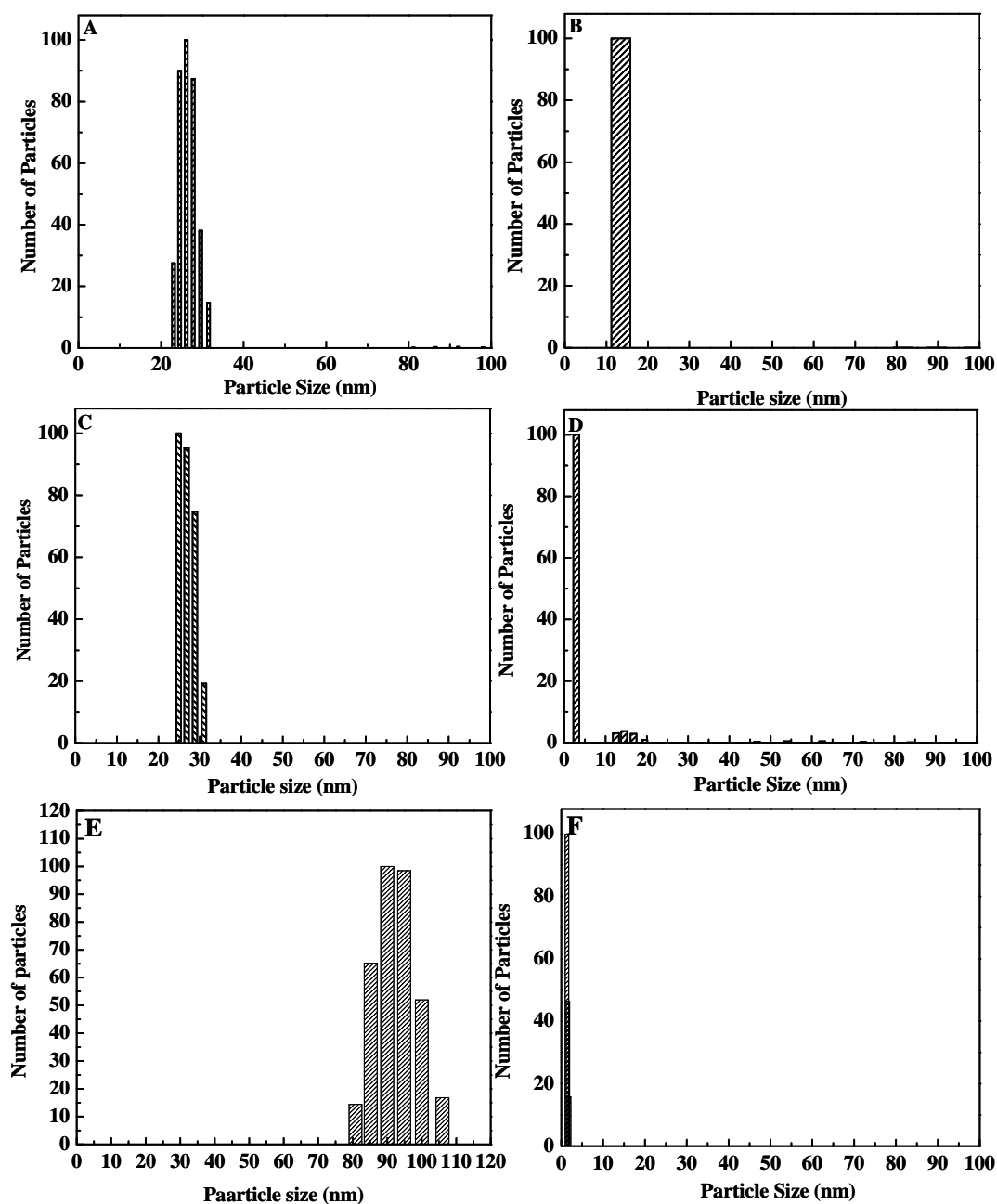


Figure 3.10: Particle size distribution of Ag nanoparticles obtained from DLS measurements at two different temperatures 40 and 90 °C for Ag_LASL (A and B), Ag_OASL(C and D) and Ag_SASL (E and F) as reducing/capping agent.

3.4.2 Time dependent studies for OASL and SASL as reducing/capping ligands.

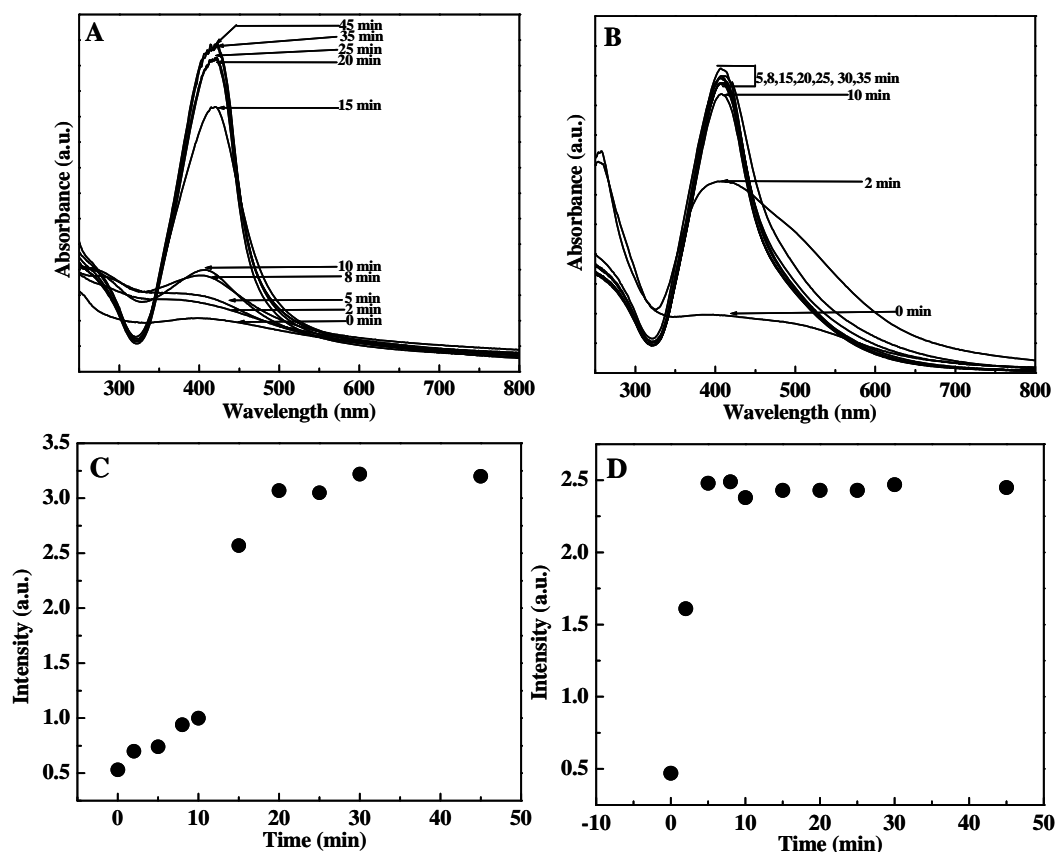


Figure 3.11: Time dependent studies for Ag_OASL (A) and Ag_SASL (B). Time scales are as indicated in figure. Figure C and D shows the intensity Vs time which informs about the saturation point obtained in both the cases.

Time dependent UV-vis studies were carried out for Ag_OASL (Figure 3.11 A) and Ag_SASL (Figure 3.11 B) at 90 °C. Time scale at which the spectra were monitored is indicated in the graph. In case of Ag_OASL, at start of the experiment the emergence of SPR is not well defined but as time increases the SPR peak builds up along with increase in intensity. In case of Ag_SASL the SPR peak intensity increases very rapidly initially and after that it remains constant. Graph of intensity vs time for Ag_OASL (Figure 3.11 C) and Ag_SASL (Figure 3.11 D) indicate the saturation time required for reaction. For Ag_OASL we see gradual increase in intensity of the SPR peak upto 20 min after which it attains a saturated value. On

the other hand, in case of Ag_SASL the intensity increases very rapidly in the first few minutes and gets saturated within 5 min of reaction time. Thus we can conclude that time required for completion of reaction in case of SASL is faster than in case of OASL.

3.5 Synthesis of Ag nanoparticles in a continuous flow manner

For details of Ag nanoparticles synthesis using continuous flow methods, see section 3.3.2. Samples collected from the SS tube micro-reactor were analyzed with UV-visible, DLS and TEM measurements.

3.5.1 UV-visible spectra.

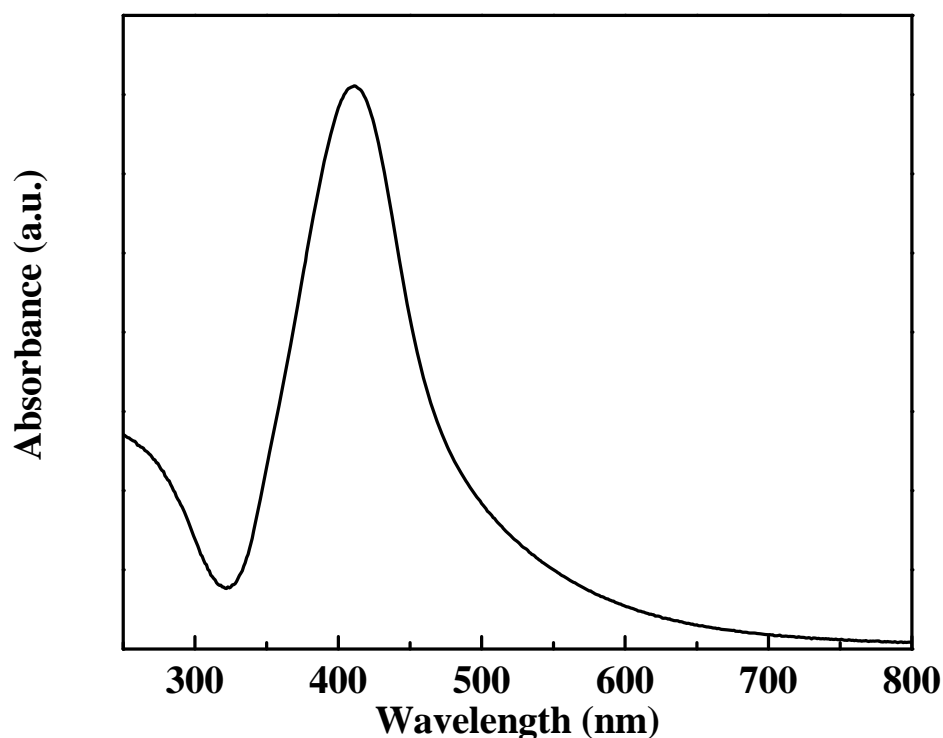


Figure 3.12 UV-visible spectrum for Ag_SASL synthesized in SS tube micro-reactor in continuous flow method.

Figure 3.12 shows the UV-visible spectrum for Ag nanoparticles reduced/capped with SASL in SS tube micro-reactor at 90 °C with 5 min residence time. From the figure, we observe a sharp surface plasmon resonance (SPR) peak centered around 420 nm which is the characteristic peak for Ag nanoparticles.^{65,66}

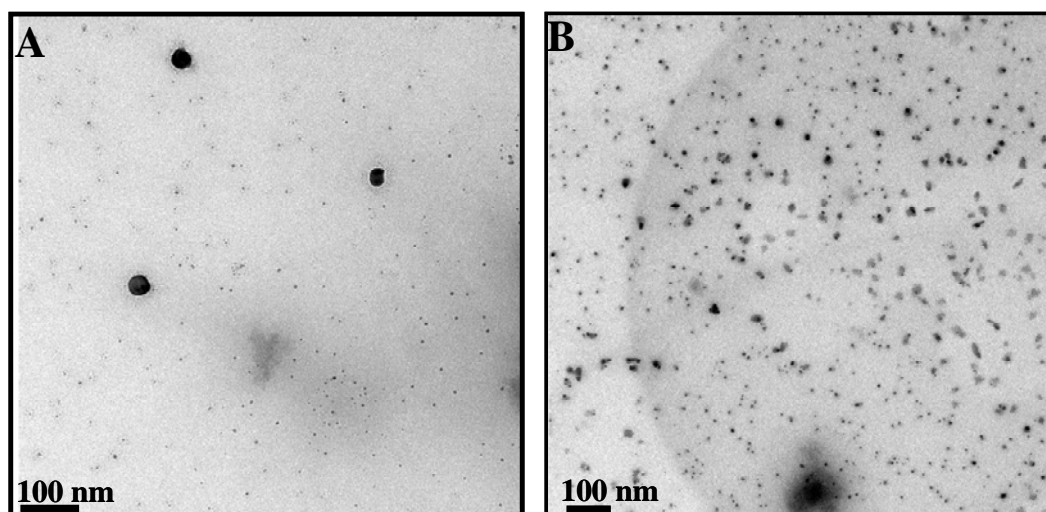
3.5.2 TEM analysis:

Figure 3.13: TEM images of SASL reduced/capped Ag nanoparticles synthesized in micro-reactor using SS tube.

TEM images corresponding to Ag nanoparticles synthesized in continuous manner in SS tube micro-reactor is depicted in Figure 3.13 which suggests the particles are almost monodisperse in nature. Particle size distribution was carried out using these images reveals the average particle size to be ~ 6.5 nm (Figure 3.13A). Particle size distribution was also carried out using dynamic light scattering measurements (DLS).

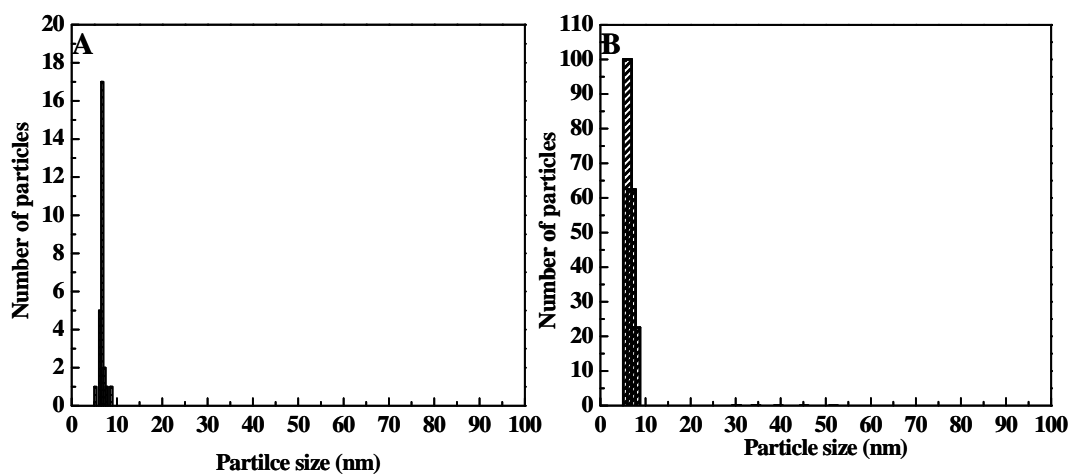


Figure 3.14: Particle size distribution of Ag nanoparticles reduced/capped with SASL using TEM measurements (A) and DLS measurements (B).

Average particle size obtained from the DLS measurements is ~ 7 nm which approximately matches with the average particle size obtained from TEM measurements (Figure 3.14 A and B).

3.5.3 XRD:

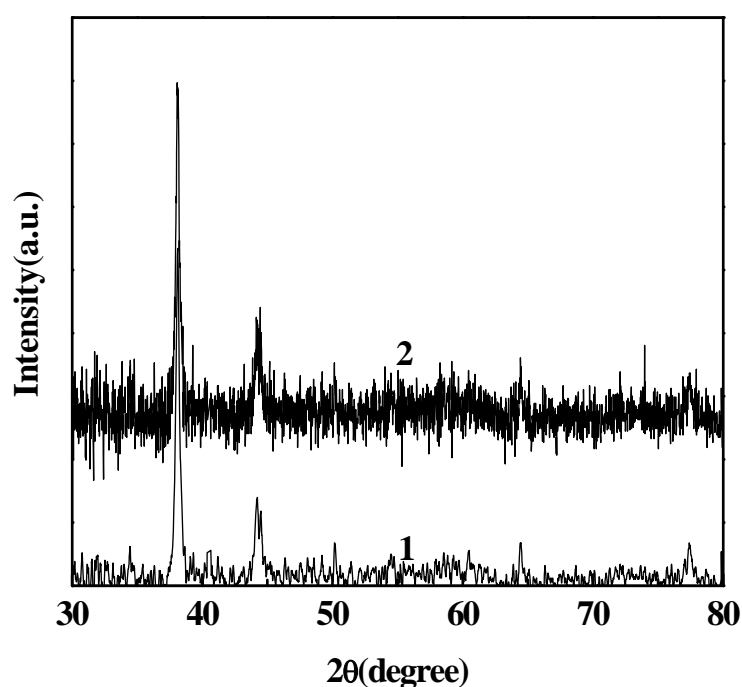


Figure 3.15: X-ray diffraction pattern recorded for Ag nanoparticles synthesized in batch process (curve 1) and continuous flow method (curve 2) using SASL as reducing/capping moiety.

X-ray diffraction analysis was carried out for Ag nanoparticles synthesized in batch process and continuous flow method using SASL as capping and reducing moiety (Figure 3.15 curve 1 and 2 respectively). The X-ray diffractograms reveal peaks at d values 2.36, 2.04, 1.44 and 1.22 Å which corresponds to Bragg's reflections (111), (200), (220) and (311) of the fcc phase of silver (Figure 3.15). XRD for both the Ag nanoparticles are same and show no difference in the structure. Thus Ag nanoparticles obtained in continuous flow method show no difference than the nanoparticles synthesized in batch process.

3.6 Discussion:

Efforts are being made to devise a method for synthesis of nanoparticles that would involve minimum number of steps and reactants. This could be possible by using multitasking ligands which can act both as reducing agent as well as capping agent. We envisaged that the bio-surfactant sophorolipids could be a good candidate that can reveal its capability of reducing and capping agent. The sophorose moiety plays the role of reducing agent in presence of the base while the lipid part acts as capping agent. In our studies, we considered three different types of sophorolipids.

1. Linoleic acid derived sophorolipid (LASL).
2. Oleic acid derived sophorolipid (OASL).
3. Stearic acid derived sophorolipid (SASL).

These three SL differ in number of cis double bonds present in their lipid part as observed from their structures shown in the Figure 3.1. Formation of Ag nanoparticles can be monitored by recording UV-visible spectrum. For Ag nanoparticles characteristic absorbance peak occurs at 420 nm. Occurrence of this peak in visible region is endorsed to the collective oscillation of conduction electrons and termed as surface plasmon resonance (SPR).^{65,66} The UV-visible spectra were recorded for Ag_LASL, Ag_OASL and Ag_SASL (Figure 3.4A, B and C respectively). The synthesis was carried out at different temperatures (25, 40, 60, 80 and 90 °C, curve 1-5 respectively). The UV-visible analysis suggests that the formation of nanoparticles is not complete for Ag_LASL and Ag_OASL at lower temperatures. This absence indicates that the reaction is incomplete at these temperatures (curve 1-4 for Ag_LASL and curve 1-3 for Ag_OASL). But as the temperature increases emergence of SPR peak becomes clear (Ag_LASL and Ag_OASL case) and at the highest temperature a well defined SPR peak is obtained. UV-visible recorded for Ag_SASL shows emergence of SPR peak even at lower temperatures (RT) and as the temperature increases, the peak becomes sharp and intense at higher temperatures. The variation observed in the UV-visible spectrum can be explained based on the double bond present in the lipid part of the sophorolipids. LASL contains two cis double bonds; OASL contains one cis double

bonds while SASL has no double bond. Silver ions bind very strongly to cis olefin bond.⁶⁷ During nanoparticle synthesis in case of LASL and OASL the silver ions bound very strongly to the cis double bonds may not get reduced quite readily. This could explain the slow reaction of Ag^+ ions with these SLs as evidenced by the slow built up of intensities in the SPR peak. In case of SASL, as there is no double bond the Ag^+ ions are easily reduced and the reaction proceeds very rapidly.

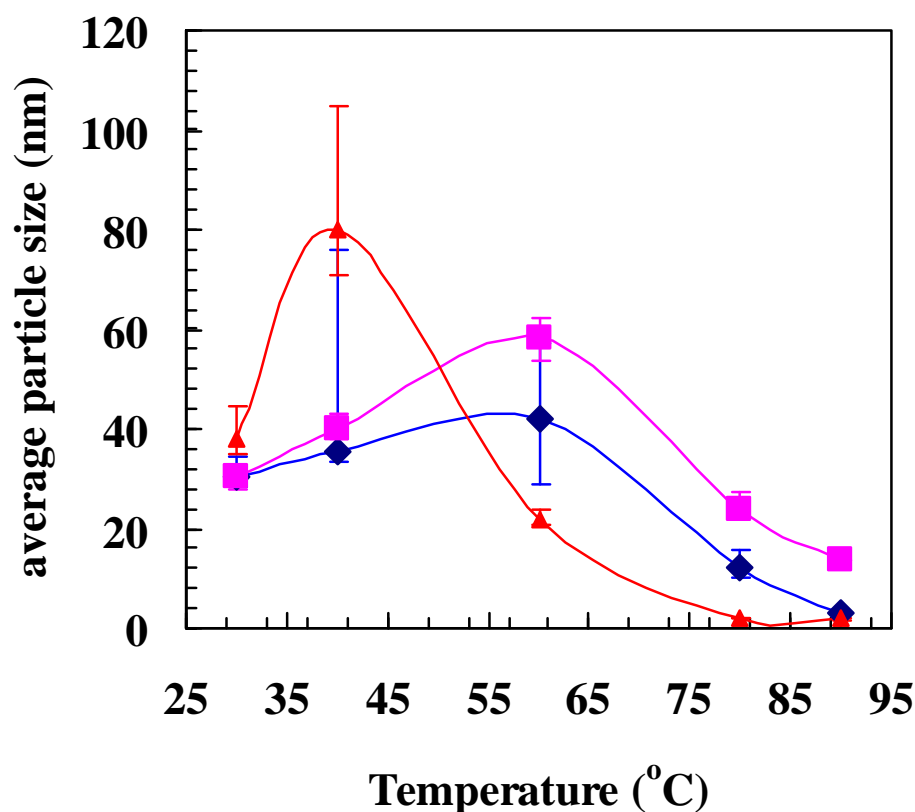


Figure 3.15: Average particle size for Ag nanoparticles obtained at different reaction temperatures using different sophorolipids SASL (red curve), OASL (blue curve) and LASL (magenta curve).

Temperature vs average particle size obtained from DLS measurement shows a peculiar trend (Figure 3.15) where the particle size initially increases with temperature and passes through a maximum. The particle size then becomes smaller with increase in temperature. This trend is observed for all the three sophorolipid cases. One of the plausible reasons for this particular behavior is that the reaction time is kept constant (5 min) while temperature is only varied. This could lead to incomplete reaction that builds some inhomogeneity in the reaction mixture leaving

unreduced metal ions along with metal nanoparticles formed. This could lead to growth of the particle on the surface of already formed nuclei. At highest temperature all the ions are reduced at once and hence the possibility of further growth is diminished. To support this hypothesis, we carried out time dependent synthesis of Ag nanoparticles using OASL at room temperature (RT) and monitored the particle growth for larger period of time (Figure 3.16). The absence of SPR peak after 5 min of the reaction indicated that the reaction has just started and is incomplete (Figure 3.16, curve1). Increase in reaction time is accompanied by increase SPR peak intensity (Figure 3.16, curves 2-5). Complete reaction is indicated by saturation of SPR peak after 21 h. Here the particle size during the initial stages of the reaction is 50 nm and at the end of 21 h the particle size observed is 12 nm.

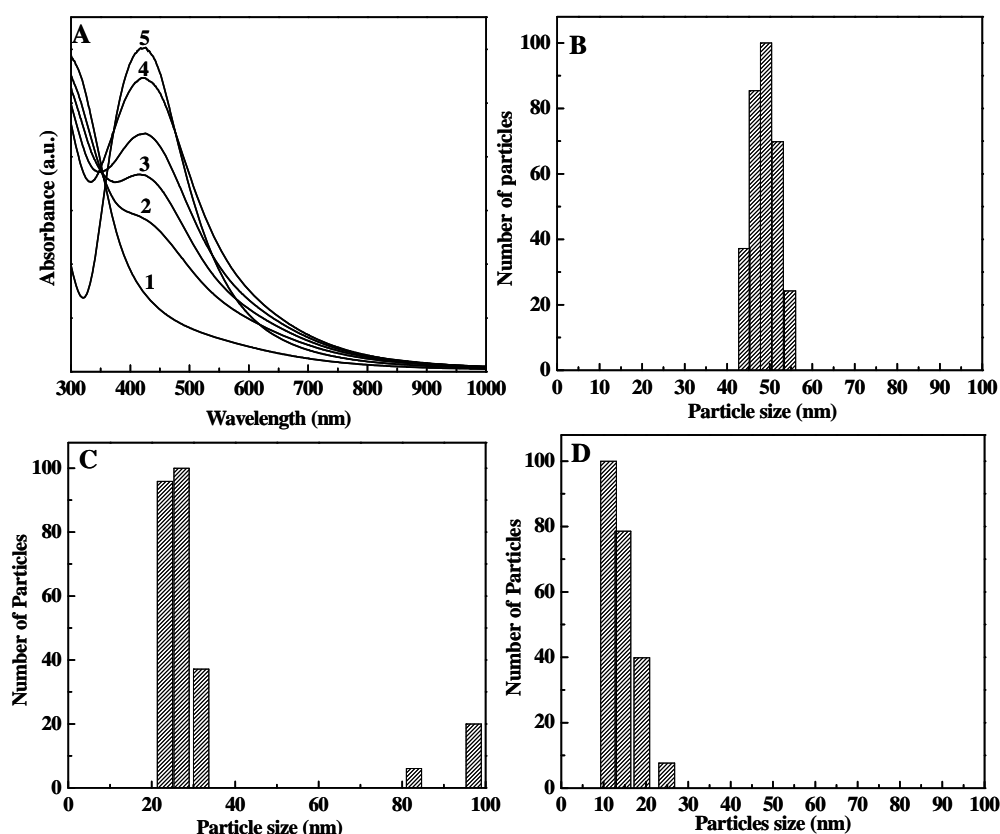


Figure 3.16: (A) Room temperature time dependent UV-visible spectroscopy curves 1-5 corresponds to 5min, 1,2,4,6, 21 hrs respectively. Figure B-D shows the particle size distribution obtained from DLS measurements recorded at different time intervals, 5min, 1h and 21 h respectively.

The time dependent (at 90 °C) results obtained by using LASL, OASL and SASL as reducing and capping ligand for Ag nanoparticles synthesis reveal that out of the above three sophorolipids, SASL leads to faster formation of Ag nanoparticles. This supports our argument that binding of Ag⁺ ions to double bond in case of OASL and LASL reduces the rate of reduction while in case of SASL, since no double bond is present, reaction is faster and occurs even at lower temperatures.

The difference in UV characteristic, particle size, nature of particle and time of reaction observed in all the experiments can be explained based on the following aspects.

1. As the number of cis double bonds present in the lipid part of the sophorolipid increased the reaction proceeds slowly. It is known that Ag⁺ ions have great affinity towards the cis double bond.⁶⁸
2. Binding of silver to cis double bond can be explained based on formation of olefinic silver complex. Strength of olefinic-silver complex is reported to depend on various factors like chain length, type of double bond (cis or trans) that follows a trend $R-CH=CH_2 > R_2C=CH_2 > cis\ R.CH=CH.R > trans\ R.CH=CH.R > R_2.C=CH.R > R_2C=CR_2$.⁶⁷
3. From the temperature dependent and time dependent particles size data (Figure 3.4 and 3.11) it can be concluded that at lower temperatures, reaction rate is slow. This favors growth process over the nucleation process while higher temperature favors nucleation over growth.⁶⁹

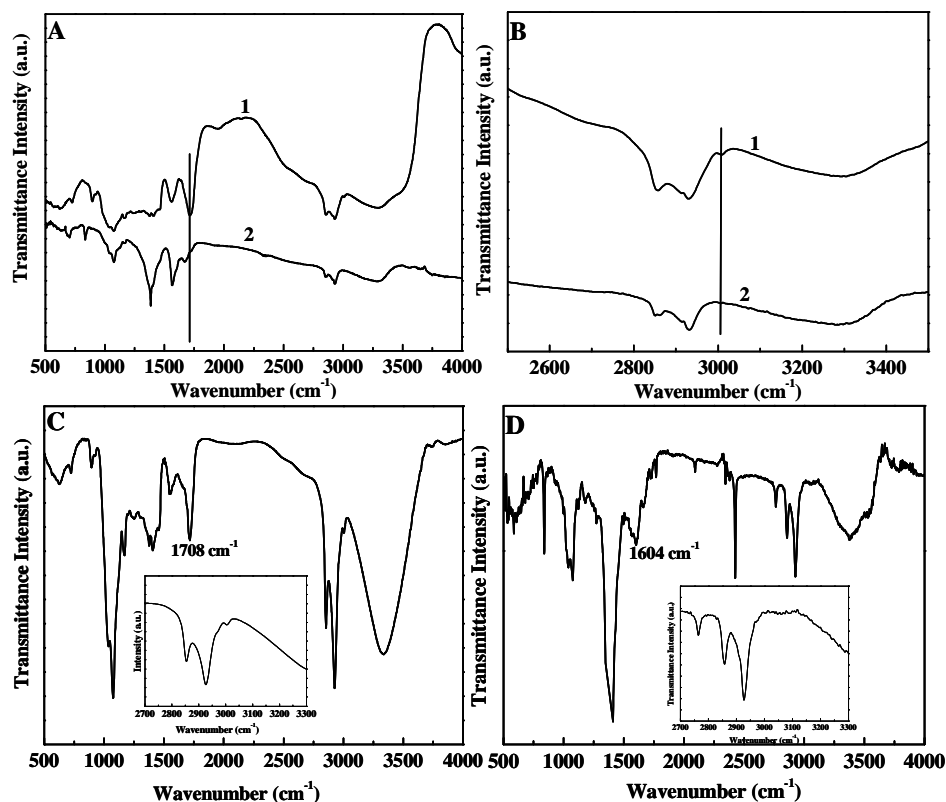


Figure 3.17: (A) FTIR spectrum for pure LASL (curve 1) and Ag_LASL (curve 2), (B) magnified spectra in the region 2700 to 3300 cm^{-1} , (C) FTIR spectrum for pure OASL, (D) Ag_OASL. Inset in C and D shows the magnified spectrum in the region 2700 to 3300 cm^{-1} highlighting the olefinic C-H band.

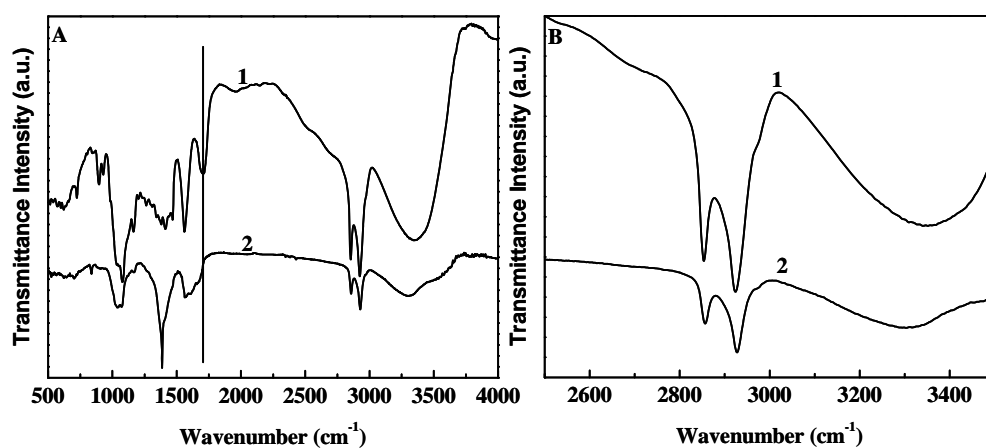


Figure 3.18: (A) Fourier infrared spectroscopy (FTIR) for SASL (curve 1) and SASL_Ag (curve 2). (B) Shows the spectra in the region 2600 cm^{-1} to 3400 cm^{-1} indicating the presence or absence of double bond

The hypothesis laid by us based on the presence of double bond can be supported by the FTIR measurements (Figure 3.17 and 3.18). The binding nature of SLs to the surface of nanoparticles is well explained by FTIR measurements. In case of SASL binding takes place only through –COOH (Figure 3.19B) end on the other hand, in case of LASL and OASL there are two possibilities through which the binding can take place: one through the –COOH end while the other is through the cis double bond (Figure 3.17 A-D).⁷⁰⁻⁷² The results endorse both the possibilities. However, one can clearly notice that whichever way the SLs bind to silver nanoparticle surface, the exterior is characterized by hydrophilic group and thus the silver particles are water re-dispersible.

From the detailed and systematic experiments carried out in the batch process, we conclude that SASL is the best candidate for experiments to be carried out in continuous flow methods as lower temperatures and shorter time intervals are required for the reaction. Therefore, using SASL as a reducing and capping agent, we synthesized silver nanoparticles in a continuous flow manner where the reaction temperature was kept at 90 °C and the residual time of 5 min. As expected, formation of very small particles with average particle size of 6.5 nm (Figure 3.14A) could be seen from TEM and DLS.

3.7 Conclusion:

Reducing and capping capabilities of sophorolipid have been unrivalled in this chapter. We used three different types of sophorolipid viz. linoleic acid sophorolipid, oleic acid sophorolipid and stearic acid sophorolipid which differ with respect to number of double bond present. Out of the three sophorolipids, SASL was adjudged to be the one which resulted faster formation of Ag nanoparticles as compared to remaining two sophorolipids. Reaction conditions for synthesis of Ag nanoparticles with respect to concentration of reactants, temperature and time were optimized in batch process. Using the optimized reaction conditions in batch process, synthesis of sophorolipid was carried out in continuous flow manner using an SS tube.

3.8 Reference:

- (1) Feldheim, D. L.; Foss, C. A. *Metal nanoparticles: synthesis, characterization, and applications*; CRC, 2001.
- (2) Maier, S. A.; Brongersma, M. L.; Kik, P. G.; Meltzer, S.; Requicha, A. A. G.; Atwater, H. A. *Adv. Mater* **2001**, *13*, 2.
- (3) Welch, C. M.; Compton, R. G. *Analytical and Bioanalytical Chemistry* **2006**, *384*, 601.
- (4) Li, Y.; Wu, Y.; Ong, B. S. *Journal of the American Chemical Society* **2005**, *127*, 3266.
- (5) Kamat, P. V. *The Journal of Physical Chemistry B* **2002**, *106*, 7729.
- (6) El-Sayed, M. A. *Accounts of Chemical Research* **2001**, *34*, 257.
- (7) Lewis, L. N. *Chemical Reviews* **1993**, *93*, 2693.
- (8) Moreno-Manas, M.; Pleixats, R. *Accounts of Chemical Research* **2003**, *36*, 638.
- (9) Murray, C. B.; Sun, S.; Doyle, H.; Betley, T. *MRS Bulletin-Materials Research Society* **2001**, *26*, 985.
- (10) Sun, S.; Murray, C. B.; Weller, D.; Folks, L.; Moser, A. *Science* **2000**, *287*, 1989.
- (11) Lam, D. M. K.; Rossiter, B. W. *Scientific American* **1991**, *265*, 48.
- (12) Jin, R.; Cao, Y.; Mirkin, C. A.; Kelly, K. L.; Schatz, G. C.; Zheng, J. G. *Science* **2001**, *294*, 1901.
- (13) Schultz, S.; Smith, D. R.; Mock, J. J.; Schultz, D. A. *Proceedings of the National Academy of Sciences of the United States of America* **2000**, *97*, 996.
- (14) Silva, T. J.; Schultz, S.; Weller, D. *Applied Physics Letters* **1994**, *65*, 658.
- (15) Han, M.; Gao, X.; Su, J. Z.; Nie, S. *Nature biotechnology* **2001**, *19*, 631.
- (16) Mirkin, C. A.; Letsinger, R. L.; Mucic, R. C.; Storhoff, J. J. *Nature* **1996**, *382*, 607.

- (17) West, J. L.; Halas, N. J. *Annual Review of Biomedical Engineering* **2003**, *5*, 285.
- (18) Liu, S. Q.; Tang, Z. Y. *Journal of Materials Chemistry*, *20*, 24.
- (19) Nicewarner-Pena, S. R.; Freeman, R. G.; Reiss, B. D.; He, L.; Pena, D. J.; Walton, I. D.; Cromer, R.; Keating, C. D.; Natan, M. J. *Science* **2001**, *294*, 137.
- (20) Kumar, A.; Vemula, P. K.; Ajayan, P. M.; John, G. *Nature Materials* **2008**, *7*, 236.
- (21) Ruparelia, J. P.; Chatterjee, A. K.; Duttagupta, S. P.; Mukherji, S. *Acta Biomaterialia* **2008**, *4*, 707.
- (22) Sanpui, P.; Murugadoss, A.; Prasad, P. V. D.; Ghosh, S. S.; Chattopadhyay, A. *International Journal of Food Microbiology* **2008**, *124*, 142.
- (23) Singh, S.; Patel, P.; Jaiswal, S.; Prabhune, A. A.; Ramana, C. V.; Prasad, B. L. V. *New Journal of Chemistry* **2009**, *33*, 646.
- (24) Sondi, I.; Salopek-Sondi, B. *Journal of colloid and interface science* **2004**, *275*, 177.
- (25) Dick, L. A.; McFarland, A. D.; Haynes, C. L.; Van Duyne, R. P. *The Journal of Physical Chemistry B* **2001**, *106*, 853.
- (26) Nie, S.; Emory, S. R. *Science* **1997**, *275*, 1102.
- (27) Hasell, T.; Lagonigro, L.; Peacock, A. C.; Yoda, S.; Brown, P. D.; Sazio, P. J. A.; Howdle, S. M. *Advanced Functional Materials* **2008**, *18*, 1265.
- (28) Yin, Y.; Li, Z. Y.; Zhong, Z.; Gates, B.; Xia, Y.; Venkateswaran, S. *Journal of Materials Chemistry* **2002**, *12*, 522.
- (29) Bonnemann, H.; Richards, R. M. *European Journal of Inorganic Chemistry* **2001**, *2001*, 2455.
- (30) Nickel, U.; Castell, A. Z.; Poppl, K.; Schneider, S. *Langmuir* **2000**, *16*, 9087.
- (31) Panacek, A.; Kvitek, L.; Prucek, R.; Kolar, M.; Vecerova, R.; Pizurova, N.; Sharma, V. K.; Nevecna, T.; Zboril, R. *J. Phys. Chem. B* **2006**, *110*, 16248.
-
-

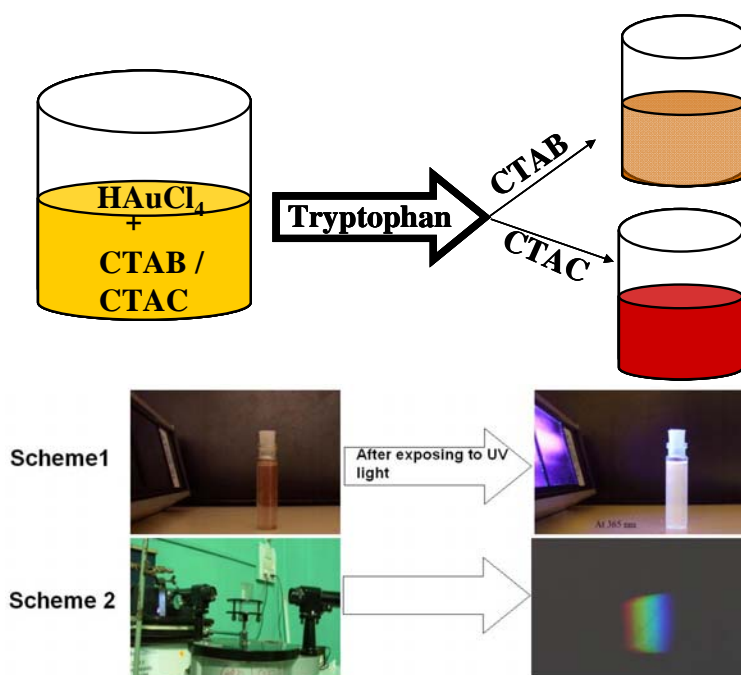
- (32) Lee, P. C.; Meisel, D. *The Journal of Physical Chemistry* **1982**, *86*, 3391.
- (33) Fievet, F.; Lagier, J. P.; Blin, B.; Beaudoin, B.; Figlarz, M. *Solid State Ionics* **1989**, *32-3*, 198.
- (34) Taleb, A.; Petit, C.; Pileni, M. P. *Chem. Mater* **1997**, *9*, 950.
- (35) Bagwe, R. P.; Khilar, K. C. *Langmuir* **2000**, *16*, 905.
- (36) Zoval, J. V.; Stiger, R. M.; Biernacki, P. R.; Penner, R. M. *J. Phys. Chem* **1996**, *100*, 837.
- (37) Yin, B.; Ma, H.; Wang, S.; Chen, S. *J. Phys. Chem. B* **2003**, *107*, 8898.
- (38) Mafune, F.; Kohno, J.; Takeda, Y.; Kondow, T.; Sawabe, H. *J. Phys. Chem. B* **2000**, *104*, 8333.
- (39) Henglein, A.; Giersig, M. *J. Phys. Chem. B* **1999**, *103*, 9533.
- (40) Cason, J. P.; Khambaswadkar, K.; Roberts, C. B. *Ind. Eng. Chem. Res* **2000**, *39*, 4749.
- (41) Si, S.; Mandal, T. K. *Chemistry-A -European Journal-* **2007**, *13*, 3160.
- (42) Si, S.; Bhattacharjee, R. R.; Banerjee, A.; Mandal, T. K. *Chemistry-A-European Journal* **2006**, *12*, 1256.
- (43) Bhattacharjee, R. R.; Das, A. K.; Haldar, D.; Si, S.; Banerjee, A.; Mandal, T. K. *Journal of Nanoscience and Nanotechnology* **2005**, *5*, 1141.
- (44) Hasell, T.; Yang, J. X.; Wang, W. X.; Brown, P. D.; Howdle, S. M. *Materials Letters* **2007**, *61*, 4906.
- (45) Raveendran, P.; Fu, J.; Wallen, S. L. *J. Am. Chem. Soc* **2003**, *125*, 13940.
- (46) Raveendran, P.; Fu, J.; Wallen, S. L. *Green Chemistry* **2006**, *8*, 34.
- (47) Huang, H.; Yang, X. *Carbohydrate research* **2004**, *339*, 2627.
- (48) Jahn, A.; Reiner, J. E.; Vreeland, W. N.; DeVoe, D. L.; Locascio, L. E.; Gaitan, M. *Journal of Nanoparticle Research* **2008**, *10*, 925.
- (49) Song, Y.; Hormes, J.; Kumar, C. *Small* **2008**, *4*, 698.

- (50) Song, Y.; Modrow, H.; Henry, L. L.; Saw, C. K.; Doomes, E. E.; Palshin, V.; Hormes, J.; Kumar, C. *Chem. Mater* **2006**, *18*, 2817.
- (51) Duraiswamy, S.; Khan, S. A. *Small* **2009**, *5*, 2828.
- (52) Chan, E. M.; Mathies, R. A.; Alivisatos, A. P. *Nano Letters* **2003**, *3*, 199.
- (53) He, S. T.; Liu, Y. L.; Uehara, M.; Maeda, H. *Materials Science and Engineering B-Solid State Materials for Advanced Technology* **2007**, *137*, 295.
- (54) Nakamura, H.; Yamaguchi, Y.; Miyazaki, M.; Maeda, H.; Uehara, M.; Mulvaney, P. *Chemical Communications* **2002**, 2844.
- (55) Nakamura, H.; Yamaguchi, Y.; Miyazaki, M.; Uehara, M.; Maeda, H.; Mulvaney, P. *Chemistry Letters* **2002**, 1072.
- (56) Edel, J. B.; Fortt, R.; deMello, J. C.; deMello, A. J. *Chemical Communications* **2002**, 1136.
- (57) Shalom, D.; Wootton, R. C. R.; Winkle, R. F.; Cottam, B. F.; Vilar, R.; deMello, A. J.; Wilde, C. P. *Materials Letters* **2007**, *61*, 1146.
- (58) Wagner, J.; Kirner, T.; Mayer, G.; Albert, J.; Kohler, J. M. *Chemical Engineering Journal* **2004**, *101*, 251.
- (59) Wagner, J.; Kohler, J. M. *Nano Letters* **2005**, *5*, 685.
- (60) Hassan, A. A.; Sandre, O.; Cabuil, V.; Tabeling, P. *Chemical Communications* **2008**, 2008, 1783.
- (61) Khan, S. A.; Jensen, K. F. *Advanced Materials* **2007**, *19*, 2556.
- (62) Shah, V.; Doncel, G. F.; Seyoum, T.; Eaton, K. M.; Zalenskaya, I.; Hagver, R.; Azim, A.; Gross, R. *Antimicrobial agents and chemotherapy* **2005**, *49*, 4093.
- (63) Singh, S. K.; Felse, A. P.; Nunez, A.; Foglia, T. A.; Gross, R. A. *Journal of Organic Chemistry* **2003**, *68*, 5466.
- (64) Van Bogaert, I. N. A.; Saerens, K.; De Muynck, C.; Develter, D.; Soetaert, W.; Vandamme, E. J. *Applied Microbiology and Biotechnology* **2007**, *76*, 23.
- (65) Henglein, A. *The Journal of Physical Chemistry* **1993**, *97*, 5457-5471.
-
-

- (66) Mulvaney, P. *Langmuir* **1996**, *12*, 788.
- (67) Giddings, J. C.; Grushka, E.; Cazes, J.; Brown, P. R. *Advances in Chromatography: Volume 14*; CRC.
- (68) Silverstein, R. M.; Webster, F. X.; *Spectrometric Identification of Organic Compounds* John Wiley & Sons, Inc, Sixth Edition 1997.
- (69) Mohamed, M. B.; Wang, Z. L.; El-Sayed, M. A. *J. Phys. Chem. A* **1999**, *103*, 10255.
- (70) Bala, T.; Swami, A.; Prasad, B. L. V.; Sastry, M. *Journal of Colloid and Interface Science* **2005**, *283*, 422.
- (71) Wang, W.; Chen, X.; Efrima, S. *Journal of Physical Chemistry B* **1999**, *103*, 7238.
- (72) Wang, W.; Efrima, S.; Regev, O. *Langmuir* **1998**, *14*, 602.

Chapter 4

Halide ion effect on shape of Au nanoparticles: Fluorescence and white light emission



This chapter discusses the effect of anions on the shape of Au nanoparticles synthesized in presence of cetyltrimethylammonium salts. Reduction of Au^{3+} ions is carried out using tryptophan. Spherical nanoparticles formed in case of cetyltrimethylammonium chloride (CTAC) while triangular shaped particles are formed when cetyltrimethylammonium bromide (CTAB) is used. The possible reasons for such a difference have been presented and are the focal point of this chapter. Interestingly emission of white light is observed from the triangular nanoparticle solution when exposed to UV-light. The possible cause for such emission characteristics has also been delineated.

Part of the work described in this chapter has been published in:

Manasi Kasture, Murali Sastry and B.L.V Prasad, *Chemical Physics Letters*, 2010, 484, 271–275.

4.1 Introduction:

Usage of stained glasses to decorate windows has been practice a wide spread from ancient times. Recently it has been realized that the beautiful colours that these glasses display are due to the noble metal nanoparticles like silver, gold, copper and their alloys that get incorporated in them during their preparation.¹ It has been realized that the color (optical absorbance) of the nanoparticle varies more dramatically with shape than size. With advancement of synthetic methods, recent focus has been shifted to the controlled synthesis of anisotropic noble metal nanoparticles like nanotriangles/prism or nanorods as these evince properties such as NIR absorption,²⁻⁶ anisotropic electrical conductivity⁷ and strong enhancement of electric fields at the vertices.⁸ Shape dependent properties of these nanomaterials enable their application in fields like cancer hyperthermia,^{8,9} electromagnetic waveguides,¹⁰ SERS¹¹⁻¹⁴ and infrared radiation absorbing optical coatings,⁴ imaging,¹⁵ enhanced fluorescence.¹⁶⁻²⁰ These exciting properties and various applications have encouraged researchers to take up the challenge to synthesize anisotropic nanoparticles more vigorously.

Synthetic methods used for making of anisotropic materials include photochemical transformation of spherical particles,²¹⁻²³ wet chemical synthesis with,⁶ or without template etc.²⁴⁻³⁰ Methods that utilize liquid crystals and polymer templates have also been found to be effective to control the shape of nanoparticles.^{31,32} A recent trend that has emerged in the syntheses of anisotropic nanoparticles is use of biological routes using plant extract, bacteria etc.^{4,8,33} Synthesis of nanoparticles of various morphologies using droplet based microfluidic techniques are also gaining lot of interest these days.³⁴

Inorganic fluorescent materials are of great interest and are considered as replacement for dyes in biolabeling and as solid state emitters.^{35,36} Amongst all the nanoparticles, semiconductor nanoparticles are well known for their unique size dependent emission characteristics. A clever combination of different sized semiconducting nanoparticles could lead to white light emission.³⁷ So lots of investigations are on to develop semiconducting nanoparticle mixtures that may emit white light.^{37,38} However, considering the toxicity of the Cd²⁺ metal ions that

constitute many of these semi conducting nanoparticles,³⁹ greater attention is being paid to the search for the substitutes of such systems. One of the features noble metal nanotriangles/prism display is enhancement of fluorescence of fluorophores attached to them. Aslan et al. have shown fluorescence enhancement of Indocyaninegreen (ICG) in presence of silver nanoprisms.^{17,19,20} It is reported that presence of metal in the proximity of fluorophores also decreases the life time thus increasing the photo stability due to less excited state time for photochemical process to occur. Thus it is observed that presence of metal in the vicinity of fluorophore leads to increased intensity and a reduction in fluorophore lifetime.⁴⁰

Work presented in this chapter deals with formation of different shapes of Au nanoparticles in presence of different surfactants. We have used two surfactants, namely cetyltrimethyl ammonium chloride (CTAC) and cetyltrimethyl ammonium chloride (CTAB) for synthesis of gold nanoparticles. Tryptophan which is an amino acid was used as reducing agent in these experiments. Particles with different morphologies are observed for CTAC (monodispersed spherical particle) and CTAB (triangular particles). The difference in the type of halide ion present with these surfactants is probably one of the main factors for the formation of different shapes. The most exciting observation is white light emission from the oxidized tryptophan –gold nanotriangular combination when exposed to UV light of 365 nm.

Part A

4.2 Synthesis of Au nanoparticles:

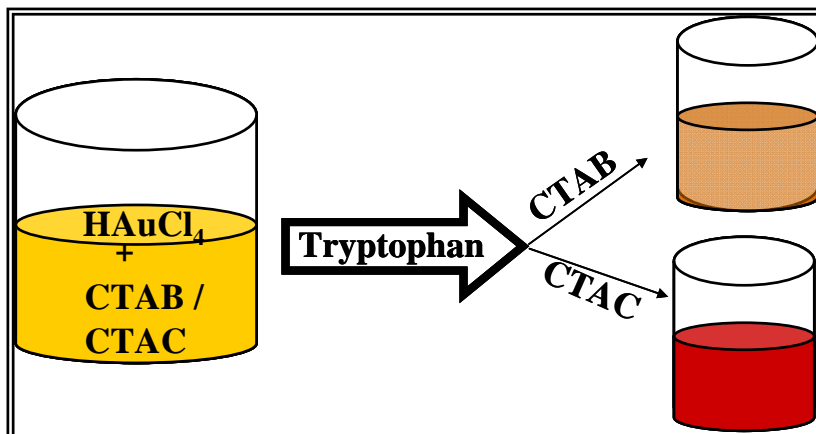


Figure 4.1: Method for synthesis of Au nanoparticles using CTAB and CTAC as surfactants and tryptophan as reducing agent.

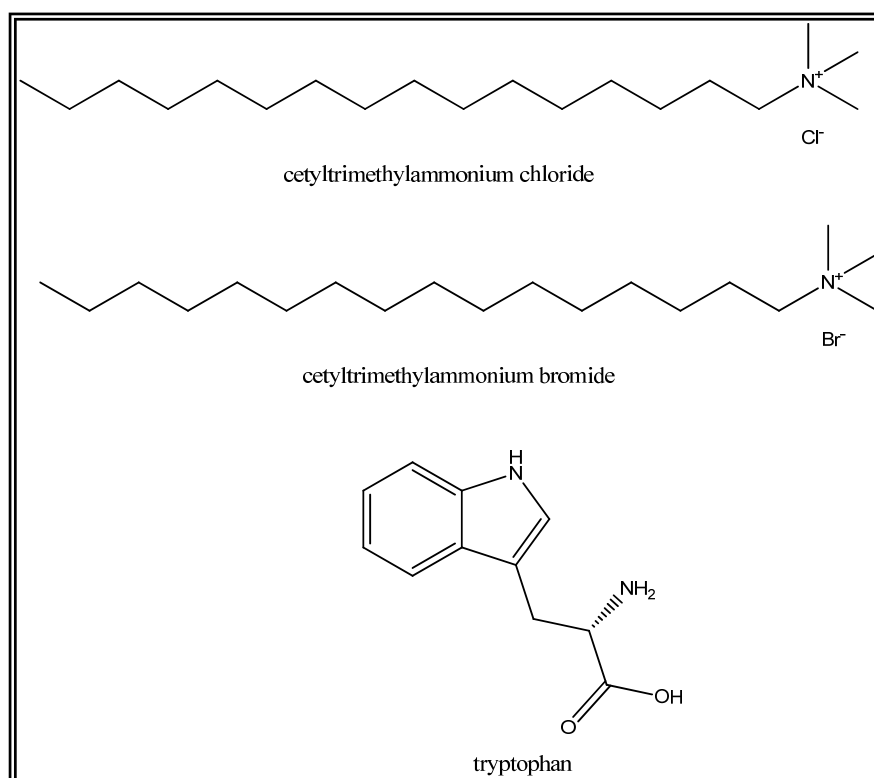


Figure 4.2: Structure of cetyltrimethyl ammonium chloride (CTAC), cetyltrimethyl ammonium bromide (CTAB) and tryptophan.

Schematic of the Au nanoparticle preparation as used for the work described in this chapter is shown in Figure 4.1. As seen from the scheme we have used CTAC and CTAB as surfactants and tryptophan as reducing agent. Structures for CTAC, CTAB and tryptophan are shown in Figure 4.2. It is well known that the critical micelle concentration (CMC) for CTAC is 16×10^{-3} M while that of CTAB is 1×10^{-3} M. In our study we considered three different concentrations of CTAC and CTAB (at CMC, above CMC 10^{-2} M and below CMC 10^{-4} M). In a typical experiment, to 100 mL solution of CTAC/CTAB, tetrachloroauric acid (HAuCl_4) was added so that it yields a final concentration of 10^{-3} M. HAuCl_4 which is now present with CTAB or CTAC is reduced by adding 10^{-3} M tryptophan. Immediate colour change from orange yellow to wine red was observed for solution where the surfactant concentration is at CMC or below CMC, while in case of solution above CMC, no immediate change was observed. These solutions were kept in static condition. For CTAC slight colour change was observed after 5 min and with increase in time the colour changed from faint red to deep wine red. After about 45 min, colour change is complete. In case of CTAB colour change was observed only after 2.5 hrs and gradually as time increases the colour developed to reddish brown. Complete colour change was observed after 6 hrs. Samples were purified by centrifuging them at 8000 rpm for 15 min. Pellet obtained were re-dispersed in de-ionized water. Centrifugation was carried out twice to ensure complete removal of excess surfactant and tryptophan.

4.3 Results:

4.3.1: UV-visible

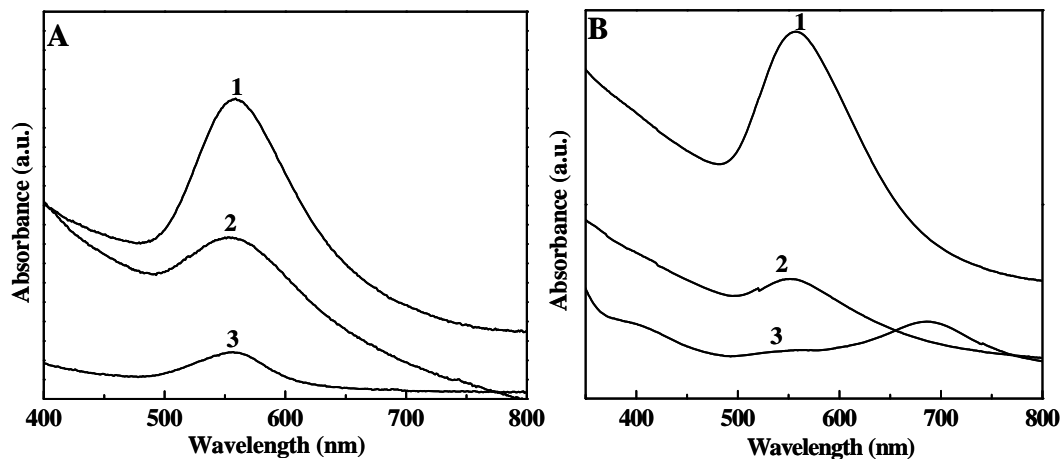


Figure 4.3: UV-Visible spectra recorded for Au nanoparticles synthesized using tryptophan as reducing agent in presence of CTAC (A) and CTAB (B). Curve 1-3 corresponds to CTAC/CTAB concentration below CMC, at CMC and above CMC respectively.

Figure 4.3 shows the UV-spectra for Au nanoparticles synthesized in presence of CTAC (A) and CTAB (B) at different concentrations as illustrated. It is seen that for CTAC at all concentrations only one peak centered around 520 nm is present. This peak is the feature of UV-visible spectra for Au nanoparticles which occurs due to surface plasmon resonance.⁴¹ In case of CTAB for concentration at CMC and below CMC are similar to the case of CTAC. But at a concentration above CMC, we observe two peaks one centered around 520 nm and other appearing at 710 nm. This indicates the formation of anisotropic nanoparticles or aggregated spherical structure. However transmission electron microscopy images (vide infra) conclude that the absorbance features are due to the formation of anisotropic triangular particles. Time dependent UV-visible spectra were recorded for this sample in order to see the development of the peak.

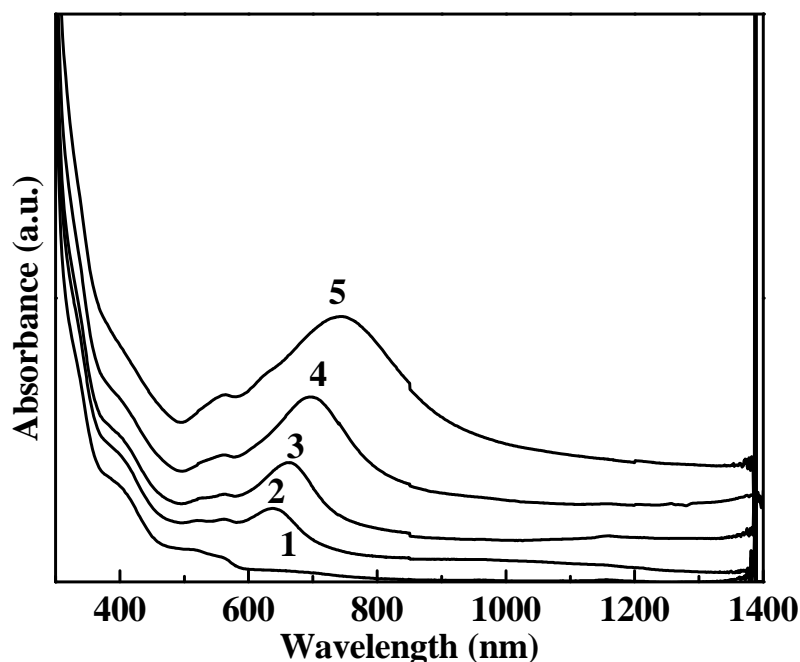


Figure 4.4: Time dependent UV-visible spectrum for Au nanoparticles synthesized in presence of CTAB with concentration above CMC. Curves 1-5 correspond to time interval of 2, 5, 8, 24 and 70 h respectively.

Figure 4.4 shows the time dependent UV-visible spectra, which shows that at about 2 h only peak at 520 nm is dominant (curve1). As time increases absorbance at around 700 nm starts increasing. In the anisotropic particles the absorbance at 520 nm is attributed to the dipolar plasmonic vibrations perpendicular to the plane of the particle called the transverse peak while that at 700 nm is attributed to the longitudinal vibrations. In the present case as time increases the longitudinal peak starts developing and becomes stronger with time and dominates the transverse peak. Finally after 5 h the longitudinal peak is observed at 620 nm which gradually shifts to 780 nm with advancement of time (by 70 h).

4.3.2: TEM Measurements

TEM measurements were carried out for Au nanoparticles synthesized in presence of CTAC (Au_CTAC) and CTAB (Au_CTAB) with their concentration

above CMC. Figure 4.5 demonstrates the TEM images of Au_CTAC along with particle size distribution.

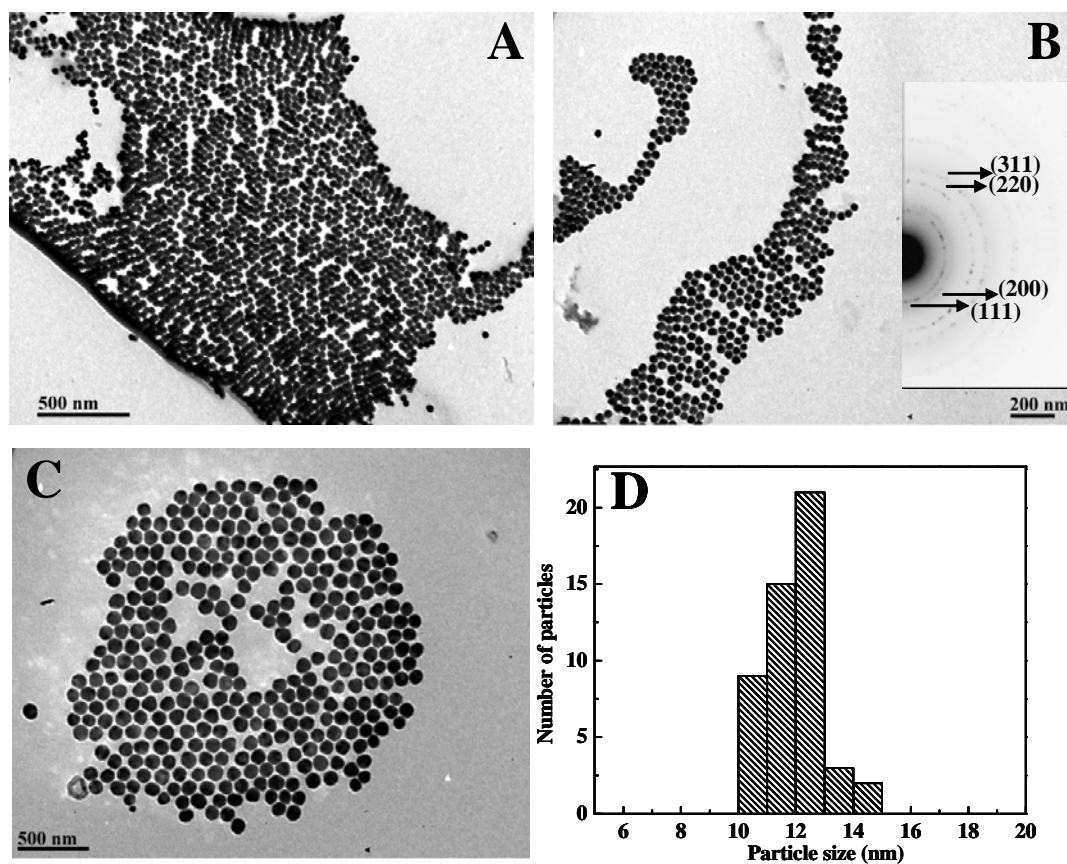


Figure 4.5: TEM micrograph image for Au_CTAC at different magnifications (A-C). Particle size distribution is shown in figure D indicating average particle size to be 13 nm. Inset in B shows the electron diffraction which is indexed as shown.

TEM analysis shows that the particles obtained in this case are spherical and mono-dispersed in nature. The average particle size obtained is 13 nm as can be observed from the histogram plotted. TEM measurements were also carried out for Au_CTAB.

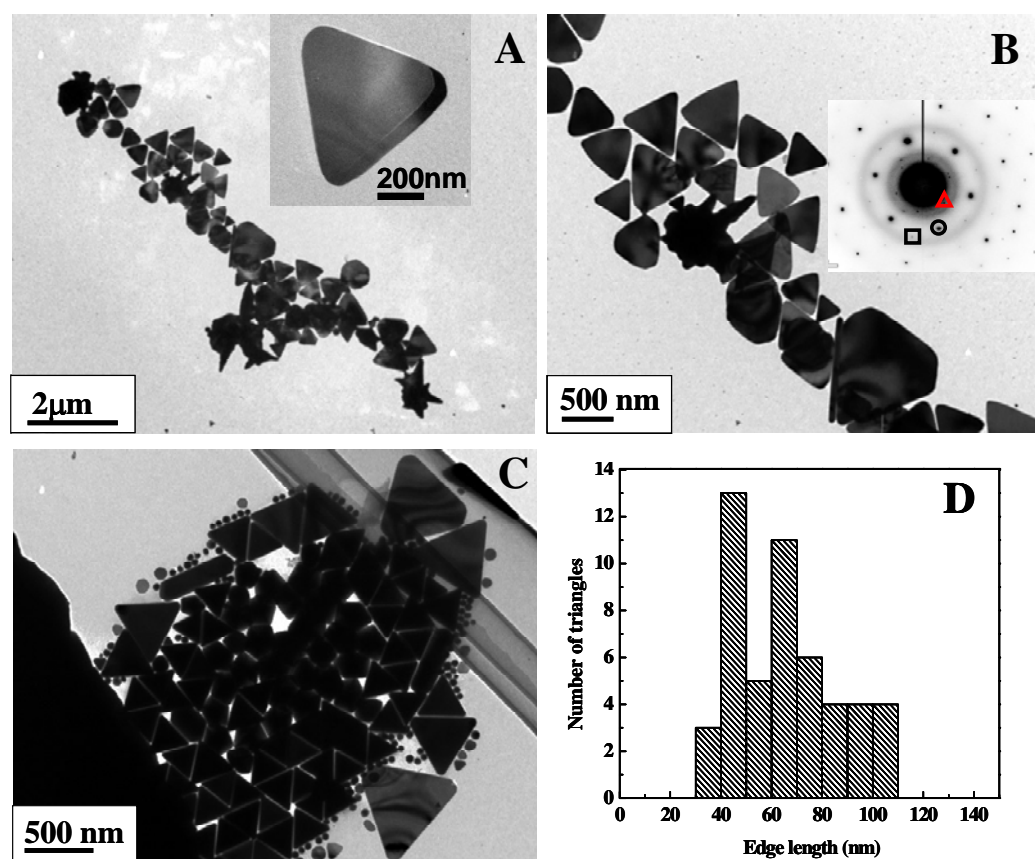


Figure 4.6: (A-C) TEM micrographs of Au_CTAB recorded at different magnifications. (D) Shows the edge length measurement for the triangular nanoparticles. Inset in B shows the electron diffraction which clearly shows the hexagonal arrangement.

Figure 4.6 (A-C) shows the representative transmission electron microscopy (TEM) images of Au nanotriangles synthesized using CTAB as surfactant when its concentration is above CMC (10^{-2} M). Selected area electron diffraction (SAED) was also recorded for Au_CTAC (Figure 4.6B, inset) and Au_CTAB (Figure 4.6B, inset). For Au_CTAC the particles are clearly polycrystalline and the rings could be indexed based on the fcc structure of Au. While SAED pattern for Au_CTAB shows a hexagonal arrangement again corresponding the fcc phase of Au nanoparticles. TEM images are recorded at different magnifications as can be seen from the scale bars. It can also be concluded that nanotriangles have varied edge length from 40 nm to 105 nm. The sizes of the nanotriangles were also verified with

atomic force microscopy measurements that are presented in Figure 4.7. The thickness obtained from AFM measurement is 27 nm.

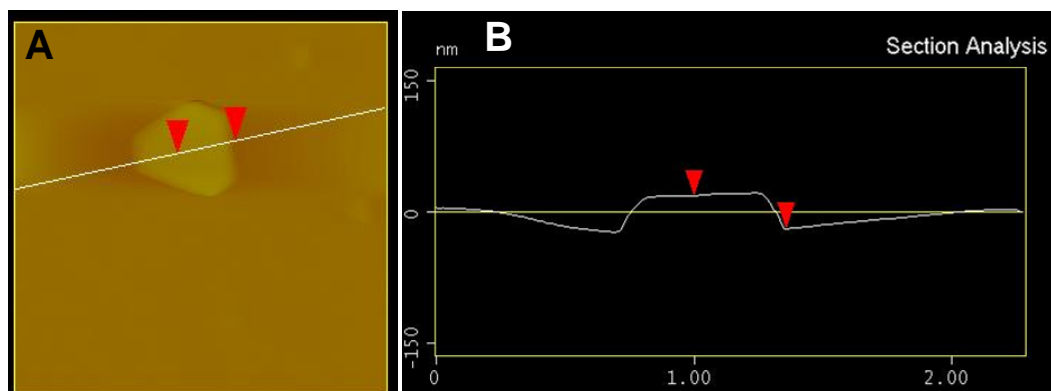


Figure 4.7: Atomic Force microscopy image of nanotriangle in contact mode (A). Height and length profile is shown in figure B.

4.3.3: X-ray Diffraction Measurements (XRD)

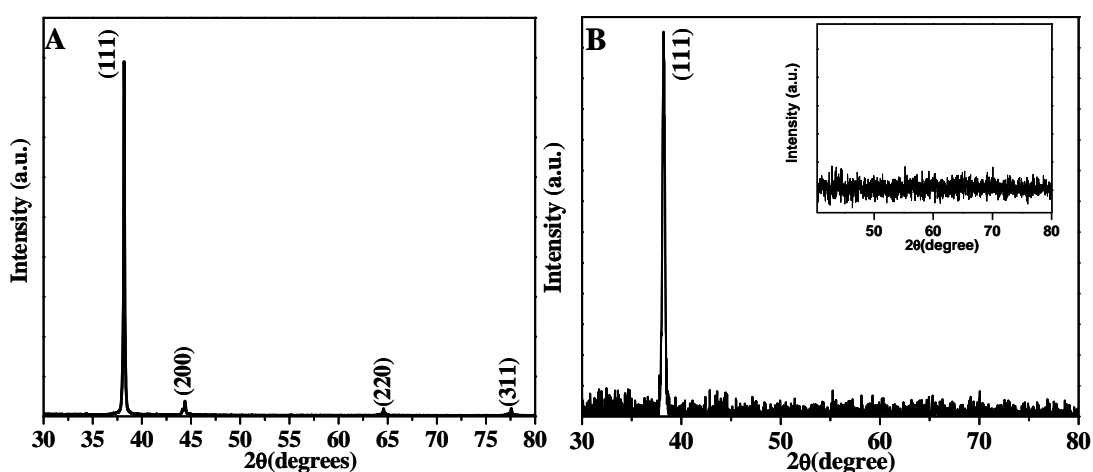


Figure 4.8: XRD measurements for Au_CTAC (A) and Au_CTAB(B). Au_CTAC can be indexed to fcc gold while we see that Au_CTAB is single crystalline in nature.

Powder diffraction pattern was recorded for Au_CTAC and Au_CTAB nanoparticles. Figure 4.8A corresponds to Au_CTAC while Figure 4.8 B corresponds to Au_CTAB. The XRD pattern in case of Au_CTAC corresponds well to the fcc crystalline phase of Au. In case of Au_CTAB we observe single peak

corresponding to (111) Bragg reflection of fcc gold. Magnified pattern (inset 4.8 B) of Au_CTAB indicates absence of peaks other than those from (111) planes from other Bragg plane of fcc gold.

4.3.4: Fourier Transform Infrared Spectroscopy (FTIR)

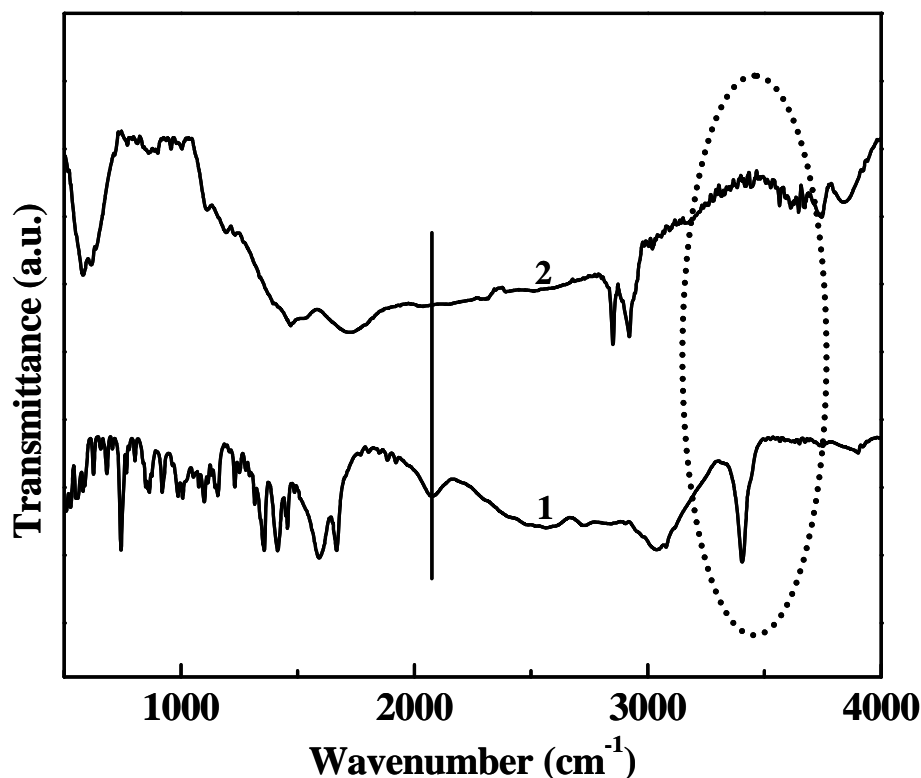


Figure 4.9: FTIR analysis for pure tryptophan (curve 1) and tryptophan reduced Au nanotriangles (curve 2).

Interaction of tryptophan with surface of Au nanotriangles was studied by FTIR analysis that is shown in Figure 4.9. Curve 1 corresponds to pure tryptophan while curve 2 represents tryptophan reduced Au nanotriangles. An FTIR spectrum of pure tryptophan shows a peak at 2073 cm^{-1} (marked by circle) due to the combination of the asymmetrical NH^{3+} bending vibration and the torsional oscillation of the NH^{3+} group. This peak is absent after reduction of chloroaurate ions with tryptophan. This is the main difference between the two spectra.

4.4 Discussion:

In this section, detail discussion on formation of anisotropic nanoparticles will be stressed upon. Various factors that could be infusing the formation of anisotropic nanoparticles are delineated. The synthesis was carried out in the presence of two surfactants namely cetyltrimethylammonium chloride (CTAC) having CMC as 16×10^{-3} M and cetyltrimethylammonium bromide (CTAB) with CMC as 1×10^{-3} M. Tryptophan was used as reducing agent. Three different concentrations of both the surfactant as mentioned in section 4.2 were considered for the synthesis purpose. From the UV visible results obtained for Au nanoparticles for CTAC and CTAB at all the three different concentrations the following observations have been made.

- a. For CTAC the surface plasmon resonance (SPR) peak corresponding to Au nanoparticles is centered at 520 nm which is the characteristic for spherical Au nanoparticles. For all the three concentrations (above, at and below CMC) SPR peak is centered at 520 nm.
- b. In case of CTAB for concentration above CMC (10^{-2} M) we observe two SPR peaks positioned at 520 nm (transverse) and 700 nm (longitudinal).
- c. Time dependent UV-visible for CTAB above CMC concentration shows that at start, the transverse peak is more prominent than the longitudinal peak. But with progress in time, the longitudinal peak becomes more sharp and strong.

TEM images recorded (Figure 4.5 and 4.6) for the samples above CMC for both the surfactants show that spherical nanoparticles are obtained in case of CTAC while for CTAB formation of triangular nanoparticles resulted. These nanoparticles are also observed to be arranged edge to edge. Selected area diffraction pattern clearly shows that the Au_CTAC nanoparticles are polycrystalline in nature and the rings can be indexed to face centered structure of gold. While the SAED pattern for Au_CTAB reveals that it is single crystalline. The hexagonal nature of the diffraction spots is a clear indication that the triangular gold nanoprisms are highly [111] oriented with the top normal to the electron beam. The spots could be indexed based on the face centered cubic (fcc) structure of gold. The circled spots, boxed

spots and spots circumscribed by triangles correspond to the forbidden $1/3\{422\}$, allowed $\{220\}$ and $\{311\}$ Bragg reflections with lattice spacing of 2.5, 1.44 and 1.23 Å respectively. The presence of the $1/3\{422\}$ reflections indicates that the gold triangles could have stacking faults along the $\langle 111 \rangle$ direction.^{42,43}

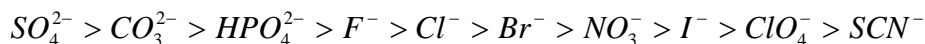
X-ray diffraction studies carried out for CTAC and CTAB also reveals preferential orientation in $\langle 111 \rangle$ directions for nanotriangles while the XRD data obtained for Au_CTAC can be indexed to fcc phase of gold particles. Thus XRD results also support the TEM measurements.

The mechanism of formation of anisotropic nanoparticles like nanosheets, nanotriangles, rods etc has been very intriguing. Reasons cited for formation of anisotropic particle formation include preferential binding of surfactant,^{44,45} oriented attachment,⁴⁵ soft templates,^{3,46} aggregation of spherical particles⁸ and kinetic control.^{5,44,46-48}

Studies carried out by Xia and co-workers clearly illustrated the role of reaction rates on the morphology of Pd nanoparticles.⁴⁸ The thermodynamically favorable shapes of Pd nanocrystals are cubooctahedral and multiple twinned particles (MTT). It was observed that when PdCl_4^{2-} is reduced by ethylene glycol to generate Pd(0), atoms formed at relatively higher rates will mould into the thermodynamically stable forms of cubooctahedral and multiple twinned particles. Slowing down the reduction rates resulted in reduction of nucleation and growth and deviation in shape from its thermodynamic state. Thus transformation from cubooctahedral and MTT to triangular nanoplates or hexagonal shape is observed on reduction of reaction rate.

Pileni et al have demonstrated that the particle shape can be controlled by using different anions.^{49,50} They have studied the effect of different anions on shape of nanoparticles keeping all the other preparation conditions same. In absence of any external anions, added spherical particles were obtained. Presence of ions like Cl⁻ during the synthesis resulted in rod formation. In case of Br⁻ ions, formation of rod with higher aspect ratio is observed. Addition of NO₃⁻ ions addition resulted in formation of aggregates. In case of SO₄⁻, slight elongation was observed. To explain the change in shape of nanoparticles on addition of these ions, Pileni and co-

workers have considered the Hofmeister series⁵¹ The Hofmeister series for anions is given as follows



When these above mentioned anions are added to an organic solvent/water-surfactant mixture, solubility of surfactant in the aqueous phase increases from left to right. The anions desorb at the water-oil interface and then decrease the solubility between water and surfactant. Water molecules are highly bound to surfactant and induce high rigidity of the water-surfactant interface. They hypothesized that such changes result in decreasing the desorption of metal ions to the water phase and thus resulting in more spherical particles than cylindrical without perturbing the template.

Ravishankar and co-workers have based their argument related to formation of anisotropic nanoparticles on a morphology diagram formulated by them.^{52,53} As a representative the morphology diagram for Au is shown in Figure 4.10. Here their argument is based on the fact that crystal growth occurs through nucleation and growth where the driving force is the volume free energy change. They have observed that depending on the nature of the driving force, the nucleation and growth pattern takes different routes as shown in Figure 4.10 A & B. Large driving force leads to continuous growth while at low driving force, growth resulted in formation of steps and a lateral motion of steps on the surface.⁵⁴⁻⁵⁶ In the morphology diagram for Au the region represented by grey colour represents the condition of $\Delta G > 0$ thus no reduction occurs in this region. As the reactant conditions are changed the free energy reverses its sign from positive to negative. In the region represented by yellow the condition is $-\Delta G < \Delta G_{2D}^{crit}$ and favors 2D structure formation. 3D structures are obtained when the free energy condition is $-\Delta G > \Delta G_{3D}^{crit}$ which is represented by the red portion. Transition from 2D to 3D is represented by the green portion. Thus, from the morphology diagram it is found that at lower temperature and low pH anisotropic nanoparticles can be obtained.

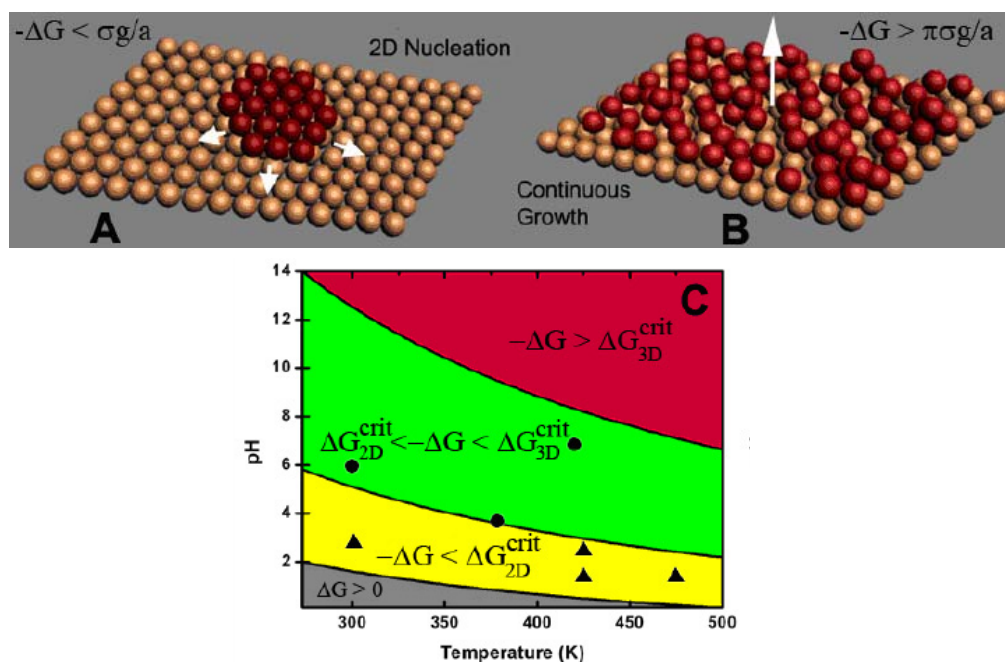


Figure 4.10: Schematic illustration of (A) two-dimensional nucleation mechanism and (B) continuous growth mechanism. Morphology diagrams illustrate pH and temperature regimes where the two-dimensional nucleation mechanism (yellow) and continuous growth (red) is operative for Au.

Another reason cited for formation of anisotropic nanoparticles is the differential stress caused by the adsorption effect of halide ions. Br^- and Cl^- are known to form a hexagonal close packed adlayer on gold nanosurface. Slight mismatch between the halide adlayers and the atomic Au (111) lattice planes might cause some residual strain at the surface and lead to the development of the defects like twin planes. This may be one of the factors that influence the formation of triangular nanoparticles as reported by Lofton and Sigmund.⁴³ This has been postulated as the reason for the observation that anisotropic particles are preferentially formed in presence of the Br^- ions and not in presence of Cl^- . Murphy and co-workers also have employed CTAB for formation of nanorods. They postulated that CTA^+ head group binds to the side surface with some preference. The preferential binding is based on sterics - the Au atom spacing on the side faces is more comparable to the size of the CTA^+ head group than the close-packed {111} face of gold, which is at the ends of the nanorods. Such binding stabilizes the side faces, which have relatively large surface energy and stress (tension) compared to

other faces. This allows material addition along the [110] common axis on {111} faces, which do not contain the CTA⁺ headgroups.⁵⁷

In the present case, formation of triangular nanoparticles in presence of CTAB can be attributed to preferential binding of bromide ions to the specific planes. There have been many reports where in presence of CTAB as surfactant leads to formation of anisotropic nanoparticles. Various reports suggest that Br⁻ ions chemisorbs onto the surface of Au more strongly and form hexagonal packed adlayer on the Au (111) surface.⁵⁸⁻⁶² Earlier report suggest that the edges of triangle are bound by the (110) and (111) faces⁴² but it appears that Br⁻ ions are strongly adsorbed on to (110) thus enhancing growth of nanotriangles in <111> direction. It is also known that there is a mismatch between the Br⁻ ion adlayer and gold lattice plane which results in strain on the small particles synthesized at initial stages. This strain leads to defect formation like twin boundary resulting in orientational growth of small nanoparticles to form nanotriangles.⁴³

We also noticed that the reaction rates with CTAB are lower than those with CTAC. Therefore this also could have had an effect on the formation of triangular particles. Apart from the above reasons, role of tryptophan and the oxidized products of tryptophan influences the shape of resulting nanoparticles cannot be ruled out.

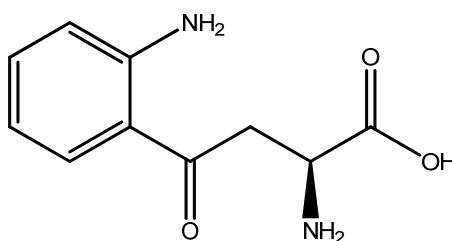


Figure 4.11: Structure of kynurenine the products obtained when tryptophan is oxidized.

It is well known that tryptophan in process of reducing Au³⁺ ions gets oxidized and leads to formation of kynurenine.⁶³ In our FTIR studies we noticed that absence of peaks corresponding to pure tryptophan but could not detect any

specific peaks that confirm the formation and adsorption of kynurenine on the gold surface. But the fluorescence studies indicate the tryptophan is getting oxidized.

Part B

4.5 White light emission:

This section of the chapter deals with emission of white light observed from Au_CTAB when exposed to UV light of 365 nm. This phenomenon was not observed for Au_CTAC (spherical nanoparticles). Experimental observations are shown in Figure 4.12 with UV light **ON** and UV light **OFF**.

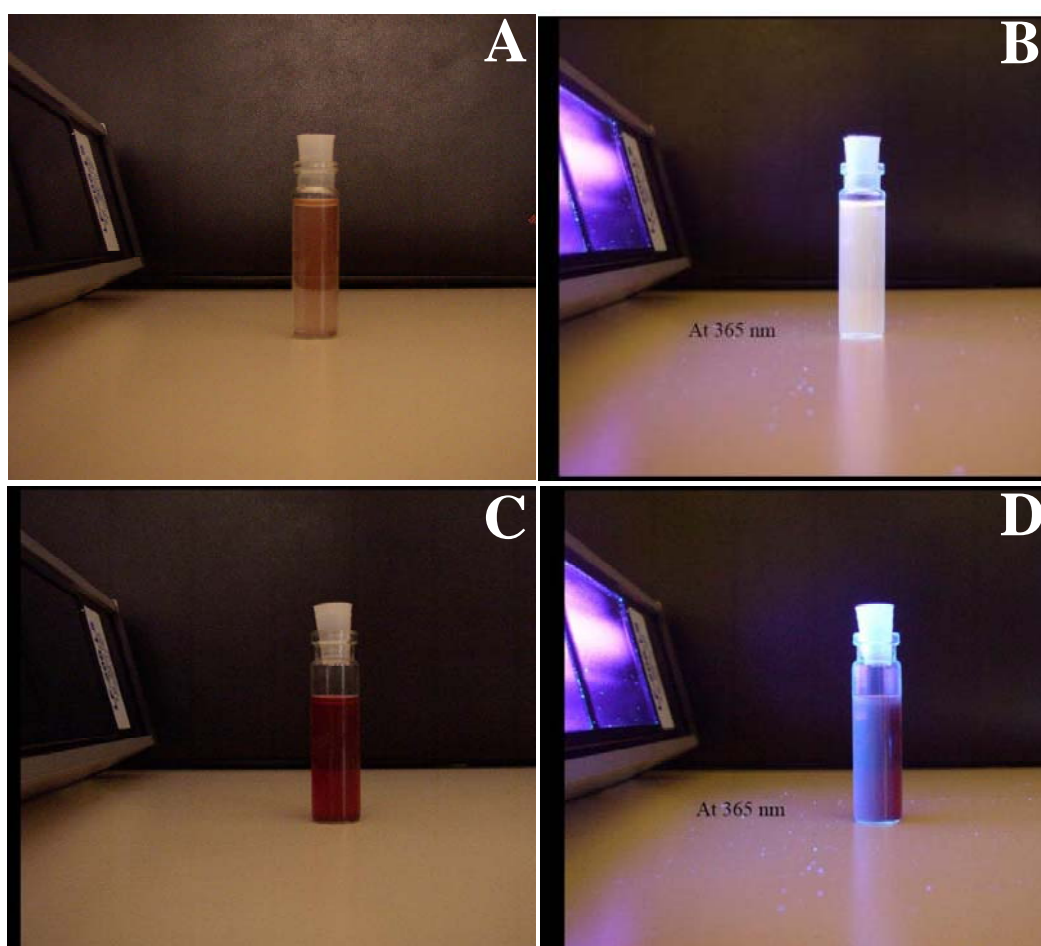


Figure 4.12: Photographs of Au_CTAB solution when UV-light is OFF (A) Au_CTAB solution exposed to UV-light of wavelength 365 nm (B). Au_CTAC solution when UV-light is OFF (C) and when exposed to UV-light of wavelength 365 nm (D).

The Au-CTAB solution is reddish brown in colour. Interestingly, when unexposed to UV-light (Figure 4.12 A) of wavelength 365 nm we observe an intense white light (Figure 4.12B) from the same sample. In case of Au_CTAC no such emission is observed when the solution is exposed to same UV-light (Figure 4.12 C and D). In order to confirm the white light which was emitted is not due to scattering it was passed through the prism. Similar experiment was carried out with just tryptophan. The observed results are shown in Figure 4.13.

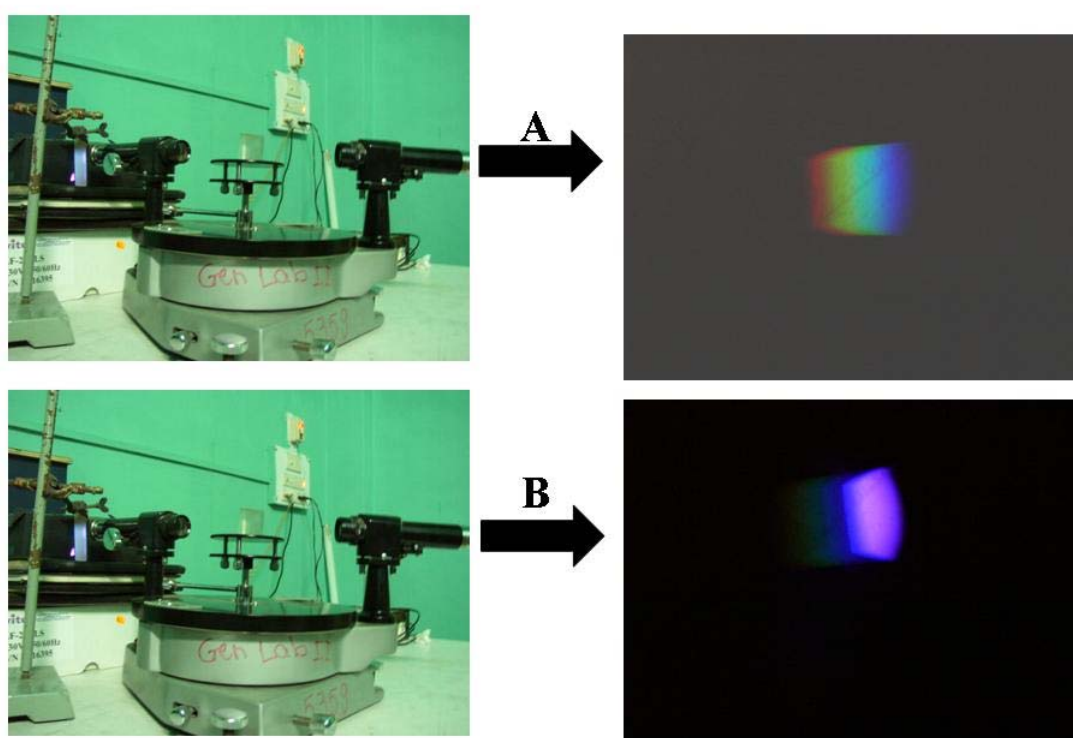


Figure 4.13: (A) Light spectrum obtained when white light emitted from Au_CTAB nanotriangles is passed through prism. (B) Spectrum obtained when light emitted from tryptophan is passed through prism.

In the case of white light emitted from Au_CTAB the splitting into various components (red, green, cyan and blue) is clearly observed (Figure 4.13 A). When same experiment was carried out by illuminating pure tryptophan only blue light was observed. To entice more information about this phenomenon detailed fluorescence and life-time measurements were carried out.

4.6: Fluorescence measurements

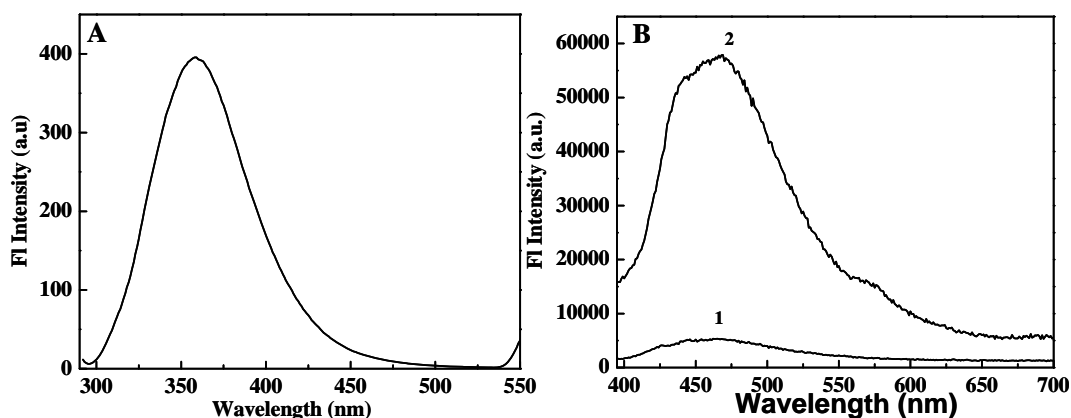


Figure 4.14: Fluorescence measurements carried for pure tryptophan (A). Excitation wavelength was 280 nm. Fluorescence spectrum for oxidized tryptophan is shown in figure B, curve 1 while fluorescence for Au_CTAB nano-triangles is represented by curve 2. For both the samples excitation was 365 nm.

Fluorescence for pure tryptophan is shown in Figure 4.14 A. The excitation for this was 280 nm. We observe that the emission for pure tryptophan is centered around 350 nm. It is known that during the reduction of Au^{3+} , the tryptophan will be oxidized. Mandal et al⁶³ have confirmed that the oxidized product of tryptophan in this reaction would be kynurenine. But in our studies we could not confirm the formation of kynurenine and hence we would restrict calling the formed product as oxidized tryptophan. To see what emission characteristic this oxidized product will have, we prepared oxidized tryptophan with H_2O_2 . Spectrum for oxidized tryptophan excited at 365 nm is shown in Figure 4.14 B. A clear peak with a weak intensity is observed at 460 nm (curve 1). In the emission spectra for Au_CTAB nanotriangles again a peak centered at 460 nm could be seen. The total initial concentration of tryptophan used to obtain the spectrum 1 and 2 is the same. From the spectra we can see that the intensities of the emission peak in case of Au_CTAB sample is much higher than that observed with H_2O_2 oxidized tryptophan. This suggests that in presence of Au_CTAB the emission intensity of oxidized tryptophan is getting enhanced.

The results obtained from the fluorescence were supported by life time measurements. Measurements were recorded for excitation of 365 nm and collected at 460 nm with accordance with fluorescence measurements. Milk was used as the reference to eliminate scattering effects. Life time measurements recorded for milk as background and oxidized tryptophan are shown in Figure 4.15.

4.7: Life time measurements:

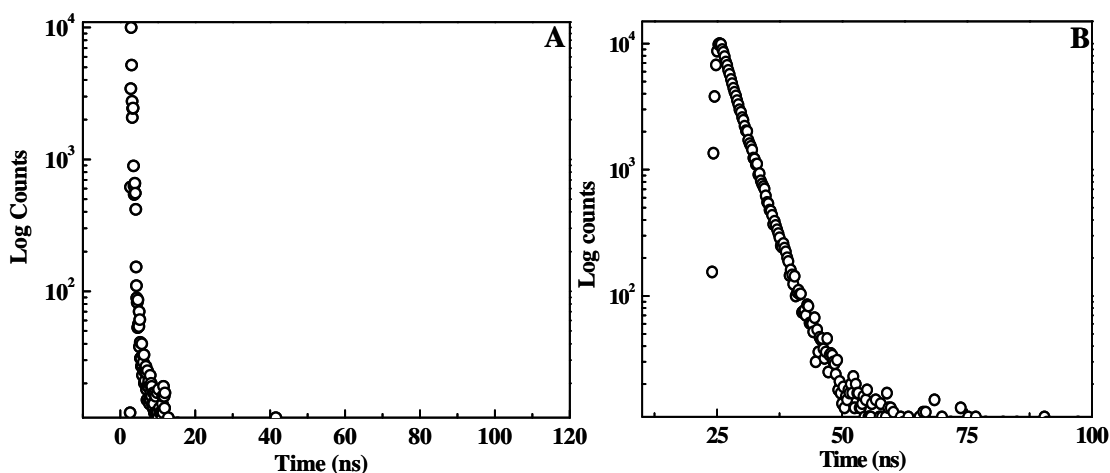


Figure 4.15: Life-time measurements recorded for milk as reference (A) and life time data for tryptophan collected at 350 nm.

The lifetime data for milk does not show any decay as can be seen from Figure 4.15 A. Lifetime measurement for tryptophan (Figure 1.15 B) was carried out by exciting the sample at 280 nm and collecting the data at 350 nm which is the wavelength of emission of pure tryptophan. The experimental data could be fitted to decay with two different life time values of 2.7 ns (90.7%) and 5.9 ns (9.3%). Our experimental life time values are in good agreement with reported values ($\tau_1=2.1 \pm 0.2$ and $\tau_2=5.4 \pm 1.1$ ns).⁶⁴

The lifetime measurements carried out for oxidized tryptophan and the Au_CTAB nanotriangles are shown in Figure 4.16. Excitation of the sample was carried out at 365 nm and the data was collected at 450 nm. The obtained lifetime values are $\tau_1=0.23$ ns (2%), $\tau_2= 2.32$ ns (10%), $\tau_3= 13.9$ ns (88%) for H_2O_2 oxidized

tryptophan and $\tau_1=1.99$ ns (9 %), $\tau_2=3.71$ ns (16 %), $\tau_3=18.2$ ns (75 %) for Au_CTAB.

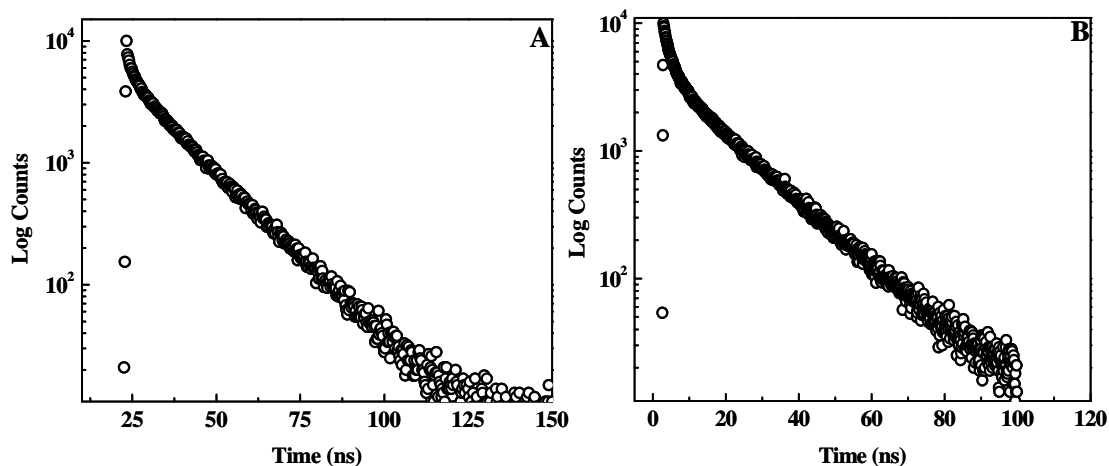


Figure 4.16: (A) Lifetime measurement for oxidized tryptophan. (B) Lifetime measurement for Au_CTAB nano-triangular solution. Both the samples were excited at 365 nm while the emission was recorded at 450 nm.

4.8 Discussion

Observance of white light from Au nanotriangles (Figure 4.12 A and B) is well studied by fluorescence and life time measurements (Figure 13-16). Tryptophan has earlier been used as reducing agent for gold nanoparticles.^{65,66} Fluorescence of pure tryptophan occurs at 345 nm when excited at 280 nm,⁶⁷ which is also observed by us for pure tryptophan (Figure 4.14 A). The most striking result in the emission experiments, is the observation of a broad peak from Au_CTAB where emission maximum is centered at 450 nm (Figure 4.14 B, curve 2). From our control experiments we could surmise that the origin of the emission could be from the oxidized tryptophan. Accordingly fluorescence was recorded for oxidized tryptophan prepared using H_2O_2 as oxidizing agent. As expected a clear peak with emission maximum again centered at 450 nm could be clearly seen (Figure 4.14 B, curve1). However the intensity of peak for Au_CTAB is much higher than the oxidized tryptophan. This enhancement is attributed to binding of oxidized tryptophan molecule to the tips of nanotriangles. Aslan et al. have shown enhancement in fluorescence spectra by ten orders of magnitude in presence of

anisotropic metal nanoparticles.^{16,17} This enhancement is attributed to increased local excitation fields around the edges of the triangles and interaction of excited state fluorophores with free electrons in the metal (surface plasmon electron).^{40,68,69} El-Sayed and co-workers have demonstrated the lightning gold nanorod effect, which is explained based on electron hole recombination and the increase in the emission yield results from the enhancement effect of the incoming and outgoing electric fields via coupling to the surface plasmon resonance in the rods.⁷⁰

Thus, our fluorescence data clearly point out the possibility of attachment of oxidized tryptophan molecules to the sharp edges of nanotriangles. The enhanced intensity of this emission which is very broad with these different life times could be the cause for white light emission observed.

4.9 Conclusion:

Au nanoparticles were prepared with two different surfactants (CTAB and CTAC) with tryptophan as reducing agent. Spherical particles are obtained in case of CTAC while use of CTAB resulted in formation of Au nanotriangles. White light emission was observed from nanotriangles when illuminated with UV-light of 365 nm. Occurrence of white light is attributed to the enhancement of fluorescence of oxidized tryptophan attached to sharp tips of nanotriangles.

4.10 Reference:

- (1) Freestone, I.; Meeks, N.; Sax, M.; Higgitt, C. *Gold Bulletin* **2007**, *40*, 270.
- (2) Diao, J. J.; Chen, H. *Journal of Chemical Physics* **2006**, *124*.
- (3) Porel, S.; Singh, S.; Radhakrishnan, T. P. *Chemical Communications* **2005**, 2387.
- (4) Shankar, S. S.; Rai, A.; Ahmad, A.; Sastry, M. *Chemistry of Materials* **2005**, *17*, 566.
- (5) Ah, C. S.; Yun, Y. J.; Park, H. J.; Kim, W. J.; Ha, D. H.; Yun, W. S. *Chem. Mater* **2005**, *17*, 5558.
- (6) Hao, E.; Schatz, G. C.; Hupp, J. T. *Journal of Fluorescence* **2004**, *14*, 331.
- (7) Singh, A.; Chaudhari, M.; Sastry, M. *Nanotechnology* **2006**, *17*, 2399.
- (8) Shankar, S. S.; Rai, A.; Ankamwar, B.; Singh, A.; Ahmad, A.; Sastry, M. *Nature Materials* **2004**, *3*, 482.
- (9) Haes, A. J.; Hall, W. P.; Chang, L.; Klein, W. L.; Van Duyne, R. P. *Nano Letters* **2004**, *4*, 1029.
- (10) Maier, S. A.; Brongersma, M. L.; Kik, P. G.; Meltzer, S.; Requicha, A. A. G.; Atwater, H. A. *Advanced Materials* **2001**, *13*, 1501.
- (11) Dick, L. A.; McFarland, A. D.; Haynes, C. L.; Van Duyne, R. P. *Journal of Physical Chemistry B* **2002**, *106*, 853.
- (12) Jana, N. R.; Pal, T. *Advanced Materials* **2007**, *19*, 1761.
- (13) Schmidt, J. P.; Cross, S. E.; Buratto, S. K. *Journal of Chemical Physics* **2004**, *121*, 10657.
- (14) Zhang, J. T.; Li, X. L.; Sun, X. M.; Li, Y. D. *Journal of Physical Chemistry B* **2005**, *109*, 12544.
- (15) Umar, A. A.; Oyama, M. *Crystal Growth & Design* **2006**, *6*, 818.
- (16) Aslan, K.; Gryczynski, I.; Malicka, J.; Matveeva, E.; Lakowicz, J. R.; Geddes, C. D. *Current Opinion in Biotechnology* **2005**, *16*, 55.
- (17) Aslan, K.; Lakowicz, J. R.; Geddes, C. D. *Analytical and Bioanalytical Chemistry* **2005**, 382, 926.

-
-
- (18) Pompa, P. P.; Martiradonna, L.; Della Torre, A.; Della Sala, F.; Manna, L.; De Vittorio, M.; Calabi, F.; Cingolani, R.; Rinaldi, R. *Nature Nanotechnology* **2006**, *1*, 126.
- (19) Aslan, K.; Lakowicz, J. R.; Geddes, C. D. *Journal of Physical Chemistry B* **2005**, *109*, 6247.
- (20) Aslan, K.; Leonenko, Z.; Lakowicz, J. R.; Geddes, C. D. *Journal of Physical Chemistry B* **2005**, *109*, 3157.
- (21) Jin, R.; Cao, Y.; Mirkin, C. A.; Kelly, K. L.; Schatz, G. C.; Zheng, J. *G. Science* **2001**, *294*, 1901.
- (22) Zhou, Y.; Wang, C. Y.; Zhu, Y. R.; Chen, Z. Y. *Chem. Mater* **1999**, *11*, 2310.
- (23) Maillard, M.; Huang, P. R.; Brus, L. *Nano Letters* **2003**, *3*, 1611.
- (24) Métraux, G. S.; Mirkin, C. A. *Advanced Materials* **2005**, *17*, 412.
- (25) Chu, H. C.; Kuo, C. H.; Huang, M. H. *Inorg. Chem* **2006**, *45*, 808.
- (26) Callegari, A.; Tonti, D.; Chergui, M. *Nano Letters* **2003**, *3*, 1565.
- (27) Xue, C.; Mirkin, C. A. *Angewandte Chemie-International Edition* **2007**, *46*, 2036.
- (28) Malikova, N.; Pastoriza-Santos, I.; Schierhorn, M.; Kotov, N. A.; Liz-Marzan, L. M. *Langmuir* **2002**, *18*, 3694.
- (29) Norman, T. J.; Grant, C. D.; Magana, D.; Zhang, J. Z.; Liu, J.; Cao, D. L.; Bridges, F.; Van Buuren, A. *Journal of Physical Chemistry B* **2002**, *106*, 7005.
- (30) Millstone, J. E.; Park, S.; Shuford, K. L.; Qin, L. D.; Schatz, G. C.; Mirkin, C. A. *Journal of the American Chemical Society* **2005**, *127*, 5312.
- (31) Kim, J. U.; Cha, S. H.; Shin, K.; Jho, J. Y.; Lee, J. C. *Advanced Materials* **2004**, *16*, 459.
- (32) Wang, L.; Chen, X.; Zhan, J.; Chai, Y.; Yang, C.; Xu, L.; Zhuang, W.; Jing, B. *Journal of Physical Chemistry B* **2005**, *109*, 3189.
- (33) Bharde, A.; Kulkarni, A.; Rao, M.; Prabhune, A.; Sastry, M. *Journal of Nanoscience and Nanotechnology* **2007**, *7*, 4369.
- (34) Duraiswamy, S.; Khan, S. A. *Small* **2009**, *5*, 2828.
-
-

-
-
- (35) Bentolila, L. A.; Ebenstein, Y.; Weiss, S. *Journal of Nuclear Medicine* **2009**, *50*, 493.
- (36) Yuhua, J.; Jimai, Z.; Zhao, D.; Shichao, X.; Xin, L.; Guo, Z.; Bo, S. In *Proceedings of SPIE - The International Society for Optical Engineering* Beijing, 2009; Vol. 7157.
- (37) Bowers, M. J.; McBride, J. R.; Rosenthal, S. J. *Journal of the American Chemical Society* **2005**, *127*, 15378.
- (38) Achermann, M.; Petruska, M. A.; Kos, S.; Smith, D. L.; Koleske, D. D.; Klimov, V. I. *Nature* **2004**, *429*, 642.
- (39) Derfus, A. M.; Chan, W. C. W.; Bhatia, S. N. *Nano Letters* **2004**, *4*, 11.
- (40) Lakowicz, J. R.; Shen, Y. B.; D'Auria, S.; Malicka, J.; Fang, J. Y.; Gryczynski, Z.; Gryczynski, I. *Analytical Biochemistry* **2002**, *301*, 261.
- (41) Kelly, K. L.; Coronado, E.; Zhao, L. L.; Schatz, G. C. *Journal of Physical Chemistry B* **2003**, *107*, 668.
- (42) Germain, V.; Li, J.; Ingert, D.; Wang, Z. L.; Pileni, M. P. *Journal of Physical Chemistry B* **2003**, *107*, 8717.
- (43) Lofton, C.; Sigmund, W. *Advanced Functional Materials* **2005**, *15*, 1197.
- (44) Lu, L.; Kobayashi, A.; Tawa, K.; Ozaki, Y. *Chemistry of Materials* **2006**, *18*, 4894.
- (45) Wang, L.; Chen, X.; Zhan, J.; Chai, Y.; Yang, C.; Xu, L.; Zhuang, W.; Jing, B. *The Journal of Physical Chemistry B* **2005**, *109*, 3189.
- (46) Sun, X. P.; Dong, S. J.; Wang, E. *Angewandte Chemie-International Edition* **2004**, *43*, 6360.
- (47) Washio, I.; Xiong, Y. J.; Yin, Y. D.; Xia, Y. *Adv Mater* **2006**, *18*, 1745.
- (48) Xiong, Y.; McLellan, J. M.; Chen, J.; Yin, Y.; Li, Z.-Y.; Xia, Y. *Journal of the American Chemical Society* **2005**, *127*, 17118.
- (49) Filankembo, A.; Pileni, M. P. *Journal of Physical Chemistry B* **2000**, *104*, 5865.
-
-

-
-
- (50) Lisiecki, I.; Bjorling, M.; Motte, L.; Ninham, B.; Pileni, M. P. *Langmuir* **1995**, *11*, 2385.
- (51) Hofmeister, F. *Arch. exper. Path. Pharm.* **1898**, *24*, 247-60.
- (52) Viswanath, B.; Kundu, P.; Mukherjee, B.; Ravishankar, N. *Nanotechnology* **2008**, *19*, 195603.
- (53) Viswanath, B.; Kundu, P.; Halder, A.; Ravishankar, N. *Journal of Physical Chemistry C* **2009**, *113*, 16866.
- (54) Burton, W. K.; Cabrera, N.; Frank, F. C. *Philosophical Transactions of the Royal Society of London Series a-Mathematical and Physical Sciences* **1951**, *243*, 299.
- (55) Cahn, J. W. *Acta Metallurgica* **1960**, *8*, 554.
- (56) Cahn, J. W.; Hillig, W. B.; Sears, G. W. *Acta Metallurgica* **1964**, *12*, 1421.
- (57) Murphy, C. J.; Sau, T. K.; Gole, A. M.; Orendorff, C. J.; Gao, J.; Gou, L.; Hunyadi, S. E.; Li, T. *J. Phys. Chem. B* **2005**, *109*, 13857.
- (58) Rai, A.; Singh, A.; Ahmad, A.; Sastry, M. *Langmuir* **2006**, *22*, 736.
- (59) Shankar, S. S.; Bhargava, S.; Sastry, M. *Journal of Nanoscience and Nanotechnology* **2005**, *5*, 1721.
- (60) Gao, P.; Weaver, M. J. *Journal of Physical Chemistry* **1986**, *90*, 4057.
- (61) Magnussen, O. M.; Ocko, B. M.; Adzic, R. R.; Wang, J. X. *Physical Review B* **1995**, *51*, 5510.
- (62) Magnussen, O. M.; Ocko, B. M.; Wang, J. X.; Adzic, R. R. *Journal of Physical Chemistry* **1996**, *100*, 5500.
- (63) Si, S.; Mandal, T. K. *Chemistry-A European Journal* **2007**, *13*, 3160.
- (64) Fleming, G. R.; Morris, J. M.; Robbins, R. J.; Woolfe, G. J.; Thistlethwaite, P. J.; Robinson, G. W. *Proceedings of the National Academy of Sciences* **1978**, *75*, 4652.
- (65) Selvakannan, P.; Mandal, S.; Phadtare, S.; Gole, A.; Pasricha, R.; Adyanthaya, S. D.; Sastry, M. *Journal of Colloid and Interface Science* **2004**, *269*, 97.
-
-

- (66) Iosin, M.; Baldeck, P.; Astilean, S. *Journal of Nanoparticle Research*, 1.
- (67) <http://omlc.ogi.edu/spectra/PhotochemCAD/html/tryptophan.html>.
- (68) Lakowicz, J. R. *Analytical Biochemistry* **2001**, 298, 1.
- (69) Lakowicz, J. R.; Shen, B.; Gryczynski, Z.; D'Auria, S.; Gryczynski, I. *Biochemical and Biophysical Research Communications* **2001**, 286, 875.
- (70) Mohamed, M. B.; Volkov, V.; Link, S.; El-Sayed, M. A. *Chemical Physics Letters* **2000**, 317, 517.

Chapter 5

Conclusion

This chapter includes summary of the work carried out in this thesis with conclusion drawn from the work. We also give the futuristic aspect of this work.

5.1 Summary of the thesis:

The work described in this thesis focuses on the use of ligands during the synthesis of nanoparticles. Effects of these ligands on the shape, size, crystalline phase of nanoparticles formed have been studied in detail. The nanoparticles considered in this these are cobalt (Co), Silver (Ag) and Gold (Au) and the ligands that have been used by us during the synthesis of these nanoparticles are

1. A biosurfactant called as sophorolipid.
2. Organically synthesized ligand 2 (Dodecyloxy) acetic acid (DDOA)
3. Cetyltrimethylammonium Chloride (CT AC).
4. Cetyltrimethylammonium Bromide (CTAB).

Applications of nanoparticles in many fields require them to be dispersed in aqueous medium. To address this issue we have picked a bio-surfactant named as sophorolipid which is derived from fatty acids like oleic acid. Oleic acid is one of the most widely used ligand in synthesis of magnetic nanoparticles. We have considered synthesis of Co nanoparticles using oleic acid derived sophorolipid (OASL) as capping ligand. We obtained stable CoNPs dispersed in aqueous medium. The second ligand that we tested in CoNPs synthesis is 2-(Dodecyloxy) acetic acid (DDOA). CoNPs obtained using these two different ligands resulted in formation of different phases of CoNPs. Mixture of hcp and ϵ -phase was obtained when OASL was used while in case of DDOA pure hcp phase is obtained.

Extending the use of sophorolipid we also explored the reducing capability of the sophorolipid in synthesis of AgNPs. To optimize the reaction condition with respect to type ligand, temperature, time of reaction we have used three different types of sophorolipids LASL, OASL and SASL. These three sophorolipid differ in number of double bonds present. LASL has 2 cis double bonds; OASL has one cis double bond while SASL contains no double bond. The presence of double bonds is found to affect the reaction rate which in turn controls the size and shape of nanoparticles. It is found that reaction rate is faster for SASL case as compared to other sophorolipids. Use of SASL also resulted in smaller and monodispersed nanoparticles. Thus, using SASL as the reducing/capping ligand Ag nanoparticle

synthesis was carried out in continuous manner in micro-reactors. The particles obtained in this case were also similar to that obtained in case of batch process.

One of the important factors that determine the property of nanoparticles is the shape of the nanoparticles. The choice of surfactants could influence the shape in a dramatic manner as revealed by our results with the Au nanoparticle synthesis in presence of CTAC and CTAB. CTAC resulted in modispersed spherical nanoparticles while CTAB resulted in formation of triangular nanoparticles. The striking feature of this study is the white light emission from the triangular nanoparticles. From the life time measurements it was concluded that the emission observed is due to the oxidized tryptophan attached to the surface of triangular nanoparticles.

5.2 Scope of future work:

Our studies shows that sophorolipid capped nanoparticles are well dispersed in aqueous medium. Taking advantage of this situation this work can be extended by tagging the sophorolipids with drug molecule. This particular system can be used in drug delivery of nanoparticles. Modification of DDOA also can be achieved to make the molecule completely water soluble and employ it for further synthesis of nanoparticles. By appropriate modification of this ligand we can target to achieve assembly of the magnetic nanoparticles and study their magnetic properties.

The mechanistic aspect of triangle formation should be further studied. Linear arrangement of nanotriangles can be achieved. Arrangement of such nanoparticles in a linear fashion could enable their usage in multiple applications such as light diodes, wave guides, solar cells etc.

APPENDIX-I

(Instruments used)

Ultraviolet-visible (UV-vis) absorption spectrophotometry: UV-vis Spectroscopic measurements were carried out on a JASCO model V- 570 dual-beam spectrophotometer operated at a resolution of 1 nm.

X-ray Diffraction: The diffractograms were recorded on a PANalytical Xpert pro machine using a $\text{CuK}\alpha$ ($\lambda=1.54\text{\AA}$) source and operating conditions of 40 mA and 30 kV at different scan rates depending upon the sample.

FTIR spectrophotometer: FTIR spectra were recorded on a Perkin Elmer Spectrum One FTIR spectrophotometer in diffuse reflectance mode, operating at a resolution of 4 cm^{-1} .

Transmission Electron Microscopy: TEM measurements were performed on a JEOL Model 1200EX instrument operated at an accelerating voltage of 80 kV. In addition, for HRTEM measurements, a TECHNAI G2 F30 S-TWIN instrument (Operated at an acceleration voltage of 300kV with a lattice resolution of 0.14 nm and a point image resolution of 0.20 nm) was also employed. The same set of instruments was used for electron diffraction analyses. TEM samples were prepared by placing drops of dispersed samples over carbon coated copper grids and allowing the solvent to evaporate.

Fluorescence spectrophotometer: Measurements were carried out on a Perkin Elmer LS55 fluorescence spectrophotometer with slit widths of 5 nm. Alternatively spectra were recorded on a Varian Cary Eclipse fluorescence spectrophotometer with slit widths of 5 nm.

Lifetime measurements: Luminescence lifetimes were measured using IBH (Fluorocube) Time-Correlated Picosecond Counting system. Solutions were excited at 365 nm and the emission was collected at 450 nm.

Atomic force microscopy: A VEECO Digital Instruments multimode scanning probe microscope equipped with a Nanoscope IV controller was used for AFM measurements. Samples were drop coated on to a Si (111) substrate and were

analyzed using contact mode AFM using long silicon nitride probes (100 μm). The height data was collected at a scanning frequency of 1Hz.

Dynamic Light Scattering: DLS measurements were carried out on Brookhaven Instrument model 90 Plus Particle Size Analyzer.

Magnetic measurements: The magnetic characteristics of the cobalt nanoparticle powder samples were measured using a EG&GPAR 4500 vibrating sample magnetometer. Zero-field-cooled (ZFC) magnetization curves were obtained after cooling the sample from room temperature to 2 K without any external magnetic field and then measuring the magnetization while warming the sample under an external field of 50 Oe. For field cooled (FC) measurements, the sample was cooled to 2 K under an external field of 50 Oe and the magnetization was measured while warming in the same field.

Ferromagnetic resonance measurements: The ferromagnetic resonance spectra of the samples were obtained using a conventional X-band ESR spectrometer (JEOL JES-TE20) at room temperature, where the magnetic field and microwave frequency were calibrated using NMR Gauss meter and a frequency counter, respectively. The ESR spectra were obtained by taking about 0.5 mg of powder samples in a quartz tube. The sample tube was purged by He before performing the room temperature experiments.

APPENDIX II

List of Abbreviations:

OA: Oleic acid.

LA: Linoleic acid.

SA: Stearic acid.

SL: Sophorolipid.

OASL: Oleic acid derived sophorolipid.

LASL: Linoleic acid derived sophorolipid.

SASL: Stearic acid sophorolipid.

SPR: Surface Plasmon Resonance.

ODA: Octadecylamine.

TOP: Trioctylphosphine.

TOPO: Trioctylphosphine oxide

DDOA: 2 (Dodecyloxy) acetic acid.

OASL-CoNPs: oleic acid derived sophorolipid capped cobalt nanoparticles.

DDOA-CoNPs: 2 Dodecyloxy acetic acid capped cobalt nanoparticles.

Ag_OASL: Ag nanoparticles synthesized using oleic acid sophorolipid.

Ag_LASL: Ag nanoparticles synthesized using linoleic acid sophorolipid.

DLS: Dynamic Light Scattering.

CTAC: Cetyltrimethyl Ammonium Chloride.

CTAB: Cetyltrimethyl Ammonium Bromide.

Au_CTAC: Au nanoparticles synthesized using

ICG: Indocyaninegreen.

CMC: Critical Micelle Concentration.

HAuCl₄: Tetrachloroauric Acid.

CoCl₂: Cobalt chloride.

NaBH₄: Sodium Borohydride.

Au: Gold.

Ag: Silver.

Pt: Platinum.

FC: Field cooled

ZFC: Zero field cooled

fcc: Face centered cubic

hcp: Hexagonal closed packed

FTIR: Fourier Transform Infrared Spectroscopy.

TEM: Transmission Electron Microscopy.

XRD: X-ray diffraction

AFM: Atomic Force Microscopy.

SAED: Selected Area Electron Diffraction.

Rpm: Rotations per minutes.

XPS: X-ray photon spectroscopy.

NMR: Nuclear Magnetic Resonance.

1D: One Dimensional.

2D: Two Dimensional.

3D: Three Dimensional.

SDS: Sodium Dodecyl Sulphate.

MPA: 3-mercaptopropionic acid.

MUA: 11-mercaptoundecanoic acid.

APPENDIX-III

(List of Publications)

1. Anita Swami, Manasi Kasture, Renu Pasricha and Murali Sastry, *Flat gold nanostructures by the reduction of chloroaurate ions constrained to a monolayer at the air–water interface*. **J.Mater.Chem**, **2004**, 14, 709.
2. P.Senthil Kumar, Manasi Kasture, Usha Raghavan, Renu Pashricha and Murali Sastry. *Synthesis of CdS and Alloyed CdMnS Nanocrystal Using Aqueous Foams*. **J.Nanosci.Nanotechnol**, **2005**, 2, 2.
3. Ajay.V.Singh, Bapurao.B. Bandgar, Manasi.Kasture, B.L.V.Prasad and Murali Sastry. *Synthesis of gold, silver and their alloy nanoparticles using Bovine serum albumin as foaming and stabilizing agent*. **J.Mater.Chem**, **2005**, 15, 5115
4. Debabrata Rautaray, Manasi. Kasture and Murali Sastry. *Role of Mg ions in modulating the growth of CaCO₃ crystals in aqueous foams*. **CrystEngComm**, **2005**, 7, 469.
5. Manasi Kasture, Sanjay Singh, Pitamber Patel, P.A.Joy, A.A. Prabhune, C.V. Ramana and B.L.V. Prasad. *Multiutility Sophorolipids as Nanoparticle Capping Agents: Synthesis of Stable and Water Dispersible Co Nanoparticles*. **Langmuir**, **2007**, 23, 11409.
6. M.B.Kasture, P.Patel, A.A.Prabhune A.A Kulkarni and BLV Prasad, *Synthesis of silver nanoparticles by sophorolipids: Effect of temperature and sophorolipid structure on the size of particles*, **J of Chem Sci** , **2008**, 120,515.
7. A.V. Singh, R. Patil, M.B. Kasture, W.N. Gade and B.L.V. Prasad, *Synthesis of Ag-Pt alloy nanoparticles in aqueous bovine serum albumin foam and their cytocompatibility against human gingival fibroblasts* **Colloid and Interface B: Biointerface**. **2009**, 69, 2,239.
8. Manasi Kasture, Murali Sastry, B.L.V. Prasad, *Halide ion controlled shape dependent gold nanoparticle synthesis with tryptophan as reducing agent: Enhanced fluorescent properties and white light emission*. **Chemical Physics Letters**, **2010**, 484, 271.

9. D. V. Ravi Kumar, ***Manasi Kasture***, A. A. Prabhune, C. V. Ramana, B. L. V. Prasad and A. A. Kulkarni *Continuous flow synthesis of functionalized silver nanoparticles using bifunctional biosurfactants*. **Green Chemistry**, **2010**, 12, 609.

Conference Proceeding:

1. A Sendilkumar, Manasi Kasture, Pitamber Patel, C.V.Ramana, B.L.V.Prasad and S Srinath, *Investigation of magnetic anisotropy in Co nanoparticles using ferromagnetic resonance technique* **Journal of Physics: Conference Series**, **2010**, 200, 075088.